Izabela Natalia Faria Gomes

STUDY OF BIOMARKERS OF CETUXIMAB RESPONSE AND PRESPECTIVE OF APPLICATION OF ANTI-EGFR "COMBI-MOLECULES" IN HEAD AND NECK AND COLORECTAL CANCER

Thesis presented to the Pio XII Foundation
postgraduate program Barretos Cancer Hospital
to obtain the Doctorate degree in health sciences.

Concentration Area: Oncology

Supervisor: Prof. Dr. Rui Manuel Reis

Co-Supervisor: Prof. Dr. Bertrand Jean-Claude

Co- Supervisor: Prof. Dr. Renato José da Silva Oliveira

Barretos, SP

2021

Izabela Natalia Faria Gomes

STUDY OF BIOMARKERS OF CETUXIMAB RESPONSE AND PRESPECTIVE OF APPLICATION OF ANTI-EGFR "COMBI-MOLECULES" IN HEAD AND NECK AND COLORECTAL CANCER

Thesis presented to the Pio XII Foundation
postgraduate program Barretos Cancer Hospital
to obtain the Doctorate degree in health sciences.

Concentration Area: Oncology

Supervisor: Prof. Dr. Rui Manuel Reis

Co-Supervisor: Prof. Dr. Bertrand Jean-Claude

Co- Supervisor: Prof. Dr. Renato José da Silva Oliveira

Barretos, SP

2021

SUPPORT TO RESEARCH BY DEVELOPMENT AGENCY

This work was supported by the Foundation for Research Support of the State of São Paulo (FAPESP) through Research Assistance – Regular (process number 2017/22305-9), DFATD x CAPES (process number 88887.137283/2017-00) and Terry Fox Foundation.

The opinions, hypotheses and conclusions or recommendations expressed in this material are those of the authors and do not necessarily reflect the views of FAPESP.

RESEARCHERS´S DECLARATION OF RESPONSIBILITY

“This thesis was prepared and is presented in accordance with the norms of the Graduate Program of the Barretos Cancer Hospital – Pio XII Foundation, based on the Regulations of the Graduate Program in Oncology and on the Manual for the Presentation of Dissertations and Theses of the Cancer Hospital of Barretos. The researchers also declare that this work was carried out in accordance with the Code of Good Scientific Practice (FAPESP), with nothing in its content that could be considered as plagiarism, fabrication or data falsification. The opinions, hypotheses and conclusions or recommendations expressed in this material are the responsibility of the authors and do not necessarily reflect the views of the Pio XII Foundation – Hospital de Câncer de Barretos”.

AGRADECIMENTOS

Apesar do restante da tese ser escrita em inglês optei por fazer os agradecimentos em português para conseguir escrever na integra a minha gratidão por cada pessoa que de um jeito ou de outro foram abrigo, um olhar diferente, o ombro e mão amiga durante esses 4 anos. Sei que ninguém vence sozinho e serei sempre grata a todos que me ajudaram e me deram força para lutar.

Agradeço primeiramente a **Deus** por ter me permitido chegar até aqui, por sempre me guiar pelos melhores caminhos, e por ter me dado força e perseverança nos momentos mais difíceis.

Aos meus pais **Francisco e Maria Helena** pelo amor incondicional, por sempre acreditarem em mim e por não terem medido esforços e abdicarem das suas próprias vontades para que eu conseguisse chegar aqui. A minha irmã **Thaynara** pelos momentos de alegria, carinho e por sempre estar ao meu lado, em todas as minhas decisões e nos momentos que mais precisei. Ao meu marido **Fábio**, por ser colo nos momentos de angústia e por compreender e viver comigo cada um dos meus sonhos e não medir esforços para realizá-los.

Ao **Prof. Dr. Rui Reis** pelo incentivo e por acreditar em meu trabalho e por poder compartilhar comigo o bem mais precioso que alguém pode dar ao próximo: o conhecimento. Obrigada por todas as oportunidades oferecidas, pelo exemplo, competência, pela confiança que depositou em mim, ao senhor minha eterna admiração e gratidão.

Ao meu co-orientador **Dr. Renato Oliveira**, faltam palavras para expressar o tamanho da minha admiração, carinho e gratidão por você. Muito obrigada pela paciência, pela dedicação, pelos ensinamentos científicos e pessoais. Muito obrigada pela confiança que você depositou em mim quando eu mesma não acreditava que seria capaz. Muito obrigada por sempre me escutar, por sempre ser o ombro amigo nos momentos de dúvida e desespero.

To my co-advisor **Prof. Dr. Bertrand Jean-Claude** for his help, for the good humor and affection I was received at McGill University, for the experience and scientific exchange, for the prompt availability to help the development of the work.

Aos queridos professores **Dr. Vladmir Lima e Drª Céline Pinheiro,** pela atenção e disponibilidade na condução das bancas de acompanhamento.

A **Drª Viviane Aline e a Drª Marcela Nunes**, duas grandes incentivadoras, obrigada por serem a mão amiga nos momentos em que nada parecia certo, por estarem junto comigo em todos os momentos e por sempre mostrarem uma nova maneira de enxergar os fatos nos momentos de dúvida.

Dear McGill University friends: Elliot Goodfellow, Julie Smith, Karine Pasteurd and Shanlong Huang, the days in Canada have been made even more special by having you around. This experience was certainly the most challenging of my professional and personal life and has remained forever in my heart and my memory. The biggest cultural and scientific exchange I could experience. Montreal has a very special place in my heart and in my life. Especially Elliot, who was like a “big brother” in the hardest days. I hope to see you again soon.

Aos amigos queridos biologistas e amigos do CPOM, **Karina Mello, Letícia Braga, Ana Carolina Laus, André Lengert** e **Marcela Nunes** cada, muito obrigada pelas conversas descontraídas, pelos cafés, pela ajuda intelectual e por terem me recebido tão bem na equipe. Também não poderia esquecer dos amigos “aleatórios” e do andar zero: **Cintia, Murilo, Weder, Ariane, Ana Laura, Ângela, Elisa, Marcela, Karen, Aline, Fernanda, Maraísa, Paula Patrik, Lucas** a caminhada ao lado de vocês tornaram os dias mais leves, muito obrigada por todos os momentos de descontração. Muito obrigada por vocês representarem sempre o ombro amigo nos momentos de alegria e tristeza, disposto a ajudar. Cada um de vocês tem um lugar todo especial na minha vida.

Ao Hospital de Amor, ao CPOM (Centro de pesquisa em Oncologia Molecular), à FAPESP, CAPES, DFATD e Terry Fox.

“What I love about science is that as you learn, you don’t really get answers.

You just get better questions.”

John Green

SUMMARY

FIGURES LIST

TABLE LIST

SYMBOL LIST

µM Micromolar

µL Microlitre

°C Celsius

≥ Bigger then

≤ Less than

M Molarity

KDa Kilodalton

CCDND2 Cyclin D2

DMEM Dulbecco's modified Eagle's medium

DMSO Dimethyl sulfoxide

DPBS Dulbecco's phosphate-buffered saline

EGFR Epidermal Growth Factor Receptor

EMT Epithelial–mesenchymal transition

ENG Endoglin

ERCC Excision repair cross-complementing

ERK Extracellular signal-regulated kinase

FBS Fetal bovine sérum

FRS2 Fibroblast Growth Factor Receptor Substrate 2

HB-EGF Heparin-binding EGF-like growth factor

HMGA2 High Mobility Group AT-Hook 2

HNSCC Head and Neck Squamous Cell Carcinoma

IC_{50} Inhibition concentration 50

ICAM-1 Intercellular cell adhesion molecule 1

KCL Potassium Chloridre

KRAS Kirsten rat sarcoma viral oncogene homolog

LAMP1 Lysosomal-associated membrane protein 1

LAMP2 lysosomal-associated membrane protein 2

MAPK Mitogen Activated Protein *Kinases*

MDM2 Mouse double minute 2 homolog

miRNA microRNA

MTOR Mechanistic Target of Rapamycin Kinase

MTS 3- (4,5-dimethylthiazol-2-yl) -5- (3-carboxymethoxyphenyl) -2- (4-sulfophenyl) -2H-tetrazolium dichloride

PARP Poly (ADP-ribose) polymerase

PD1 Programmed cell death 1

PIK3A Phosphoinositide 3-kinase

PTEN Phosphatase and Tensin Homolog

RHOA Ras homolog family member A

SHH Sonic hedgehog

TCA Trichloroacetic acid

TGF-β Transforming growth factor beta

WES Whole exome sequencing

WT1 Wilms tumor suppressor

XRCC X Ray Repair Cross Complementing

RESUMO EM PORTUGUÊS

O receptor do fator de crescimento epidérmico (EGFR) é uma proteína cuja ativação leva à ativação da sinalização de vias intracelulares que atuam diretamente na proliferação, migração e sobrevivência celular. O cetuximabe (CTX) é um anticorpo monoclonal anti-EGFR aprovado para o tratamento de pacientes com carcinoma espinocelular de cabeça e pescoço (CECP) e câncer colorretal metastático (mCRC). A resposta de pacientes com mCRC ao CTX está associada ao *KRAS, NRAS* e *BRAF* de tipo selvagem. No entanto, para pacientes com CECP até agora, nenhum biomarcador preditivo de resposta CTX foi validado, sendo um desafio selecionar pacientes que poderiam se beneficiar deste agente. Além disso, considerando a resistência adquirida das células cancerosas às terapias moleculares e à comunicação cruzada intracelular, o design de "moléculas combinadas" ou “moléculas híbridas” é uma abordagem inovadora e promissora. As denominadas "combi-moléculas" são projetadas para ter dois ou três alvos, como a inibição do reparo de DNA e, ao mesmo tempo, o bloqueio da sinalização mediada por EGFR. Portanto, este projeto teve como objetivos: a) encontrar biomarcadores preditivos de resposta CTX em linhagens de células resistentes a CECP; b) avaliar a atividade antineoplásica de "combi-moléculas" em tumores sólidos. Para atingir esses objetivos, estabelecemos um modelo de resistência ao cetuximabe (FaDu), usando concentrações crescentes de cetuximabe por cerca de oito meses. As linhagens resistentes e parental foram avaliadas quanto à viabilidade celular, ensaios clonogênicos, de migração e de adesão. O perfil de expressão da proteína foi analisado por Western blot e por um painel de proteínas de superfície celular humana. O perfil mutacional, a análise do cariótipo e as alterações do número de cópias (CNA) foram analisados usando sequenciamento do exoma completo (WES) e a plataforma NanoString. Para avaliar o potencial das “combi-moléculas” como uma nova abordagem terapêutica em tumores sólidos, analisamos a viabilidade celular, clonogênica, migração, bem como a inibição da sinalização de EGFR usando um grande painel de cabeça e pescoço e linhagens de células colorretais. Os clones resistentes exibiram IC_{50} pelo menos 2 vezes maior em comparação com a linhagem celular parental. O WES mostrou mutações relevantes em vários genes relacionados ao

câncer, e a análise comparativa da expressão de mRNA mostrou 36 genes diferencialmente expressos associados à resistência aos inibidores da tirosina quinase *EGFR, RAS, MAPK* e sinalização de *mTOR*. É importante ressaltar que observamos que a superexpressão de RhoA e CD44, bem como a expressão aumentada de marcadores da transição epitélio-mesenquimal (EMT) e de marcadores de células-tronco, foram associados à resistência ao cetuximabe. A análise de proteínas revelou inibição da fosforilação de EGFR e aumento de mTOR nas células resistentes. Além disso, a linhagem celular resistente demonstrou um fenótipo agressivo com um aumento significativo na adesão, no número de colônias e nas taxas de migração. As combi-moléculas exibiram um efeito citotóxico dependente da dose em um grande painel de células colorretais e de cabeça e pescoço. Os valores de IC_{50} de ZR2002 foram significativamente mais baixos quando comparados com geftinib, clorambucil e da combinação entre geftinib e clorambucil. Em seguida, avaliamos o impacto funcional do ZR2002 em umas linhagens celulares sensiveis (FaDu, Difi) e resistentes (JHU28, HCT15). Além de reduzir os níveis das proteínas relacionadas à via do EGFR, o tratamento com ZR2002 também aumentou os níveis das proteínas p-H2AX e PARP, sugerindo dano ao DNA. ZR2002 também aumentou células na apoptose tardia / necrose. Além disso, o ZR2002 reduziu a formação de colônias em comparação com o DMSO e demonstrou taxas de migração mais baixas em comparação com seus controles. No geral, identificamos várias alterações moleculares na linhagem celular resistentes ao cetuximabe que representam potenciais novos biomarcadores de resposta a cetuximabe. Além disso, nossos resultados sugerem que ZR2002 é capaz de inibir EGFR e promover danos ao DNA, indicando que esta nova abordagem terapêutica através da utilização de “moléculas-combinadas” pode ser uma estratégia promissora para superar a resistência a agentes anti-EGFR.

Palavras-chave: EGFR, Cetuximabe, resistência a drogas, receptores tirosina-quinase, Combi-moléculas

ABSTRACT

The epidermal growth factor receptor (EGFR) is an important protein which activation leads to the signaling of intracellular pathways that act directly on cell proliferation, migration and survival. Cetuximab (CTX) is an anti-EGFR monoclonal antibody that has been approved for the treatment of head and neck squamous cell carcinoma (HNSCC) patients and metastatic colorectal cancer (mCRC). The response of mCRC patients to CTX is associated with genetic tumor features, such as wild type *KRAS, NRAS* and *BRAF.* However, for HNSCC patients until now, any biomarker predictive of CTX response was validate, making harder the selection of patients who could benefit from this agent. Also, considering the acquired resistance of cancer cells to molecular therapies and intracellular cross-communication, the design of "combinate- molecules" or "hybrid molecules" is an innovative and promising approach. "combi-molecules" are designed to have two or more targets, such as inhibition of DNA repair, and at the same time blockage of EGFR-mediated signaling. Therefore, this project aims to: a) find biomarkers predictive of CTX response in HNSCC resistant cell lines; and b) evaluate the antineoplastic activity of "combi-molecules" in HNSCC and CRC cell lines. To achieve these goals, we established a cetuximab resistant model (FaDu), using increased cetuximab concentrations for more than eight months. The resistance and parental cells were evaluated for cell viability, clonogenic, migration, and adhesion assays. The protein expression profile was analyzed by western blot and human cell surface panel by lyoplate. The mutational profile, karyotype analysis, and copy number alterations (CNA) were analyzed using whole-exome sequencing (WES) and the NanoString platform. To assess the potential of three combi-molecules that target EGFR and alkylated DNA, as a new therapeutical approach in solid tumors we analyzed the cell viability, clonogenic, migration as well as the EGFR signaling inhibition using a large panel of head and neck and colorectal cell lines. FaDu resistant clones exhibited at least 2-fold higher IC_{50} compared to the parental cell line. WES showed relevant mutations in several cancer-related genes, and the comparative mRNA expression analysis showed 36 differentially expressed genes associated with EGFR tyrosine kinase inhibitors resistance, RAS, MAPK, and mTOR signaling. Importantly, we observed that

overexpression of RhoA, and CD44, as well as upregulation of epithelial–mesenchymal transition (EMT) and stem cell mechanisms, were associated with cetuximab resistance. Protein analysis revealed EGFR phosphorylation inhibition and mTOR increase in resistant cells. Moreover, the resistant cell line demonstrated an aggressive phenotype with a significant increase in adhesion, the number of colonies, and migration rates. The combi-molecules exhibited dose-dependent cytotoxic effect in a panel of colorretal and head and neck cancer cell lines. The IC_{50} values of ZR2002 were significantly lower when compared to Geftinib chlorambucil and Geftinib combinated with chlorambucil. Then, we evaluate the functional impact of ZR2002 in one sensitive (FaDu, Difi) and one resistant (JHU28, HCT15) cell line. Besides reducing levels of EGFR pathway proteins, ZR2002 treatment also increased levels of p-H2AX and PARP proteins, suggesting DNA damage and cell death process, in all cell lines analyzed. ZR2002 also increased cells on late apoptosis/necrosis. Furthermore, ZR2002 reduced colony formation compared with DMSO and demonstrated lower migration rates compared with their controls. Overall, we identified several molecular alterations in the cetuximab CTX resistant cell line that may constitute novel biomarkers of cetuximab response, and our results suggested that ZR2002 is able to inhibit EGFR and to promote DNA damage, indicating that this new therapeutical approach might be a promising strategy to overcome anti-EGFR resistance.

Key words: EGFR, Cetuximab, Drug resistance, Tyrosine kinase receptors, Combi-molecules.

1. BACKGROUND

1.1. Cancer

Cancer is characterized by a set of malignancies that have in common exacerbated and uncontrolled cell growth, as well as the capacity of cellular invasion to organs other than the primary site[1]. According to GLOBOCAN estimates, up to the year 2020, more than 17 million new cases of cancer diagnosed worldwide are expected, and around 10 million deaths from the disease[2], being solid tumors responsible for about 85% of the total cases [3].

In this context, head and neck and colorectal tumors comprise the 8th and 3rd most frequent neoplasms in men worldwide [4-6]. In Brazil, these tumor subtypes correspond to the 2nd and 5th most incident among men, with an estimation, for the year 2020, of approximately 11.000 cases for head and neck tumors and about 16,660 cases for colorectal tumors[7]. Among the histological subtypes, the most frequent head and neck cancer is squamous cell carcinoma (HNSCC), which comprises 90% of all cases. This type of tumor is more common in men, and it is estimated that about two-thirds of all cases are diagnosed in males [8]. In turn, the most incident subtype for colorectal is adenocarcinoma, accounting for about 90% of the cases, with a similar incidence in both sexes [9].

Tobacco is the main risk factor associated with the development of head and neck cancer [10, 11]. Tobacco and alcohol consumption have shown a synergistic relationship that contributes to disease progression in HNSCC, as well as the presence of HPV (human papilloma virus), especially the oncogenic subtypes 16 and 18 [11-13]. Concerning CRC, 90% are sporadic and their main risk factors are diet, tobacco and alcohol[14]. For both HNSCC and colorectal tumors the therapeutic approach adopted is based on staging of the disease[14-17]. For HNSCC patients, the association of chemotherapeutic agents based on platinum drugs and taxanes represents the standard treatment for locally advanced tumors. Promising results have also been observed with the use of the docetaxel-cisplatin-5'-flurax scheme as a neoadjuvant

therapy in clinical trials[15, 18, 19]. Although in recent years the therapeutic behaviors have contributed to the disease control for HNSCC, the rate of local recurrence is still considerable (between 20-30%)[20].Cytotoxic therapy for colorectal tumors using 5'-fluoracil has shown effective results as adjuvant therapy for metastatic tumors. Other cytotoxic drugs have been studied and validated, including capecitabine, tegafur, irinotecan and oxaliplatin, leading to its incorporation into practical guidelines and widespread use in clinical practice[21].

In addition to chemotherapy, there is also the targeted therapy, with EGFR being one of these promissory targets in the context of solid tumors. Regarding head and neck cancer, among the many available anti-EGFR drugs, only cetuximab was approved[22]. The first targeted agent for CRC approved by the Food and Drug Administration (FDA) was cetuximab in 2004 followed by anti-angiogenesis agent bevacizumab in the same year[23]. Immune checkpoint inhibitors aims to enhance immune surveillance and suppression against cancer by blocking the tumor's attempt to escape from T cell detection.[24] Currently, checkpoint inhibitors have been investigated in various solid tumors with promising responses[24]. Although, there are plentiful choices of targeted treatments which one or more could ultimately be beneficial. The development of new therapeutic arsenals even more individualized are necessary to promote even longer survival and have fewer adverse reactions. Thus, the development of new therapeutic arsenals for the control of head and neck and colorectal cancer is necessary.

1.2 Epidermal growth factor receptor (EGFR)

EGFR (ErbB1) is tyrosine kinase receptor that mediates the cellular processes associated with proliferation, survival, migration and invasion [25]. This receptor is a conserved transmembrane glycoprotein belongs to the ErbB family, which has three closely related transmembrane receptor tyrosine kinases (ErbB2, ErbB3, ErbB4). Mature EGFR has about 170 kDa and is subdivided into an extracellular ectodomain with 4 subdomains named I, II, III and IV, as well as an intracellular C-terminal portion with a tyrosine kinase domain and an autophosphorylation domain[26]. This receptor can be activated by homo or hetero-dimmerization by allosteric stimulation of its ligands [25, 26]. Once dimerized, EGFR has the ability to autophosphorylate the tyrosine

residues present in the C-terminal portion, thereby recruiting effector proteins capable of transducing the extracellular signals, activating a signaling cascade that culminates in the transcription of target genes involved in proliferation [27] . Activation of EGFR is promoted by binding of specific ligands and results in the activation of some proliferative pathways such as MAPK, PI3KA / AKT and STAT [28, 29 30] (figure 1).

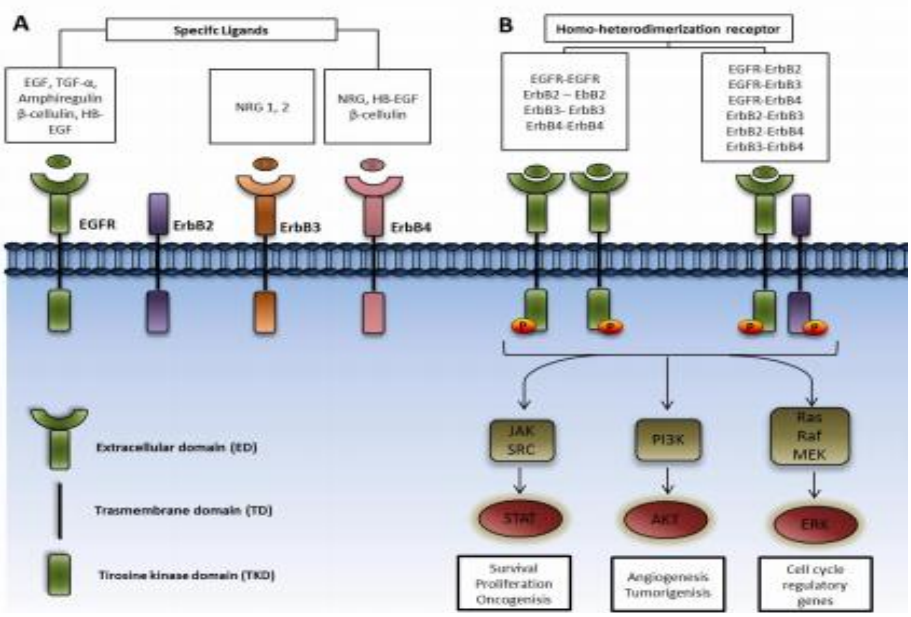

Figure 1-Activation of ErbB family receptors. A) ErbB family receptors and their specific ligands. B) EGFR activation by homo / heterodimerization. Adapted from Silva-Oliveira et.al, 2016

Due to EGFR importance in modulating cell proliferation, the balance between the expression/activation of EGFR must be regulated to ensure basal proliferative levels. Alterations in EGFR activity may result from alterations in mechanisms of secretion of autocrine/paracrine factors, gene amplification, mutations (mainly in the intracellular domain), and nuclear translocation of the receptor[22]. Typically, EGFR is overexpressed in a variety of tumors, including solid tumors, which include lung (40-80%), colorectal (25-77%) and head and neck tumors (30-95%) [30-34].

1.3 EGFR Targeted therapy and the search for predictive biomarkers

Anti-EGFR targeted approaches, have shown promising results for a variety of tumor types, including lung, head and neck, and colorectal tumors[35]. Cetuximab, an anti-EGFR monoclonal antibody, has been inserted in clinical practice for HNSCC patients and recurrent or metastatic colorectal patients, in which previous therapies

have failed and can be used as monotherapy or in combination with radiotherapy [36, 37]. Cetuximab acts by competitive inhibition, preventing the interaction of the receptor with its natural ligands. Once the binding site is blocked, ligand-receptor interaction is prevented, resulting in blockade of receptor dimerization and inhibition of proliferative intracellular pathways, which, among other events, can trigger cell cycle disruption, induction of apoptosis, inhibition of metastases and receptor degradation itself [22, 38] (Figure 2). This therapeutic approach has demonstrated effective results with low toxicity rates, high efficacy, and improved overall survival from 29.3 months compared to 49 months, in HNSCC patients treated with radiotherapy only [22, 39, 40].

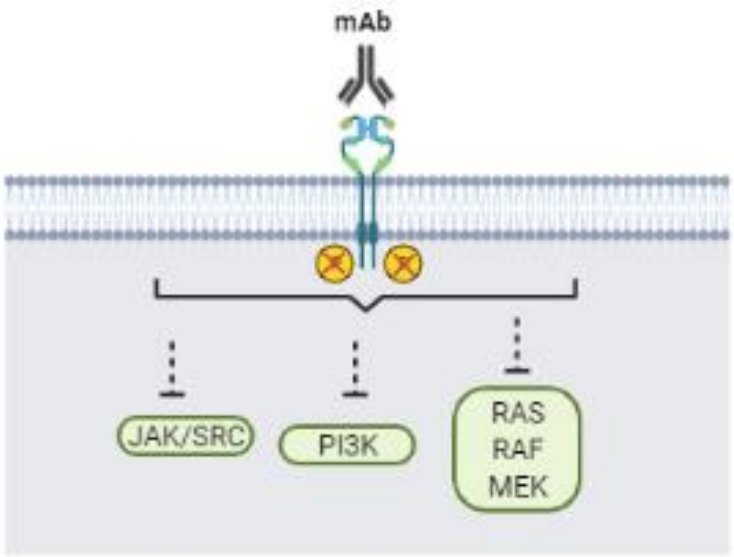

Figure 2-Cetuximab mechanism of action. Adapted from Silva-Oliveira et al, 2016

Although cetuximab-directed therapy has shown promise in its first years, intrinsic or acquired resistance has limited the promising results obtained [41, 42]. In CRC, activating KRAS mutations, which are present in 30–40% of CRC serve as a key useful biomarker for cetuximab response as well as the introduction of BRAF V600E allele, high p38 (MAPK) and NRAS could predict the response to cetuximab in patients with CRC harboring WT KRAS [43-46]. Moreover, there are no solid molecular bases that explain the resistance mechanisms in HNSCC. In this way, the search for predictive biomarkers is necessary to identify molecular targets that determine the mechanisms of cetuximab resistance, especially in HNSCC tumors [47-49].

Considering *KRAS* mutations are practically absent in HNSCC (<1%)[50], the mutational status of *KRAS* does not represent a predictive biomarker as in the case of colorectal tumors, nor EGFR mutations since they are present in only 5% of cases [51]. However, some findings indicate changes that may be associated with persistence of the resistant phenotype in HNSCC patients such as the mutational status of *PIK3CA41* and *HRAS* [52], *HB-EGF* increased expression, as well as variation in the genes of control of the AP-1 transcription factor[49] and *EGFR* copy number variation[53].

1.4 The "combi-molecules" concept as a new approach to the rational development of anticancer drugs

Another important mechanism of therapy resistance is the cross-communication between different intracellular signaling pathways [54]. The implication of several signaling proteins in a complex network of signal transduction pathways is a commonly occurring event in advanced cancers. This communication functions as a compensatory mechanism when one of the signaling cascades is blocked [55]. In this manner, inhibition of a single target may not be sufficient to induce tumor regression[35, 56]. Therefore, there is a need for the development of new therapeutic approaches, such as "combi-molecules", with the aim of increasing the selectivity and improving the effectiveness in refractory tumors[57].

The development of multi-target drugs, named "combi- molecules" or "hybrid molecules", has been "shown to be a promising strategy and trend for the development of new anticancer drugs, since this approach allows the construction of molecules that can promote the tandem blockade of multiple targets responsible for tumor progression [56, 58]. The design of "Combi-molecules" was develop by Prof. Bertrand Jean-Claude Group (Chemical medicine McGill University), are able to block two or three targets simultaneously and are divide into three types: (i) Type I molecule was designed to block tyrosine kinase receptor (I) and promote DNA damage as an intact structure or upon undergoing hydrolysis (figure 3a, step 1)[59]. (ii) Type II form was designed to inhibit tyrosine kinase receptor and damage DNA without requirement for hydrolysis (Fig. 3B, steps 1 and 2)[60]. (iii) The type III reconciles the type I and II targeting models. As shown in Fig. 1C (step 1), to target a cell expressing kinase 1 (Kin-1) and kinase 2 (Kin-2) as an intact structure or upon undergoing hydrolysis [61]. Thus,

the combi-targeting concept is a tandem approach to chemosensitivity and chemoselectivity.

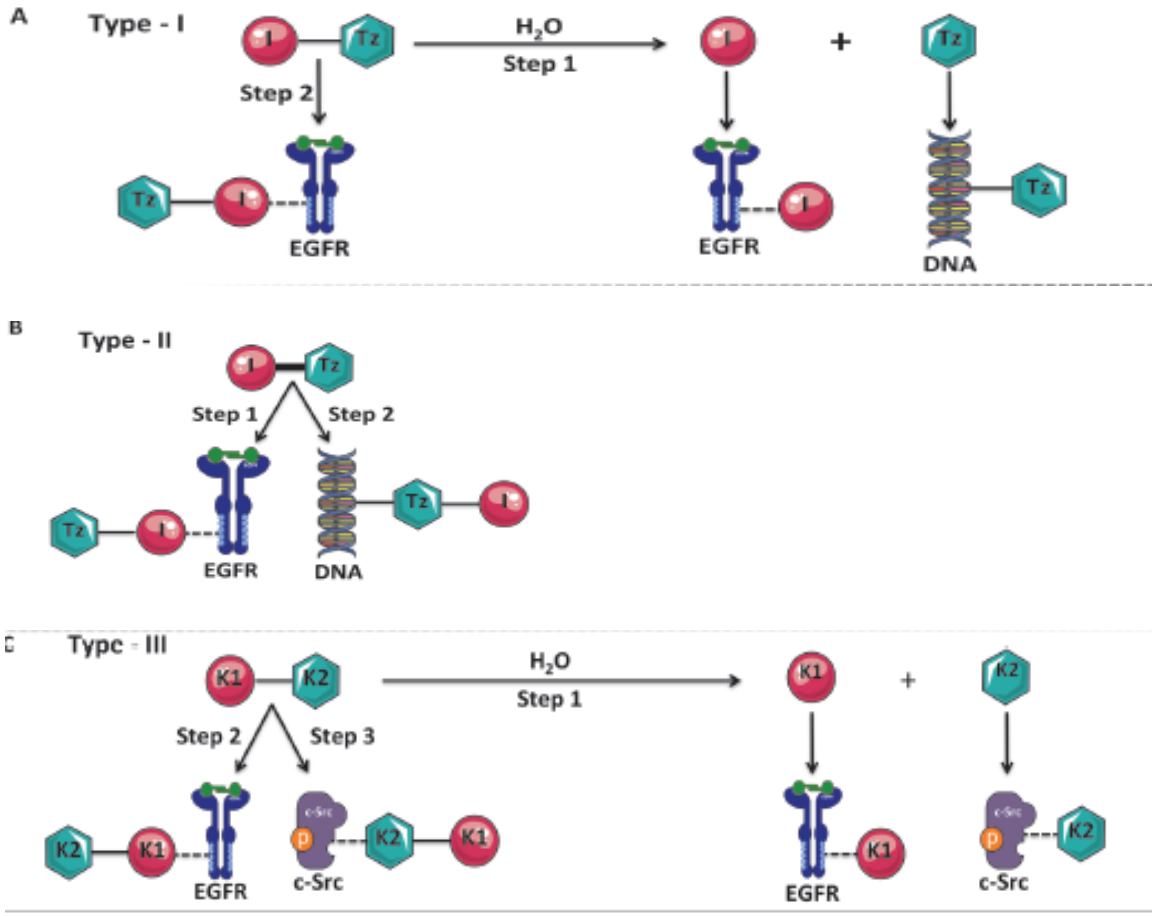

Figure 3- Combi-molecules classification. **A-** Combi-molecule type I was designed to contain a tyrosine kinase inhibitor (I) and a DNA alkylating agent (Tz) moiety. The type I can inhibit tyrosine kinase receptor as an intact struture (step 2), or upon undergoing hydrolysis, but the molecule is only capable of targeting DNA through the release of its Tz moiety (step 1). **B**- Combi-molecule type II was was designed to contain a tyrosine kinase inhibitor (I) and a DNA alkylating agent (Tz) moiety connected by a non-hydrolysable linker. This type-II molecule can target both tyrosine kinase receptor and DNA as an intact structure through each of its targeting arm (steps 1 and 2). **C-** Combi-molecule type III was designed to contain two tyrosine kinase inhibitors connected by hydrolysable linker. Adapted by Rao *et al*,2015

The combi- molecules are able, for example, to inhibit EGFR-mediated signaling by inhibiting receptor phosphorylation, and may also promote DNA damage by inhibiting repair mechanisms and thereby activating the cell death[62, 63]. Since blockade of EGFR

signaling can negatively regulate proteins and genes involved in repair processes such as *ERCC* and *XRCC*, the use of so-called PARP inhibitors has also shown promising results in inhibiting repair mechanisms, especially for mutated tumors in *BRCA1 /2* [64]. In addition, there are reports that attribute the inhibition of proteins involved in apoptosis signaling as BAD to EGFR signaling [65-70]. Taking these findings together, it is suggested that the combination of anti-EGFR agents and genome targeting agents may promote a potential antineoplastic effect against solid tumors that overexpress EGFR, including head and neck and colorectal tumors.

Promising results have been demonstrated in prostate tumor cell lines where the use of a "combi-molecule" called RB24 that inhibits EGFR and promotes DNA methylation was about 100 times more effective than its precursor alone and had a potency four times greater than gefitinib. This same work shows that RB24 can negatively regulate XRCC1 and BAD, thereby maximizing cell damage and promoting the activation of mechanisms of death[71] . Moreover, it has been demonstrated, *in vitro*, that such "combi-molecules" have a tendency to accumulate in the cytoplasm of the tumor cell, thereby conferring selectivity to this molecules[72]. It has also been demonstrated *in vitro* that ZR2002, a “combi-molecule” designed to alkylate DNA and promote DNA damage plus induce irreversible EGFR tyrosine kinase inhibition, induced anti-proliferative effects and suppressed neurosphere formation in glioblastoma cell lines with marginal effects on normal human astrocytes[73]. ZR2002 was able to block EGFR, downstream Erk1/2 phosphorylation, and increased DNA strand breaks. Moreover, ZR2002 improved survival of mice harboring intracranial mesenchymal TMZ-resistant glioblastoma cell lines[73]. These results together provide evidence to the potential of “combi-molecules” as a new approach to anticancer therapy in solid tumors.

JUSTIFICATION/ RATIONALE

The EGFR is an important cancer target due to its central role in the carcinogenesis of several solid tumors, and several therapies against EGFR have been developed and are currently in clinical used for cancer patients.

Cetuximab is a monoclonal antibody against EGFR, approved for colorectal and head-neck metastatic tumors. However, only a fraction of patients responds favorably to the drug. The mutational status of *KRAS, NRAS* and *BRAF* are currently predictive biomarkers of colorectal resistance, yet, for HNSCC patients, there is no predictive biomarker.

Moreover, in the context of targeted therapy, it has already been identified that there is activation of several compensatory pathways in the tumor environment. In this way, multi-target therapy has emerged as a new therapeutic promise for refractory and not responsive tumors to single anti-EGFR therapy. In this context, has worked on the synthesis of a new class of molecules denominated "combi-molecules". This new approach in drug design promotes the tandem blockade of multiple oncogenic targets, such as genomic DNA, while blocking EGFR-mediated signaling simultaneously. Given the importance of the development of new therapeutic formulations for the treatment and control of solid tumors, the concept of "combi-molecules" promises to be a more effective, selective and less toxic strategy to control these tumors.

2. AIMS

2.1 GENERAL AIM

To identify and validate predictive biomarkers to cetuximab in head and neck cetuximab-resistant cell line and evaluate the antineoplastic activity of "combi-molecules" in head and neck and colorectal cancer cell lines.

2.2. SPECIFIC AIMS

2.2.1. To validate an *in vitro* cetuximab resistant model previously developed by our group;

2.2.2 To identify biomarkers associated with acquired resistance to cetuximab (anti-EGFR) in resistant head and neck cell lines, using a multi-omics approach;

2.2.3. To evaluate the antineoplastic effect of "combi-molecules" (anti-EGFR + alkylating agents) in a panel of solid tumors cell lines, including head and neck and colorectal tumors, by functional assays.

3. MATERIALS AND METHODS

3.1 Cetuximab resistance model development

A cetuximab-resistant in vitro model was previously established by our group[74]. Briefly, FaDu cell line was exposed to increasing doses of cetuximab (200-3200 µg / mL) for 72 hours, after which time the medium was removed and the cells were maintained in complete medium until the repopulation of cell culture (Figure 4). Thus, all the next steps were performed using the FaDu parental (FaDu P) and FaDu cetuximab-resistant (FaDu R) cell lines, to verify the changes that occurred from the acquired resistance to cetuximab.

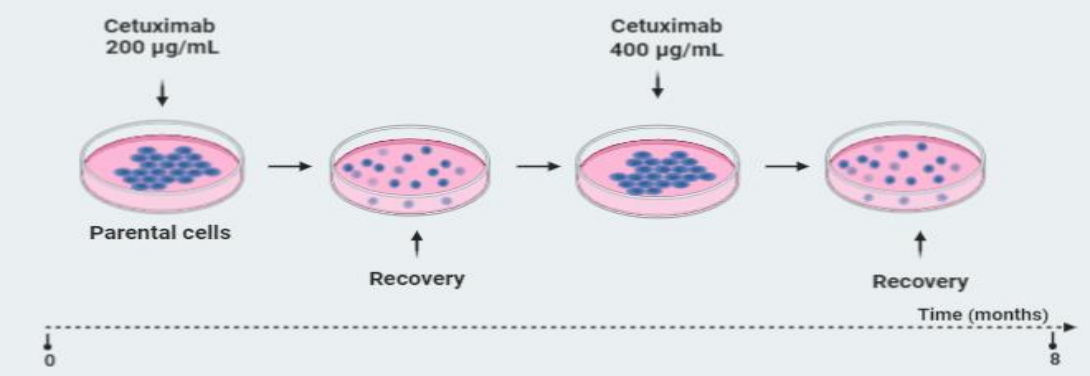

Figure 4- Scheme representative of cetuximab-established resistance model. Created in Biorender.com

3.2. Cell lines

The cell lines used in this work as well as cultivation conditions and molecular status are described in Table 1

Table 1- Molecular characterization and culture conditions of the Head and Neck and Colorectal cancer cell lines panel used in this work

Cell line	Tissue	Culture Conditions	*NRAS* mutation	*KRAS* mutation	*PIK3CA* mutation	*BRAF* mutation	*EGFR* mutation	*EGFR* amplification	HPV	Microsatellite Instability
SCC25	Head and Neck	DMEM + 10% FBS + 1% P/S	WT	WT	WT	WT	WT	No amplification	Negative	-
UM-SCC47	Head and Neck	DMEM + 10% FBS + 1% P/S	-	-	-	-	-	-	Positive	-
HN13	Head and Neck	DMEM + 10% FBS + 1% P/S	WT	WT	WT	WT	p.H773Y	No amplification	Negative	-
JHU28	Head and Neck	DMEM + 10% FBS + 1% P/S	WT	p.G12S	WT	WT	WT	No amplification	Negative	-
FaDu	Head and Neck	DMEM + 10% FBS + 1% P/S	WT	WT	WT	WT	WT	No amplification	Negative	-
HCT 15	Colorrectal	RPMI + 10% FBS + 1% P/S	WT	p.G13D	p.E545K, p.D549N	WT	WT	No amplification	-	MSI-L
CACO-2	Colorrectal	DMEM + 10% FBS + 1% P/S	WT	WT	WT	WT	WT	No amplification	-	MSS
DIFI	Colorrectal	DMEM + 10% FBS + 1% P/S	WT	WT	WT	WT	WT	Amplification	-	MSS
HCT 116	Colorrectal	RPMI + 10% FBS + 1% P/S	p.G13D	WT	p.H1047R	WT	WT	No amplification	-	MSI-H

MSI-L: Microsatellite instability low; MSS: Microsatellite instability stable; MSI-H: Microsatellite instability high

The cell lines were cultivated in DMEM medium (Dulbecco's modified Eagle's medium-SIGMA) or RPMI 1640 (Roswell Park Memorial Institute) supplemented with 10% fetal bovine serum (Gibco-SFB-code 12657-029) and 1% streptomycin / penicillin (SIGMA-code P4333), incubated in a 5% CO_2 incubator at 37 °C. All cell lines were analyzed for their authenticity by the short tandem repeat (STR) profile using international reference standardization for cell line authentication using a panel of 8 fluorescent primers (D5S818, D13S317, D7S820, D16S539, vWA, TH01, TPOX and CSF1P063) [75], at the Molecular Diagnostic Center of the Barretos Cancer Hospital. Also, all cell lines were tested for Mycoplasm contamination by Mycoalert™ (Lonza).

3.3. Drugs

The anti-EGFR "combi-molecules", namely JS61, JS84 and ZR2002 (figure 5) were developed and kindly provided by Prof. Bertrand Jean-Claude (McGill University)69, co-supervisor of the present Ph.D. The combi-molecules were diluted in DMSO to obtain 10 mM stock and conditioned at -20 ° C for the future use. As showed in figure 5, ZR2002 and JS84 are “combi-molecules” with a single alkylating group and JS61 has two alkylating groups. Gefitinib (anti-EGFR) and chlorambucil (alkylating agent, chemistry structurally control to combi-molecules) (Selleck Chemicals) were diluted in DMSO to obtain stock at the concentration of 10 mM and conditioned at -20 ° C The monoclonal antibody cetuximab (Merck), used in this work was obtained from industrially diluted 5 mg / mL suspension and conditioned at 4 ° C.

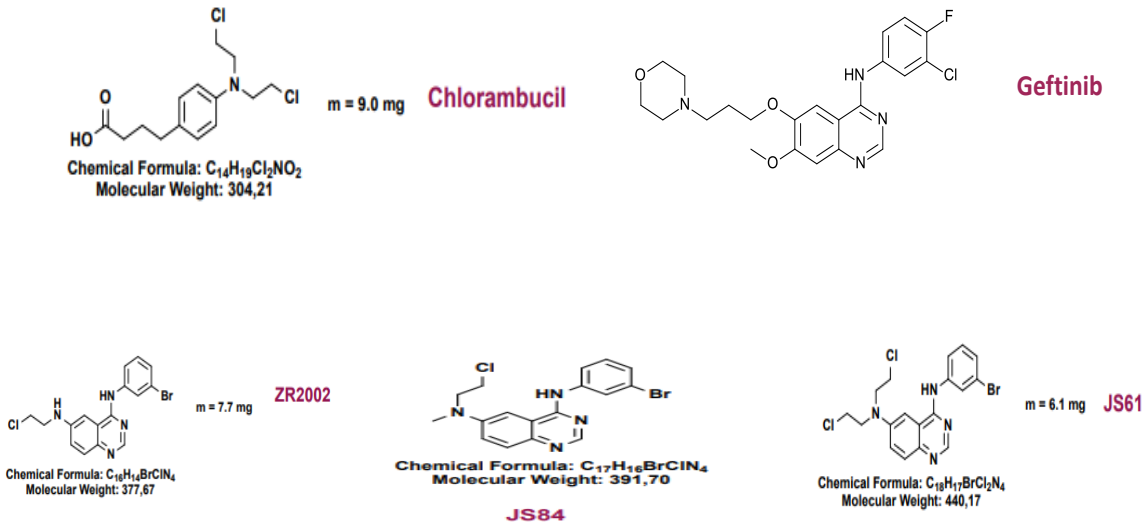

Figure 5- Chemical structure of JS61, JS84 and ZR2002, Chlorambucil and Gefitinib.

3.4. DNA and RNA isolation

Fadu Parental (Fadu P) and Fadu Resistant (Fadu R) cells were cultured in DMEM medium supplemented with 10% fetal bovine serum and 1% penicillin/streptomycin, kept in an incubator of CO_2 at 37 ° C until complete third passage. At about 90% confluence the cells were disaggregated with trypsin and the obtained pellet washed with DPBS.

The genomic DNA of the cells was obtained using the Biopur Mini spin plus kit (biometrix) and the RNA was isolated using the RecoverAll total nucleic acid isolation (Ambion) kit. Genetic material quantifications were performed using the Qubit platform (Thermo Fisher).

3.5. Nanostring

The nCounter® technology (NanoString Technologies, Seattle, WI) enables precise, digital quantification of up to 800 nucleic acid targets in a single reaction. This technology has delivered high-quality data for gene expression, miRNA and copy number alterations (CNA) analysis of all types of samples, including the high degraded ones (e.g., FFPE) without the need of DNA or RNA amplification. Each nCounter probe pair is identified by the "color code" generated by six ordered fluorescent spots present on the Reporter Probe[76]. The Capture Probe carries biotin molecules for immobilization on a streptavidin surface over the cartridge. The complexes comprised of Reporter and Capture Probes and the targets are placed on the surface of the cartridge and are then counted and tabulated.

3.5.1 Copy Number Alterations (CNA)

The nCounter® v2 Cancer CN Assay was developed to quantify in a single multiplexed reaction 87 CNAs known to be associated with cancer including *KRAS, PIK3CA, AKT, PTEN, BRCA, ERBB2, ERBB1,* and *MYC*. This assay accurately quantifies genes that are amplified to dozens or even hundreds of copies. The DNA input used for the assay was 600ng for both cell lines (resistance and parental). Firstly, the DNA double strands were submitted to the fragmentation by AluI enzymatic digestion followed by a denaturation step, which yielded single-stranded templates for hybridization with nCounter® probes comprised of a Reporter Probe, which carries the

signal, and a Capture Probe, which allows the immobilization of the targets over the cartridge for data capture. After the hybridization step, samples were transferred to the nCounter® Prep Station, which is an automated platform, for removal of probes excess and for probe/target complexes alignment and immobilization over the nCounter® cartridge. Then, cartridges were placed in the nCounter® Digital Analyzer for data capture. Raw data was captured by the *nSolverAnalysis Software* v4.0® (NanoString Technologies) and normalized by the average of 54 probes targeting invariant regions (invariant controls). For final data estimation, CN was estimated as twice ratio of the average probe count per gene in the resistant cell line compared with the parental cell line as previously described[77].

3.5.2 miRNAs expression profiling

The nCounter® Human v3 miRNA Expression Assay was developed to efficiently quantify in a single multiplexed assay 800 highly curated human miRNAs. This assay provides a highly sensitive and reproducible method for detecting specific miRNAs covering 100% coverage of the miRBase high confidence and published clinical miRNAs[78]. Control RNA were also included in the assay to monitor ligation efficiency and specificity through each step of the reaction. Firstly, miRNAs were specifically ligated to unique tags (miRtags) onto the 3' end of target miRNAs so that short RNA targets can be detected by nCounter probes followed by an enzymatic purification to remove non-ligated tags, thus this approach specifically captures all mature miRNAs. Lastly, ligated samples were denaturated for downstream detection via hybridization with the nCounter® CodeSet as described above. Raw data was captured by the *nSolverAnalysis Software* v4.0® (NanoString Technologies) and normalized by NanoStringNorm package using geometric mean of positive controls plus genes with low coefficient of variation (housekeeping candidates). Subsequently, the normalized data was submitted to differential expression analysis, which was conducted as following: filter by missing miRNAs (all miRNA presenting low counts were removed), filter by upper/lower fold change (all miRNA presenting fold change between -3.99 and +3.99 were removed) and finally filter by statistically significant expression considering p value lower than 0.05 (all miRNA presenting no statistically significant expression were removed) All analyses for differential expression were conducted in Galaxy

platform . Next, to determine the association between miRNA targets and Head and Neck neoplasm involvement, we used the plugin Reactome FI on Cytoscape (Version 3.6.0, Seattle, WA, USA). We focused on tumor suppressor genes and oncogenes in human cancers according to described in the Catalogue of Somatic Mutations in Cancer (COSMIC) database (https:// cancer.sanger.ac.uk/cosmic). Molecular pathway enrichment was performed with a false discovery rate-corrected (FDR-corrected) p value <0.001. The interaction network was performed by Cytoscape[79].

3.5.3 mRNA NanoString™ analysis

Gene expression analysis on FaDu Parental and FaDu resistant were performed using the NanoString nCounter PanCancer Pathways panel (730 gene transcripts) according to the manufacturers' standard (NanoString Technologies, Seattle, WA), which assess thirteen canonical pathways analyzed (Notch, Wnt, Hedgehog, Chromatin modification, Transcriptional Regulation, DNA Damage Control, TGF-beta, MAPK, STAT, PI3K, RAS, Cell Cycle and Apoptosis). Briefly, 100 ng aliquots of RNA were hybridized with probe pools, hybridization buffer, and TagSet reagents in a total volume of 30 µL and incubated at 65°C for 20h. After codeset hybridization overnight, the samples were washed and immobilized to a cartridge using the Nanostring nCounter Prep Station (NanoString Technologies, Seattle, WA) for 4 hours. Finally, the cartridges containing immobilized and aligned reporter complexes were scanned in the nCounter Digital Analyzer (NanoString Technologies), and image data were subsequently generated using the high-resolution setting. Quality control assessment and normalization of raw NanoString gene expression counts were performed with nSolver Analysis Software version 2.5 and the default settings (NanoString Technologies, Seattle, WA). The normalized log2 mRNA expression values were used for subsequent data analysis. Genes with log2 fold change (Log2FC) ≥ ±2 and p<0.001 were considered significant. The functional analysis was done using STRING software.

3.6. DNA isolation and Whole exome sequencing (WES) analysis

The DNA from FaDu Parental and FaDu Resistant were used for WES, with input of 50 ng on the Illumina HiSeq2500 ™ System by a commercial company (Sophia

Genetics, São Paulo, Brazil). Sequence reads were aligned to the human reference genome build 37 (hs37d5-decoy) using BWA-MEM with Burrows–Wheeler Aligner version 0.7.10-789[80]. Duplicate reads were marked with Picard-Tools 1.92 (http://broadinstitute.github.io/picard/). MuTect version 1.1.4; (http://www.broadinstitute.org/cancer/cga/mutect) and Varscan2[81] were used to call somatic SNVs and indels in parental cell line, respectively. MuTect was run using default parameters with files from COSMIC version 54 and dbSNP version 132 included as input[82, 83]. We used Ensembl Variant Effect Predictor (VEP)[84] to annotate and determine functional consequences of tumor specific variants. The results from SIFT, Polyphen-2, ClinVar were considered. It was also excluded variants that were likely to be germline, i.e., listed in ESP6500 (http://evs.gs.washington.edu/EVS/), 1000 Genome or ExAC[85, 86] . The candidate mutations were validated visually using the Integrated Genomics Viewer (IGV)[87]. Copy number abnormalities (CNA) were identifed using Nexus Copy Number version 9.0 (BioDiscovery; El Segundo, CA; https://www.biodiscovery.com/products/ Nexus-Copy-Number) with default parameter for BAM ngCGH (matched) input with homozygous frequency threshold and value at 0.97 and 0.8 respectively, hemizygous loss threshold at −0.18, single copy gain at 0.18 and high copy gain at 0.6. Mutational signature was defined using the package Somatic Signatures of Bioconductor Software, as described by Gehring *et al.*[88]

3.7 Chromosome preparation and C-banding

The karyotyping analysis was performed as described previously[89]. Fadu Parental and FaDu Resistant were incubated with 120 ng/ml colcemid (Life Technologies-Gibco) for 125 min. The cells were harvested by treatment with 0.025% trypsin EDTA, suspended in KCl 0.075 M solution at room temperature for 5 minutes, and fixed with methanol/acetic acid (3:1) five times. To examine the chromosomal distribution of constitutive heterochromatin, C-banding was performed using the standard barium hydroxide/saline/Giemsa method[90]. At least 20 metaphase spreads/cell line were observed to examine the ploidy level, and ten metaphase spreads/cell lines determined chromosome alteration in both structure and number.

3.8 Expression Microarray

Fadu cells expression profiles were analyzed by microarray slides Gene Expression Microarray, 4 × 44K (Agilent Technologies, Santa Clara, CA, USA) in dual-color methodology (Cy3 and Cy5), following the manufacturer's recommendations. 500 ng of total RNA with the addition of control RNA (spike in), were carried out to reverse transcription with the aid of the enzyme MMLV-RT (Maloney Murine Leukemia Virus-Reverse Transcriptase). Subsequently, nucleotides marked with the fluorochromes cyanine 3 (Cy3) were added to the T7 polymerase enzyme to the parental Fadu cells cDNA, called in this control approach, and cyanine 5 (Cy5) to the resistant cells cDNA, called in this clone approach. The respective cDNAs were purified with commercial columns, and then hybridized on the slides for 17 hours at a constant temperature of 65 ° C in a hybridization oven (Agilent Tecnologies). Finally, the hybridized slides were washed in Wash Buffer 1 and Wash Buffer 2 buffers, according to the manufacturer's. The slides were scanned at 550 nM (green spectrum - Cy3) and 640 nM (red spectrum - Cy5) on the Agilent Scanner Surescan (Agilent Technologies). Data extraction and quality control was performed using the Feature extraction software, version 10.7 (Agilent Tecnologies). Oligonucleotides were identified by the customized protocol GE2_107_Sep09. After quantification, the raw data means (gMeanSignal) were selected, in addition to the background means (gBGMeanSignal) used for future analyzes. The expression data were analyzed in an R environment, version 2.11.0. For the inclusion of data, identification of flags and generation of expression matrices, the limArray package was used to remove positive and negative controls, values that overlapped the background, and data conversion on a logarithmic scale. Then, the data were normalized by the quantile methodology. The category that presented at least 3 genes and a classification $p \leq 0.05$ was considered significant, after Benjamini-Hochberg correction.

3.9 Sanger Sequencing

The analysis of ROS1 mutation (c.6341A>G) was performed by PCR followed by direct Sanger sequencing, as described previously [91]. Briefly, using specific pairs of primers (Supplementary Table S1), the target regions were amplified by PCR using a Veriti PCR thermal cycler (Applied Biosystems, Foster City, CA). We used an initial

denaturation at 95°C for 1 minute followed by 35 cycles of 95°C denaturation for 30 seconds; specific annealing temperature was for 30 seconds and the 72°C elongation phase for 30 seconds followed by a 72°C final elongation for 2 minutes. Amplification of PCR products was confirmed by gel electrophoresis. Sequencing PCR was performed using a BigDye Terminator v3.1 Cycle Sequencing Kit (Applied Biosystems) and a 3500xL Genetic Analyzer (Applied Biosystems). Confirmation of all mutations was performed by repeating the PCR and sequencing the altered regions.

3.10. Evaluation of the impact of cetuximab acquired resistance on tumoral phenotype of head and neck cells and evaluation of antineoplastic activity of "combi-molecules" in head and neck and colorectal cancer cell lines.

3.10.1. Cell viability

For the viability assay, 5 x 10^3 were seeded in cells-well-plate in triplicate and incubated for adherence in DMEM medium supplemented with 10% fetal bovine serum (FBS) overnight in a $C0_2$ incubator. After incubation, cells were treated with the compounds diluted in culture medium (0.5% FBS). After 72 hours, cell viability was quantified using the commercial Cell Titer 96 Aqueous One Solution Cell Proliferation Assay kit (Promega - code G3581, which is based on the conjugation of MTS ([3- (4,5-dimethylthiazol-2-yl) -5- (3-carboxymethoxyphenyl) -2- (4-sulfophenyl) -2H-tetrazolium dichloride) with a PES electron coupling reagent (phenazin ethosulfate). Samples were measured in the ELISA reader (Varioskan Flash-Thermo scientific), at the wavelength of 490 nm, after 4 hours of incubation. The results were expressed as a percentage of the mean number of viable cells in the treatments compared to the control (considered as 100% viability). The IC_{50} was calculated by non-linear regression analysis using the software GraphPad Prism 7.

3.10.2. Morphological data

The images of cell morphology at baseline and after acquiring cetuximab resistance were obtained with the Olympus XT01 microscope, in the 100x magnification.

3.10.3. Immunofluorescence analysis

Epidermal Growth factor receptor (EGFR) and mammalian target of rapamycin (mTOR) were stained as described[92]. Briefly, $2.5x10^4$ cells were seeded in 12-well-plate in DMEM-10%. The next day, cells were washed in PBS and permeabilized with 0.3% Triton X-100 for 10 mins. Cells were incubated with the primary antibodies, goat anti-EGFR (1:1000, Dako) and Rabbit anti-mTOR (1:200, cell signalling) for 24 hrs at 4°C. After the wash step, cells were incubated for 1 hour at room temperature with Alexa560 labeled anti-goat secondary antibodies (1:400, Invitrogen). Sections were then stained with Hoechst (Thermo Scientific) and washed with PBS three times. Cells were analyzed using a fluorescence microscopy (InCell analyzer, GE) in the 40x magnification.

3.10.4. Apoptosis – Flow cytometry

For apoptotic analysis, $2x10^5$ cells were seeded into 6-well plates. After reaching about 80% confluence, cells were treated with fixed doses of the compounds for 24 hours at 37°C. After the incubation period, apoptotic cells were analyzed by flow cytometry with the commercial PE Annexin V Apoptosis Detection Kit (BD Pharmingen, code 559763).

3.10.5. Cell surface markers screening

The cell surface markers were analyzed as previously described[93]. BD Lyoplate Human Cell Surface Marker Screening Panel was utilized (cat. 560747; BD Biosciences, Franklin Lakes, NJ) containing 242 purified monoclonal antibodies and corresponding isotype controls following the manufacturer's instructions. Briefly, $5x10^3$ cells were seeded in a 96-well-plate in fluorescence-activated cell sorting (FACS) buffer containing 10 mg/mL DNAse. Primary antibody incubation was carried out in 100 mL volume for 30 min on ice followed by 2 washes in FACS buffer washes. Next, cells were incubated

with biotinylated secondary antibodies (goat anti-mouse 1:200, goat anti-rat 1:200). Tertiary incubation with Alexa Fluor 647 Streptavidin (1:4000) was carried out in 100 mL volume for 30 min in ice. DAPI was used as the viability dye. Analysis was performed using BD ACCURI flow cytometer.

3.10.6. Adhesion assay

Cell adhesion of FaDu Parental and FaDu resistant cell lines was evaluated as described previously[94]. Briefly, wells in a 96-well plate were coated for 24 h with PBS/ BSA solution (bovine serum albumin, 10 µg/ml, Sigma-Aldrich), Matrigel®. Matrigel® was diluted to 1:10 in PBS. The next day, excess liquids were removed, and culture plates were incubated with 100 µl/well of 0.1 % BSA for 2 h and washed with PBS. $6x10^3$ cells of FaDu P and FaDu R cells were added to each well were added to each well in serum-free medium and incubated at 37 °C in a 5 % CO_2 humidified atmosphere for 2 h. Non-adherent cells were rinsed off, and the remaining cells were fixed with 10 % trichloroacetic acid (TCA), stained with crystal violet and quantified using an ELISA reader at 540 nm.

3.10.7. Migration -Wound Healing

For wound healing assay, $2x10^5$ cells were seeded in 6-well plates and cultured in 10% SFB culture medium until reaching confluence of 95%. The cell monolayer was washed with DPBS and a wound was made with a 200 µl plastic pipette. Cells was treated or not with fixed doses of the compounds. Images were obtained using the Olympus IX71 microscope. The relative migration distances were analyzed using Image J Software. The relative migration distance was calculated by the following formula as previously described[95]: percentage of wound closure (%) = (A–B), where A is the width of cell wounds before incubation (0H), and B is the width of cell wounds after incubation and them normalized by the control. Results are expressed as the mean ± SD. The assay was done in triplicate at least three time

3.10.8. Anchorage-dependent Colony formation assay

FaDu Parental and FaDu resistant were seeded at a density of $5x10^3$ and $1x10^4$ cells/well in six-well plates and then grown in a culture medium for 8-10 days at 37°C. After the incubation period, the colonies formed were fixed in formaldehyde and

stained with 0.005% violet crystal. The colonies formed were photographed under a 40x magnification microscope. Colonies were photographed under the light microscope Eclipse 2200 (Nikon) and the number of colonies was analyzed by open CFU (Plos One- http://opencfu.sourceforge.net/) [96]. In all experiments the results represent the mean of at least three independent experiments.

3.10.9 Real time PCR

Quantitative PCR was performed for specific genes linked to epithelium-mesenchymal transition, migration and invasion (Table 2) using the GoTaq® DNA Polymerase system (Promega) according to the manufacturer's instructions. Real-time PCR was performed using a Step One Plus instrument (Life Technologies, Carlsbad, CA, USA). PCR conditions were 95 ° C for 2 minutes to activate DNA polymerase, followed by 40 cycles at 94 ° C for 15 seconds and 40 cycles at the annealing temperature of each primer (Table 2). The difference in cycle threshold value (Ct) of parental versus internal control ($^{\Delta}$Ct) was used to determine gene expression in the resistant cell line.

Table 2-Genes analyzed by real time PCR and Sanger sequencing

	Gene	Primer Foward (5' - 3')	Primer Reverse (5' - 3')	Size (pb)	Annealing temperature °C
Genes EMT/Migration/Invasion	*β-actin*	GGACTTCGAGCAAGAGATGG	AGCACTGTGTTGGCGTACAG	234	63
	Plakoglobin	AAGGTGCTATCCGTGTGTCC	GTTGTTGCATGTCAGGTTGG	261	63
	Snail	CTCTAGGCCCTGGCTGCTAC	TGACATCTGAGTGGGTCTGG	134	63
	Slug	CTTTTTCTTGCCCTCACTGC	ACAGCAGCCAGATTCCTCAT	161	63
	E-cadherin	TGCCCAGAAAATGAAAAAGG	GTGTATGTGGCAATGCGTTC	200	61
	N-cadherin	ACAGTGGCCACCTACAAAGG	TGATCCCTCAGGAACTGTCC	392	64
	Vimentin	GGGACCTCTACGAGGAGGAG	AAGATTGCAGGGTGTTTTCG	177	63
	Fibronectin	TCGAGGAGGAAATTCCAATG	CTCTTCATGACGCTTGTGGA	382	61
	Nanog	ATACCTCAGCCTCCAGCAGA	CTGGGGTAGGTAGGTGCTGA	174	59
	ITGA11a	ATCTCGCAGTCAGCAAACCT	AAGAGGACGTCAGCCTCGTA	305	61
	MMP2	CAGGGAATGAGTACTGGGTCTATT	ACTCCAGTTAAAGGCAGCATCTAC	119	59
	MMP9	GCACGACGTCTTCCAGTACC	CAGGATGTCATAGGTCACGTAGC	124	59
	MMP 14	CACTGCCTACGAGAGGAAGG	TCCCTTCCCAGACTTTGATG	269	63
	MMP 24	TGAAGGCATTGACACAGCTC	CGCTCAGTTTCTGGTTGTCA	242	63
ROS 1- Validation	*ROS 1*	AGCATTACTCTGTGTCCCGT	AGGGATCTGGCAGCTAGAAA	232	59

3.10.10 Western Blot, Human RTK and Cytokines Arrays

To assess the effect of cetuximab resistance in the intracellular signaling pathways and RTKs, the cells were cultured in DMEM-10% FBS in T25 culture flasks, grown to 85% of confluence and then serum-starved for 2 hours. The cells were washed and scraped in cold PBS and lysed in buffer containing 50 mM Tris (pH 7.6–8), 150 mM NaCl, 5 mM EDTA, 1 mM Na_3VO_4, 10 mM NaF, 10 mM sodium pyrophosphate, 1% NP-40, and 1/7 of protease cocktail inhibitors (Roche, Amadora, Portugal). Western blot analysis was done using a standard 10% sodium dodecyl sulfate-polyacrylamide gel electrophoresis, loading 20 µg of protein per lane. All the antibodies were used as recommended by the manufacturer. The conditions used for each antibody are described in table 3. Concerning the RTK phosphorylation assessment, a proteome human RTK Phosphorylation Antibody Array (ab193662; Abcam, Cambridge) and Human XL Cytokine Array Kit (ARY022; R&D systems, Minneapolis,USA) was used according to the manufacturer's instructions. A total of 500 µg of fresh protein lysates was briefly incubated overnight at 4°C with nitrocellulose membranes dotted with duplicated spots for 71 anti-RTK, 102 anti-Cytokines and control antibodies. Bound phospho-RTKs and cytokines were incubated with a pan anti-phosphotyrosine-HRP antibody for 2 hours at room temperature. Blot detection was done by chemiluminescence (ECL Western Blotting Detection Reagents, RPN2109; GE Healthcare, Piscataway, NJ) in ImageQuant LAS 4000 mini (GE Healthcare) or using X100 Hyperfilm ECL (Amersham, GE Healthcare).

Table 3- Antibody conditions utilized in western blot analysis.

Antibody	Dilution	Condition	Manufacturer / Code
Anti - β actin	1/1000	4ºC- Overnight	Cell signaling/ #4967
Anti- EGFR	1/1000	4ºC- Overnight	Cell signaling/ #4267
Anti- phospho-EGFR	1/1000	4ºC- Overnight	Cell signaling/ #2234
Anti- phospho- AKT	1/1000	4ºC- Overnight	Cell signaling/ #9271
Anti- AKT (total)	1/1000	4ºC- Overnight	Cell signaling/ #9272
Anti- phospho- p44/42 MAPK	1/1000	4ºC- Overnight	Cell signaling/ #9101
Anti- p44/42 MAPK (total)	1/1000	4ºC- Overnight	Cell signaling/ #9102

Anti-mTOR	1/1000	4ºC- Overnight	Cell signaling/ #2983
Anti-Laminin B1	1/1000	4ºC- Overnight	Cell signaling/ #13435
Anti-FADD	1/1000	4ºC- Overnight	Cell signaling/ #2782
Anti-CD44	1/1000	4ºC- Overnight	Cell signaling/ #37259
Anti-E-cadherin	1/1000	4ºC- Overnight	Cell signaling/ #3195
Anti-N-cadherin	1/1000	4ºC- Overnight	Cell signaling/ #13116
Anti- α-Smooth Muscle	1/1000	4ºC- Overnight	Cell signaling/ #19245
Anti-SLUG	1/1000	4ºC- Overnight	Cell signaling/# 9585
Anti-SNAIL	1/1000	4ºC- Overnight	Cell signaling/ #3879
Anti- TGF-β	1/1000	4ºC- Overnight	Cell signaling/#3711
Anti-mouse IgG HPR	1/5000	TA- 1 hour	Cell signaling/ #7076
Anti-rabbit IgG HPR	1/5000	TA- 1 hour	Cell signaling/ #7074

3.10.11 Transwell chamber assay

Cell migration was assessed with a Transwell assay. Cells were collected and suspended at a density of 3×10^5 cells in 500µL of serum-free medium and the IC_{50} value of each compound and seeded in the upper compartment of the chamber. 700µL of complete medium containing 10% FBS was added into the lower chamber. After incubation for another 24h, the chambers were removed and the cells on the upper surface of membrane were wiped off with cotton swabs. Then, the cells that had migrated into the microporous membrane were washed three times with PBS, fixed with methanol for 15min, and stained with Hematoxylin and Eosin for 5 min. Finally, images were obtained using 10x magnification microscope Eclipse 2220 (Nikon) and the cells were counted in all the fields of the membrane. The results are expressed in relation to the DMSO control (considered as 100% of migration) as the mean percentage of invasion ± SD.

3.10.12 Statistical Analysis

For the simple comparisons between the different conditions studied, the student's T test was used, and the differences between the groups were tested using the One-way ANOVA followed by the Bonferroni test. All statistical analyzes were

performed using GraphPadPrism software version 7. The level of significance established for the analyzes was considered 5%.

4. RESULTS

4.1 Cetuximab resistance model establishment and identification of biomarkers associated with acquired resistance in head and neck cells.

The results present in this section correspond to specific objective 2.2.1 and 2.2.2.

4.1.1 Cetuximab-resistance model establishment and characterization.

As previously reported, a cetuximab-resistant in vitro model was previously established by our group [74]. The HNSCC cetuximab-resistant in vitro model was established with the exposure of FaDu cells with increasing cetuximab doses for 72 hours after which time medium was removed, and cells were allowed to recover and re-populate in complete medium. This cetuximab exposition process was done in a period of at least eight months, leading to the establishment of six resistant clones. All resistant clones exhibited at least a 2-fold higher IC_{50} ranging from 400 µg/mL to 9350 µg/mL (Figure 1A) and EGFR pathway inhibition with a loss of EGFR phosphorylation comparing to parental cells (Figure 1B). The optical microscopy revealed a marked alteration of cellular morphology in cetuximab-resistant cells, with parental cells maintained epithelial morphology, whereas FaDu resistant cells exhibited spindle shape and scattering profile, suggesting loose cell-cell interaction (Figure 1C).

In the present thesis, we select the resistant clone C5 to perform the next steps. The clone C5 was evaluated 24 months after cetuximab resistant establishment and exhibited a significant difference between FaDu parental proliferation (Figure 1D). The IC_{50} was 17-fold higher when compared with FaDu parental (216,9 µg/mL in FaDu parental against 3722 µg/mL in FaDu resistant). Moreover, this long time cetuximab-resistant cells demonstrated a decrease in EGFR phosphorylation (Figure 1E).

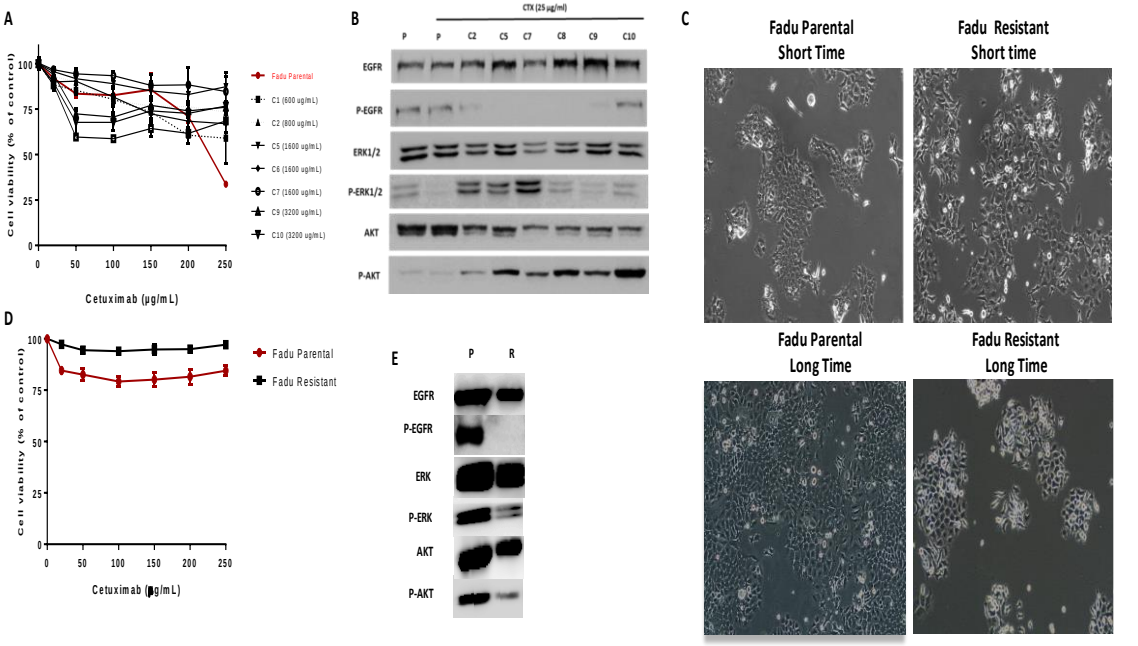

Figure 6-Cetuximab resistant model establishment and characterization. A) Cell viability assay after selection in a short time (8 months of increasing doses of cetuximab exposition), cell viability assay of parental and resistant clones upon cetuximab exposition. The dose in parentheses represents the concentration that the clone was selected B) EGFR signaling of parental and resistant clones in a short time of establishment. C) Morphological changes upon CTX exposition after 8 months of exposition. D) Cell viability assay of parental and C5 resistant clone upon cetuximab exposition, after selection in a long time (24 months after cetuximab resistant clones' establishment). E) Cell viability assay after long time of exposition that correspond to 8 months after cetuximab resistant model establishment F) Morphological changes upon CTX exposition after 24 months of exposition P: FaDu Parental; R: FaDu Resistant; C: Clone. Cetuximab (CTX).

4.1.2 Cetuximab resistance is associated with chromosomal abnormalities

To evaluate the molecular impact of cetuximab resistance, we performed a detailed genomic and transcriptomic profile comparison between parental and FaDu resistance cells. The karyotyping analysis of Fadu parental and Fadu resistant cell lines revealed severe aneuploidy, with 51-57 chromosomes figures, with 11 numerical alterations and several structural changes (Figure 7 A and B). The parental cells presented hyperdiploid and compound karyotype with 51 to 53 chromosome figures, with several aberrations such as trisomy of chromosomes 1, 2, 3, 6, 7, 8, 9, 10,11, 12, 16 and 17, monosomy of chromosomes 5, 13, 19, 20, 21 and 22, and tetrasomy of

chromosome 18. The resistant cells exhibited hyperdiploid and compound karyotype with many chromosomes ranging from 52 to 56, showing several alterations such as trisomy of X, 1, 2, 3, 6, 8, 11, 16, 17 and 18 chromosomes, monosomy of chromosomes 4, 5, 13, 14, 19, 20, 21 and 22, and tetrasomy of chromosomes 7, 9, 10 and 12.

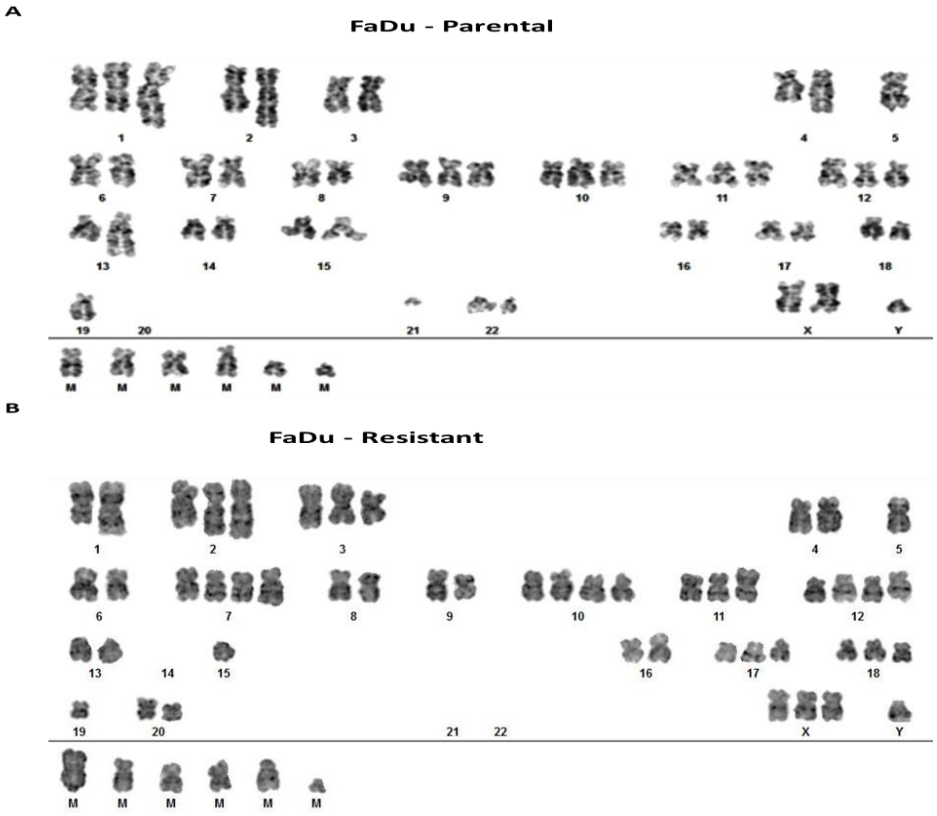

Figure 7-Chromosomal abnormalities in FaDu parental and FaDu resistant by karyotyping. A) FaDu parental numerical and structural changes. B) FaDu resistant numerical and structural changes**.**

The chromosomal changes or copy number aberrations (CNA) were also evaluated by whole exome sequencing (WES) and by the Copy Number Aberrations (CNA) Nanostring panel of 87 genes. The WES showed 31 chromosomal regions harboring a large number of genes with CNA (Figure 8 A). There were 15 amplified regions harboring genes such as *RHOA*, *KRAS, MYB, MAP3K5, BCL2L2* and *YAP1* (Table 4). These data corroborate the karyotyping analysis, where we also founded amplification of chromosome 7 and 12 containing the same amplified genes found in CNA analysis such as, *KRAS*, *MDM2*, *HMGA2*, *SHH*, *CCDND2* and *FRS2*. Deletions were

found in 15 regions, harboring genes such as *TP53, PTEN, WT1, BRCA1, MAP2K4,* and *NF1*. Many of the altered genes identified are related to MTOR-PI3K-AKT and MAPK proliferation signaling pathways. Other altered regions harbored genes mostly related to the DNA repair process, apoptosis, and transcriptional factors. All genes are reported as tumor driver by Cancer Genome Interpreter (CGI)[97] are shown in table 4.

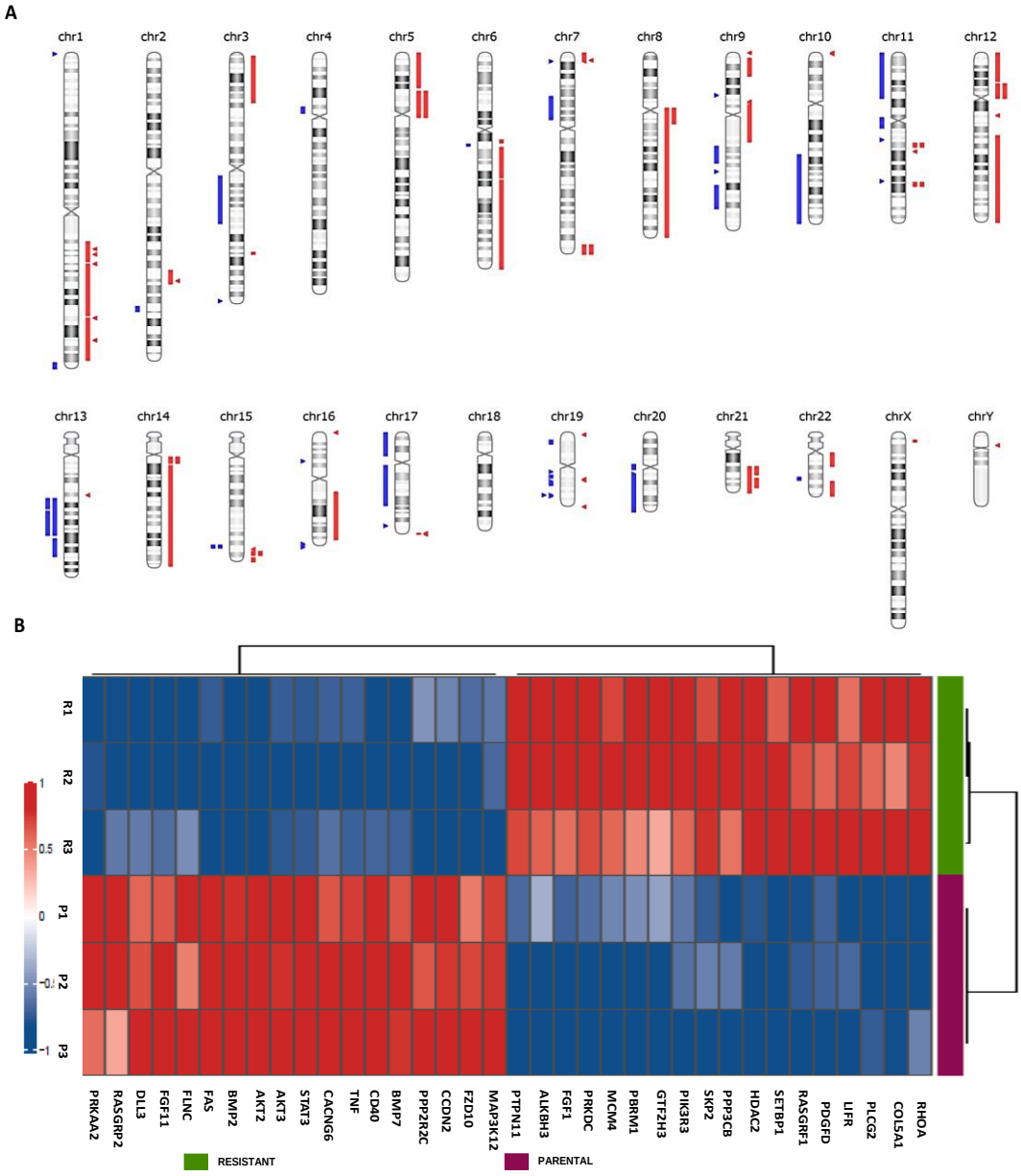

Figure 8- Molecular characterization after cetuximab-acquired resistance. A) Overview of the significant CNA'S founded in FaDu resistant cells in comparison with FaDu parental cells. In red are shown gains and in blue deletions. B) Heatmap of genes altered in FaDu parental and FaDu resistant cells. In red are represent the

overexpressed genes and in blue the downregulated genes. The p value considered for cut-off was $p<0.001$.

Table 4- Copy number alterations founded in FaDu Resistant compared with FaDu Parental cell line by whole exome analysis and nanostring validated as driver by CGI platform.

Chromosome Region	Event	Cytoband	Cancer Gene	Driver statement
chr 17	Deletion	p13.3 - p11.2	MAP2K4	known in: PA;BRCA;COREAD
chr 17	Deletion	p13.3 - p11.2	TP53	known in: BCL;THYM
chr 11	Deletion	p15.5 - p12	WT1	known in: WT;DSRCT
chr10	Deletion	q22.3 - q26.3	PTEN	known in: G;PRAD;ED;CM;TH;BRCA;L;OV;PA
chr 7	Deletion	p14.3 - p12.1	IKZF1	known in: ALL;DLBCL
chr 10	Deletion	q22.3 - q26.3	SUFU	known in: MB
chr 16	Deletion	q24.3	FANCA	known in: AML;LK;PRAD
chr 17	Deletion	p13.3 - p11.2	FLCN	known in: TH
chr 17	Deletion	q11.1 - q23.1	NF1	known in: NF;G;MPN;CM;PLEN;HNC;SG;LK
chr 17	Deletion	q11.1 - q23.1	SUZ12	known in: CANCER
chr 17	Deletion	q11.1 - q23.1	BRCA1	known in: OV;BRCA
chr 14	Amplification	q12 - q32.33	NKX2-1	known in: NSCLC
chr 1	Amplification	q32.1 - q32.2	MDM4	known in: GBM;BLCA;RB;S
chr 12	Amplification	q14.3 - q24.33	MDM2	known in: S;G;COREAD;LIP
chr 9	Amplification	p24.2 - p22.1	JAK2	known in: BRCA
chr 9	Amplification	p24.2 - p22.1	CD274	known in: BCC
chr 8	Amplification	q12.1 - q24.3	MYC	known in: BLY;CLL;NB;COREAD;MYMA;PRAD
chr 5	High Amplification	p13.3 - q11.2	RICTOR	known in: L
chr 6	Amplification	q16.2 - q27	ESR1	known in: UCEC;BRCA;OV
chr 12	Amplification	p13.33 - p12.1	CCND2	known in: L
chr 12	Amplification	q14.3 - q24.33	FRS2	known in: LIP
chr 14	Amplification	q12 - q32.33	FOXA1	known in: COREAD

PA: Pancreas; BRCA: Breast Adenocarcinoma; COREAD: Colorectal Adenocarcinoma; ; BCL: B cell Lymphoma; THYM: Thymic; WT: Wilms tumor; G: Glioma; TH: Thyroid DSRCT: Desmoplastic small round cell tumor; PRAD: Prostate Adenocarcinoma; ED: Endometrium; CM: Cutaneous melanoma; L: Lung; OV: Ovary; ALL: Acute Lymphoblastic Leukemia; DLBCL: Difuse Large B Cell Lymphoma; MB: Medulloblastoma; AML: Acute Myeloid Leukemia;LK: Leukemia; NF: Neurofibroma; MPN: Malignant Peripheral Nerve Sheat Tumor; PLEN: Plexiform Neurofibroma; HNC: Head and Neck; SG: Salivary Glands; NSCLC: Non-small Lung Cancer; BLCA: Bladder; GBM: Glioblastoma Multiforme; RB: Retinoblastoma; S: Sarcoma; LIP: Liposarcoma; BCC: Basal Cell Carcinoma; BLY: Burkitt Lymphoma; CLL: Chronic Lymphocytic Leukemia; NB: Neuroblastoma; MYMA: Myeloma; UCEC: Uterine Corpus Endometroid Carcinoma.

4.1.3 Differential gene expression and mutation profile

The differential transcriptomic profile of Fadu parental and resistant cells were evaluated using the NanoString PanCancer Pathways Panel. Of the 770 genes evaluated, 36 were differentially (p. adjusted <0.001; FC>±2) gene, being 18 upregulated (*RHOA, COL5A1, PLCG2, LIFR, PDGFD, RASGRF1, SETBP1, HDAC2, PPP3CB, SKP2, PIK3R3, GTF2H3, PBRM1, MCM4, PRKDC, FGF1, ALKBH3, PTPN11*) and 18 downregulated (*MAP3K12, FZD10, CCND2, PPP2R2C, BMP7, CD40, TNF, CACNG6, STAT3, AKT3, AKT2, BMP2, FAZ, FLNC, FGF11, DLL3, RASGRP2, PRKAA2*) (Figure 8B). In accordance with CNA results, we founded the differential expression of genes associated with the MAPK signaling, Ras signaling, mTOR-P3IK-AKT signaling (Figure 9). It was also performed an analysis of the functional connections among the proteins encoded by the 36 genes differently expressed by STRING software. In particular, FaDu resistant cells, 28 of 36 genes, had at least two connections (Figure 9). Notably, of these 28 genes, 9 demonstrated stronger connections centered around them (*PTPN11, RHOA, PLCG2, PPP2R2C, PP3CB, AKT2, AKT3, PIK3R3,* and *STAT3*). These findings suggest the involvement of MAPK signaling, Ras signaling, mTOR-PI3K-AKT signaling in cetuximab resistance.

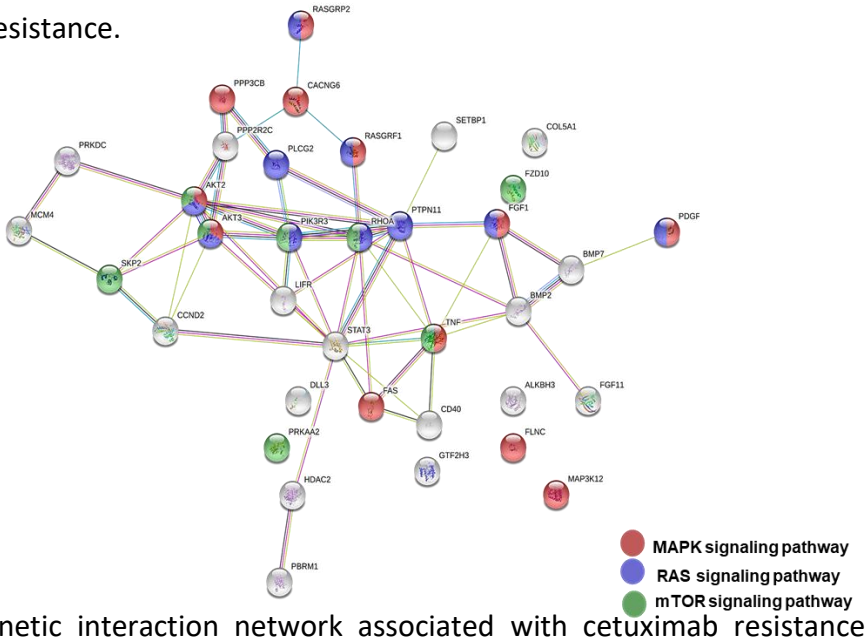

Figure 9-Genetic interaction network associated with cetuximab resistance on the String platform. In this figure, each circle represents a gene (node), and each connection represents a direct or indirect connection (edge). Line color indicates the type of interaction evidence, and line thickness indicates the strength of data support.

MAPK associated genes are show in red, RAS associated genes are show in blue and mTOR signaling related genes are show in yellow**.**

Furthermore, we performed the whole-exome sequencing in both parental and resistant FaDU cells and found 394 mutations present only in the resistant cells. Mutations with important biological significance are summarized in Table 5, and included genes *NOTCH1, EPHA2, TSC1, ALK*, and *ROS1*, which were previously described as tumor drivers[97].

Table 5- Somatic mutations present in FaDu Resistant compared with FaDu Parental cell line.

Chromosome	cDNA	Protein	Consequence	Gene	Driver status
chr 1	c.2492A>T	p.N831I	Missense	EPHA2	Tumor Driver
chr 2	c.2074G>T	p.G692W	Missense	ALK	Tumor Driver
chr 6	c.6341A>G	p.Y2114C	Missense	ROS1	Tumor Driver
chr 6	c.3391A>T	p.K1131*	Nonsense	ZNF292	Tumor Driver
chr 8	c.1648delT	p.S550Qfs*12	Frameshift	UBR5	Tumor Driver
chr 9	c.3127_3129delAGC	p.S1043delS	In Frame Deletion	TSC1	Tumor Driver
chr 9	c.740delC	p.P247Qfs*30	Frameshift	NOTCH1	Tumor Driver
chr 9	c.250_252delGAA	p.E84delE	In Frame Deletion	XPA	Tumor Driver
chr 13	c.3273dupG	p.K1092Efs*233	Frameshift	IRS2	Tumor Driver
chr 14	c.928delG	p.E310Kfs*68	Frameshift	ARID4A	Tumor Driver
chr 15	c.3416delG	p.G1139Efs*25	Frameshift	FANCI	Tumor Driver
chr 16	c.1183delC	p.H395Tfs*78	Frameshift	TRAF7	Tumor Driver
chr 17	c.1420_1422delCAT	p.H474delH	InFrameDeletion	AXIN2	Tumor Driver
chr 19	c.209A>T	p.N70I	Missense	ARHGAP35	Tumor Driver
chr 21	c.146delC	p.P49Qfs*4	Frameshift	RUNX1	Tumor Driver

ROS1 (c.6341A>G) demonstrated the higher variant allele frequency (VAF) (24%) in the resistant cells, and it was also further validated by Sanger sequencing (Figure 10).

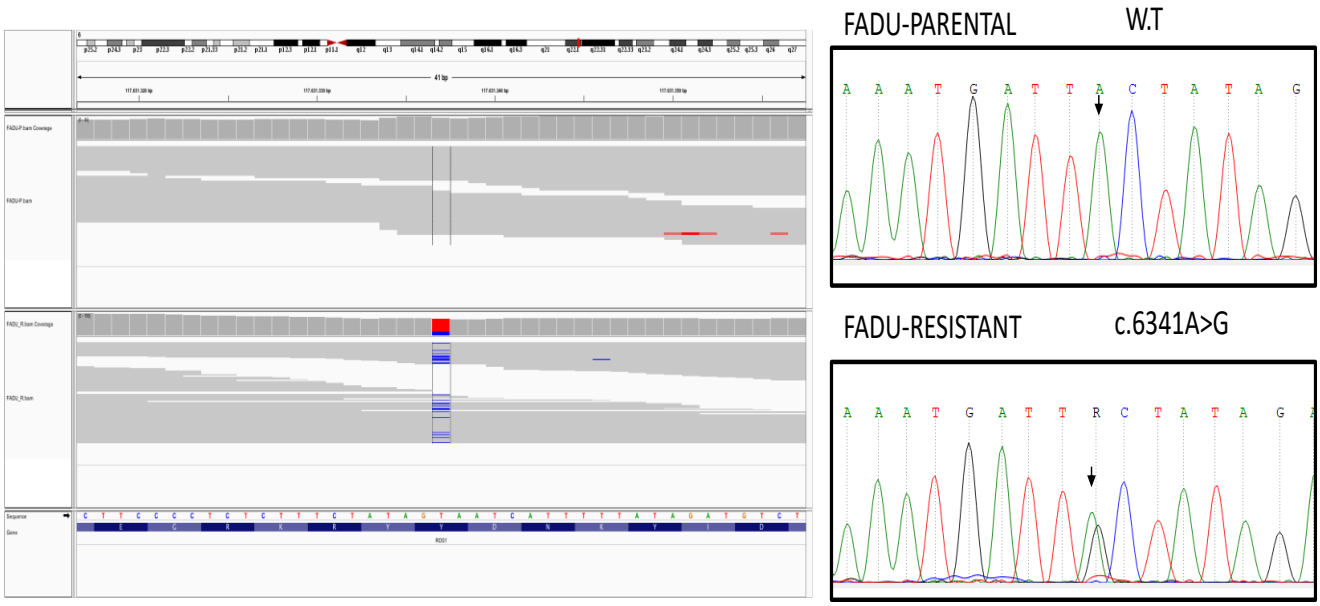

Figure 10-Sanger sequencing of ROS 1 C.6341A>G mutation in parental and resistant cells. The electropherogram depicts a ROS1 mutation C.6341A>G in the resistant cell line.

4.1.4 Overexpression of cell surface markers and cytokines may be associated with cetuximab resistant phenotype

Parental and resistant cells were analyzed by flow cytometry using lyoplate, an extensive screening panel of 242 human surface proteins. To control changes in surface marker expression, both cell lines were cultured for equal periods (21 days). We found 131 cell surface markers differentially expressed between parental and resistant cells. Among them, we found the overexpression of some mesenchymal stem cells markers (MSCs), like CD44 and other cell surface markers such as Intercellular cell adhesion molecule 1 (ICAM-1), endoglin (ENG) and programmed death-ligand 1 (PD-L1), lysosomal-associated membrane protein 1 (LAMP1) and lysosomal-associated membrane protein 2 (LAMP2) (FC>1.5; p<0.001; Figure 11A)(17, 18). To validate the lyoplate results, some cytokines were next assessed by the human cytokines array protein and corroborate the overexpression of some markers such as ICAM1, TFRC and ENG (Figure 11B and C).

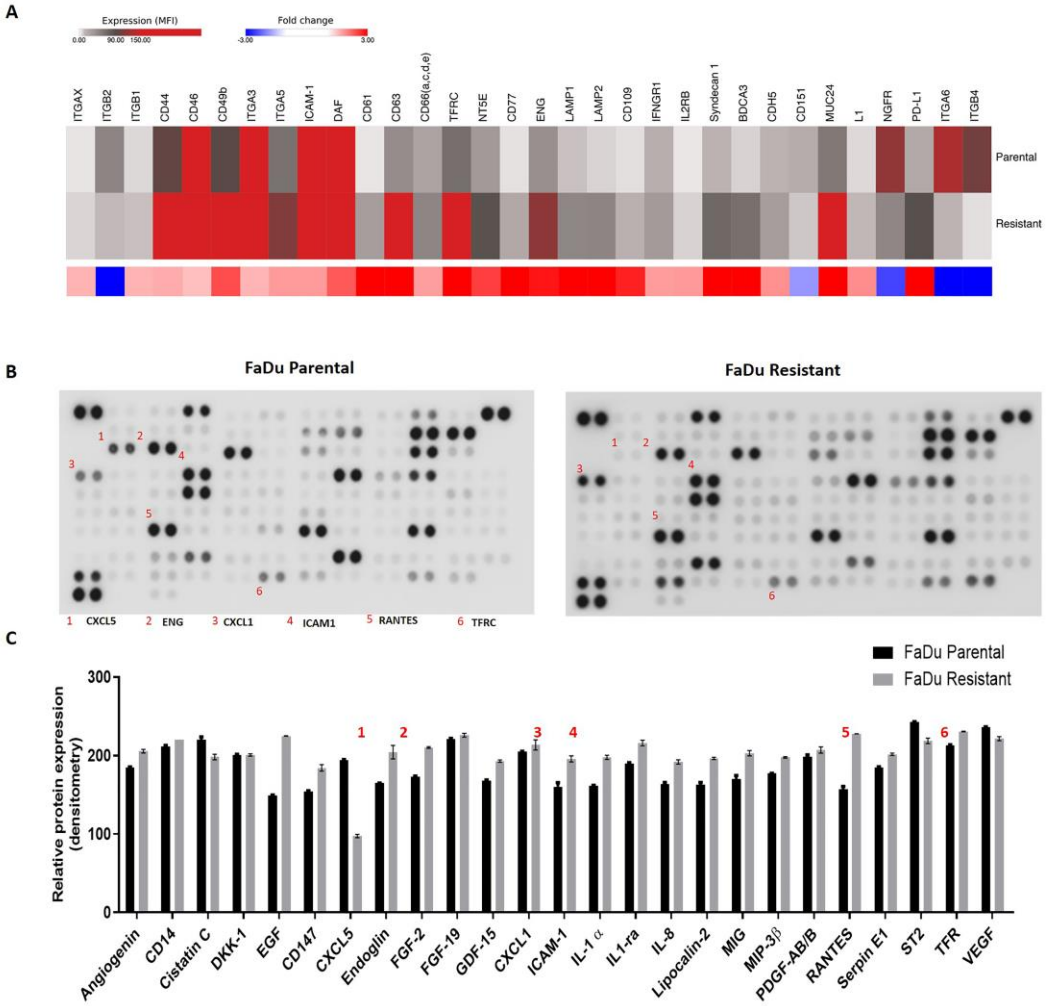

Figure 11-Cell surface markers and cytokines profile expression in FaDu parental and FaDu resistant cells. A) Heatmap of cell-surface markers expression in FaDu parental and FaDu resistant cells. In red are represent the overexpressed markers and in blue the downexpressed markers. Fold-change≥1,5. B) Representative images of Cytokines protein array in FaDu parental and FaDu resistant cells. C) Bars demonstrated the cytokines differential expression in FaDu cells**.**

4.1.5 EGFR nuclear translocation and overexpression of mTOR are associated with cetuximab resistant phenotype

We further evaluate whether cetuximab resistance is associated with EGFR nuclear translocation. The resistant cells showed loss of EGFR in the plasma membrane (membrane fraction – MF) and cytoplasm (cytoplasm fraction – CF) compared with the parental cell line (Figure 12A). The EGFR nuclear translocation in resistant cells was confirmed by immunofluorescence, where we observed the presence of EGFR in the perinuclear region in resistant cells instead of the plasma membrane as well was found in parental cells (Figure 12B). Moreover, since the mTOR expression had been

associated with cetuximab response and EGFR nuclear translocation[98-100] and considering that our results from the Nanostring we founded an enrichment of genes involved in mTOR signaling (Figure 9), we evaluated the mTOR expression in our resistant model. We observed an increase of mTOR-related genes and protein in FaDu resistant cells compared to parental cells (Figure 12A and 12D). The overexpression of mTOR was also confirmed by immunofluorescence (Figure 12C).

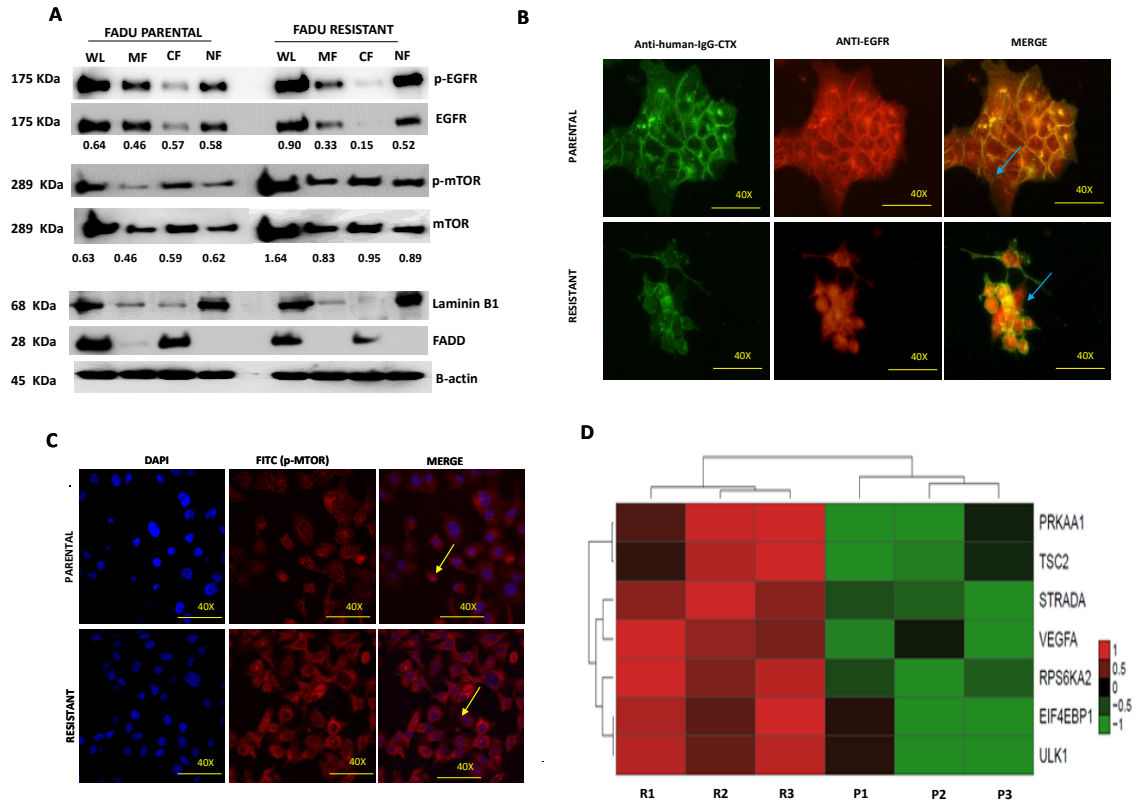

Figure 12-EGFR-FITC+ MTOR-FITC expression in FaDu parental and FaDu resistant cells. A) Subcellular protein fractionation assay for EGFR detection in parental and resistant cells. B) p-EGFR nuclear translocation in resistant cells by Immunofluorescence assay. C)p-mTOR immnunoflouorescence assay in resistant and parental cells D) mTOR-related genes by microarray of expression in green are show genes downregulated and in red genes upregulated. DAPI (Hoescht) staining in blue. p-EGFR-FITC+ p-mTOR-FITC+ and is expressed in parental and resistant cells. Arrows indicate EGFR-FITC+ and p-mTOR-FITC+ localization.

4.1.6 Cetuximab resistant cells display an increase of aggressiveness phenotype and differential expression of epithelial-mesenchymal transition markers (EMT)

Due to overexpression of genes involved in proliferation, migration, adhesion and invasion in FaDu resistant cell, we performed functional assays to evaluate phenotype changes caused by cetuximab resistance. First, we evaluated the migration, the wound-healing assay showed that resistant cells migrate in a higher rate than the parental cells independent of time, as assessed by wound-healing assay (Figure 13A and 13B). Moreover, resistant cells showed higher adhesion by protein-based assay comparing to parental cells (Figure 13C and 13D). The proliferation capacity of parental and resistant cells was assessed using the clonogenic assay. There was a significantly higher fraction of colonies of resistant cells relative to parental cells (Figure 13C and 13E). These results suggest the higher aggressive phenotype of cetuximab-resistant compared with parent cells.

Epithelial-mesenchymal transition (EMT) is a highly conserved cellular process, that involved acquire mesenchymal and stem cell signatures, usually involved in tumor progression, including metastasis, therapy resistance, and disease recurrence [101]. The stemness marker CD44 is increased during EMT and the increased levels of mTOR could modulate the EMT by TGF- β[102] . FaDu resistant cells demonstrated the change in morphology and an increase of aggressiveness phenotype as well as overexpression of CD44 and mTOR-related genes (Figure 11A and 9). We evaluated EMT markers in the established resistance model and the FaDu resistant cells demonstrated a decreased expression of N-cadherin (Figure 13F) and increased expression of slug, and TGF-β and CD44 (Figure 13F, H, I and J).

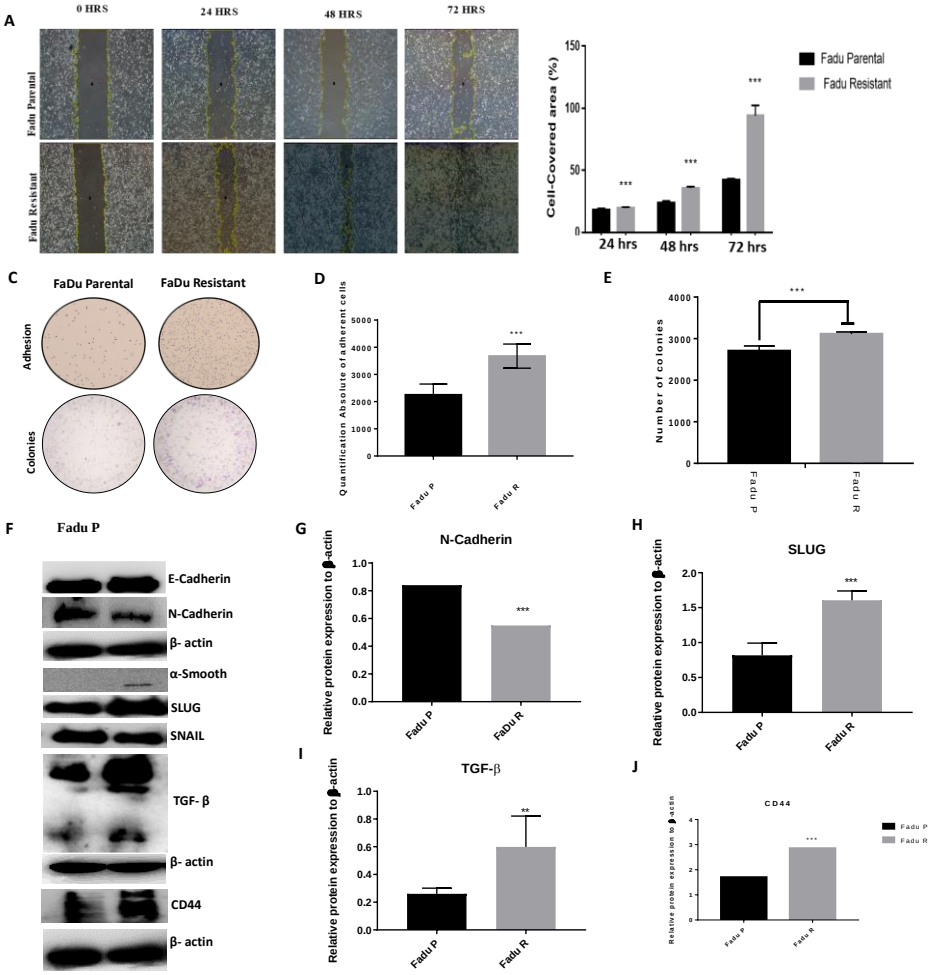

Figure 13-Malignant phenotype acquired after CTX resistance establishment and Epithelial-mesenchymal transition (EMT) markers expression in FaDu parental and FaDu resistant cells. A) Representative images of wound healing assay of FaDu Parental and FaDu Resistant cell lines in 24 h, 48h, and 72 h. B) Migration rates of FaDu Parental and FaDu resistant cells in a wound-healing assay. C) Representative images of Adhesion and Clonogenic assay for Parental and Resistant cells. D)Absolute quantification of adherent cells. E) Absolute number of colonies in Clonogenic cell assay for anchorage-dependent in parental and Resistant cells. F) Representative images of EMT proteins detected in western blot assay in parental and resistant cells. G) N-cadherin densitometry. H) Slug densitometry. I) TGF-β densitometry. J) CD44 densitometry.The yellow lines represent the distance between both edges of the wound; Scale bars, 200 µm. (.**p<0.05 ;***p<0.001).

To validate these findings, we also performed real-time PCR, corroborating with protein levels by western blot analysis (Figure 14). In accordance with our functional assays, we founded increased levels of *MMP14, MMP9,* and *ITGA11A*, whereas

NANOG, MMP2, MMP24, and plakoglobin were downregulated in resistance cells compared with parental cells that is involved with adhesion, invasion, and migration.

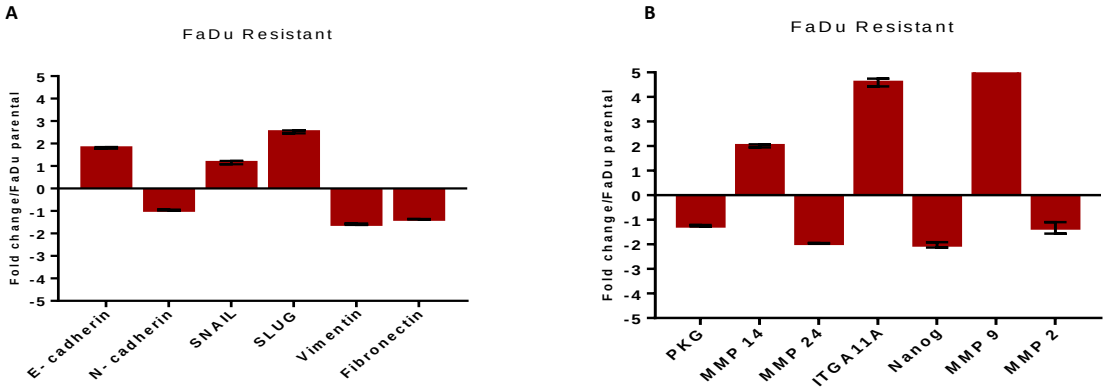

Figure 14- Expression of EMT markers, invasion and migration. A) Expression of EMT markers by PCR in real time. Data are presented in fold-change compared to parental FaDu. B) Expression of invasion and migration markers by RT-PCR. Data are presented in fold-change compared to parental FaDu.

4.1.7 The establishment of cetuximab resistance induces miRNA´s differential expression

In addition, we also analyzed the expression of microRNA´s between the cell lines. Using the Nanostring® platform, we analyzed about 800 miRNAs known to be involved in tumorigenesis. As shown in figure 15, we found 23 miRNAs differentially expressed between the parental and resistant cell lines, 13 miRNAs showed a overexpressed and 10 with reduced expression

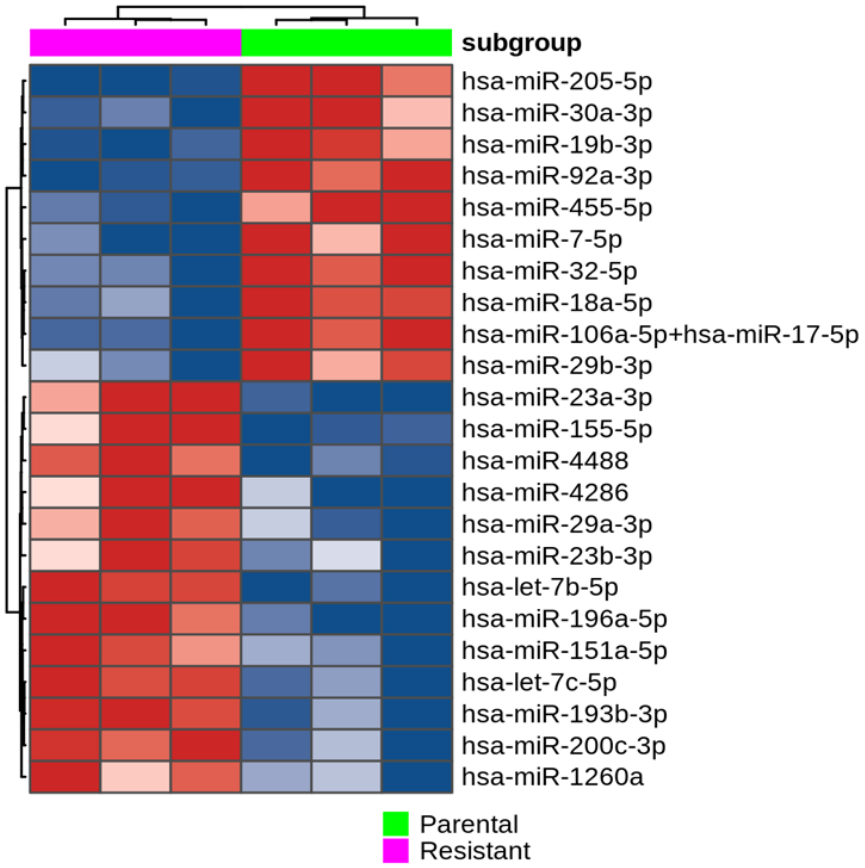

Figure 15- Matrix of expression of microRNAs between Fadu Parental and Fadu Resistant. The mirRNA upregulated are show in red and the mirRNA downregulated are show in blue. Green= resistant, Red: parental.

For this initial analysis, cell culture pellet was used for the extraction of genetic material. Thinking of mimicking the paraffined blocks with tumor tissue, the cell lines were processed and paraffined similar to the processing of the tumor tissue. The blocks containing the paraffin cells were cut and the RNA was extracted from the slides. The analysis of the microRNA´s profile revealed a different microRNA´S profile than that found in the cell pellet (non-paraffin processes) (Figure 16).

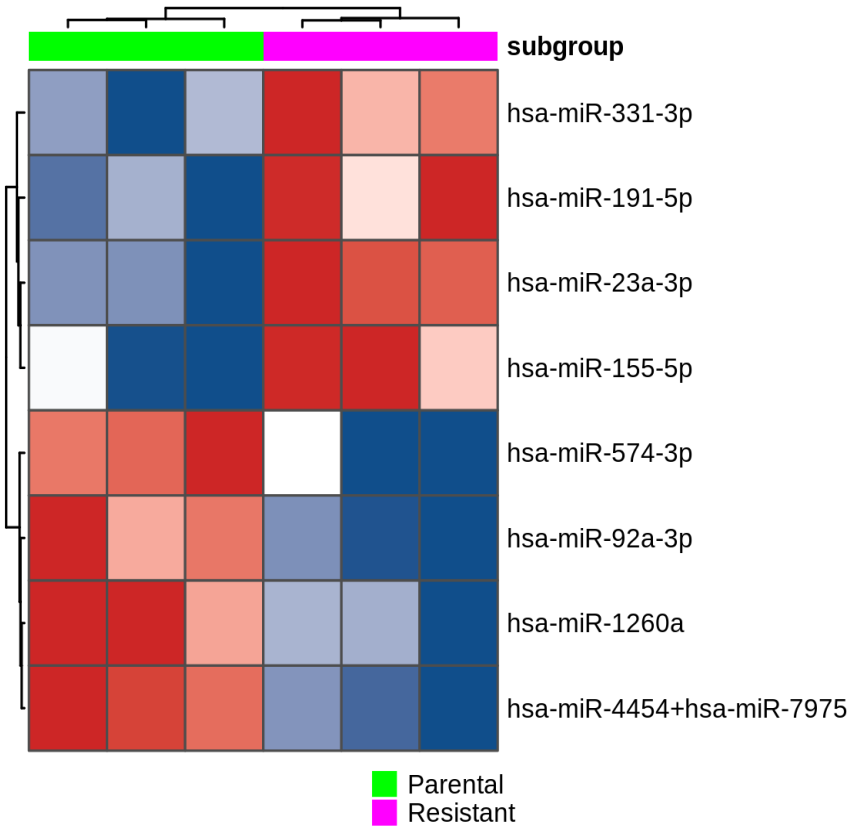

Figure 16-miRNA´s expression profile between the FaDu Parental and FaDu resistant cells. FaDu parental expression cluster is represented in green and the FaDu resistant in pink. Overexpressed miRNA´s are represented in red and the little expressed miRNA´s in blue. The material used for the extraction was the cell block of the cell lines.

We found only 8 microRNA´s differentially expressed between the parental and resistant cells, 4 of which were overexpressed and 4 with reduced expression. Among the microRNA´s found in the analysis of the cell pellet, only 3 microRNA´S were preserved in the analysis made with the cell block: hsa-miR-92a-3p, hsa-miR-155-5p and hsa-miR-23a-3p. These data together provide evidence that the expression of microRNA's is influenced by the type and processing of the sample. To further explore the target and roles of these 3 microRNA´S conservated between the analysis, we performed a functional analysis (Figure 17). The genes are involved meanly in focal adhesion (67), regulation of cytoskeleton (66) MAPK signaling (72), endocytosis (57) and mTOR signaling (24).

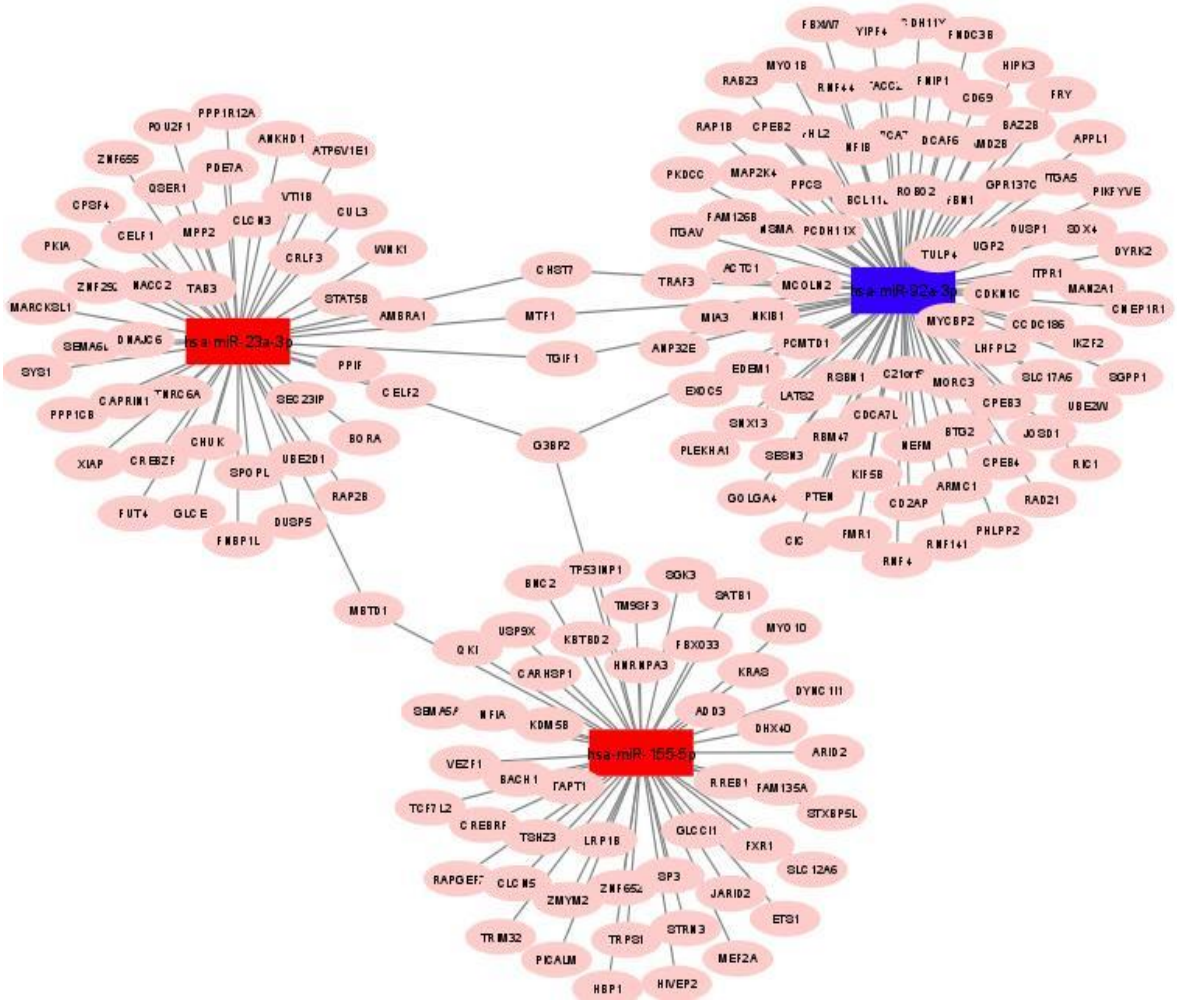

Figure 17-Molecular interaction network between hsa-miR-92a-3p, hsa-miR-155-5p and hsa-miR-23a-3p and their targets. In this figure, each circle represents a gene (node), and each connection represents a direct or indirect connection (edge).

4.2. Comparative study of the cytotoxic effect of anti-EGFR combi-molecules in head and neck and colorectal cell lines.

The results present in this section correspond to specific objective 2.2.3.

4.2.1 Combi-molecules anti-EGFR + alkylating agents reduce cell viability of the head and neck and colorectal cells.

To assess the cytotoxic potential of combi-molecules, we conduced cell viability assays using head and neck cancer cell lines: FaDu parental, FaDu resistant, JHU28, SCC25, HN13 and UM-SCC47. To assess the effectiveness of combi-molecules in reducing cell viability, initially a screening was performed using 3 combi-molecules (JS61, JS84 and ZR2002) diluted in DMSO in increasing concentrations ranging from 0 to 100 µM. As a positive control, geftinib (anti-EGFR), chlorambucil (alkylated agent and chemical structurally like "combi-molecules") and the combination of both (G + C) were used. For this purpose, dilution curves ranging from 0 to 200 µM (0, 0,0625, 0,625, 6,25, 12,5, 25, 50, 100, 200) were exposed to the strains for 72 hours. As shown in figure 18, all combi-molecules tested were able to reach the IC_{50} for all cells tested. In addition, all combi-molecules analyzed showed a dose-dependent effect on the strains (Figure 18). Moreover, ZR2002 and JS84, showed lower IC_{50} values than geftinib, chlorambucil and the combination of both. In addition, chlorambucil did not obtain IC_{50} values detectable for most cells analyzed.

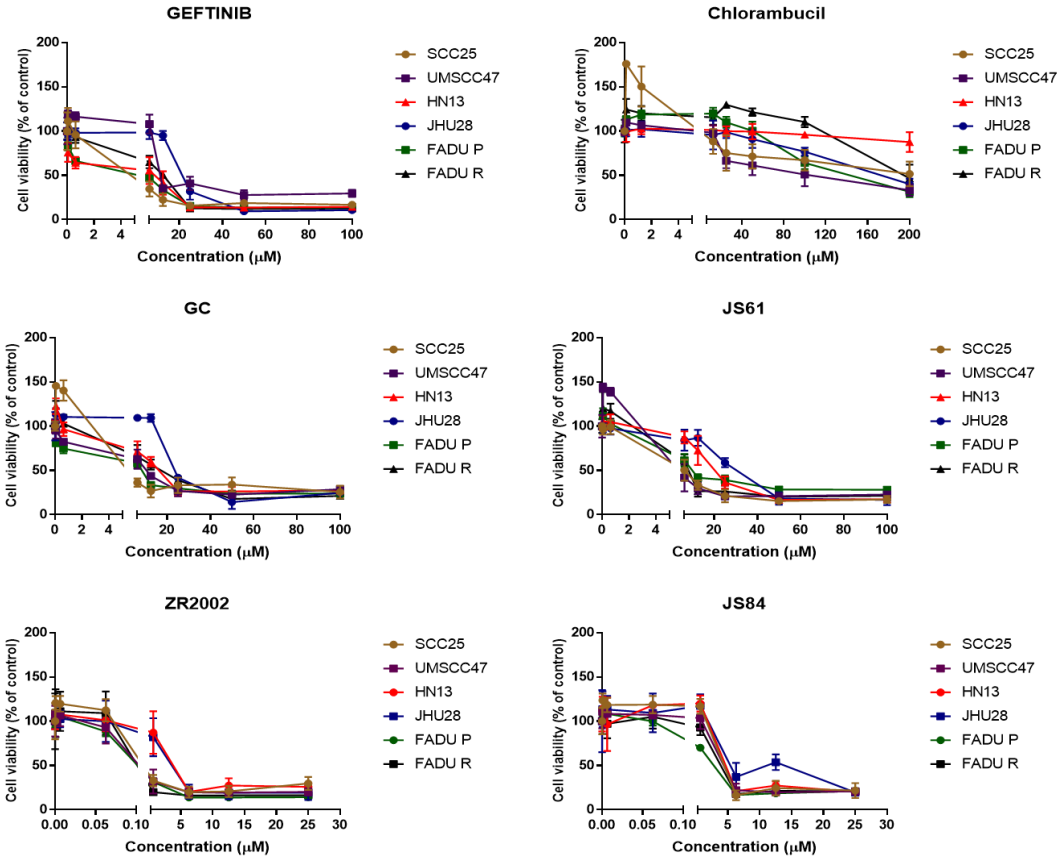

Figure 18-Dose-response curves for combi-molecules and their respective controls in HNSCC cells.

The IC_{50} values for the most resistant cell line to combi-molecules, JHU28, varied from 2.5 to 40 µM. For the FaDu parental considered the most sensitive, the values ranged from 0.4 to 13.2µM (Table 6).

Table 6-IC_{50} values for combi-molecules and their respective controls in the head and neck lines

	IC_{50} µM (Mean ± SD)					
	GEFTINIB	**CHLORAMBUCIL**	**G+C**	**ZR2002**	**JS61**	**JS84**
FaDu Parental	4.9 ± 0.2	ND	8.8 ± 3.3	0.4 ± 0.2	13.2 ± 6.7	2.2 ± 0.3
FaDu Resistant	9.7 ± 0.5	ND	15.9 ± 5.0	0.5 ± 0.2	13.5 ± 4.4	4.7 ± 1.2
JHU28	26.3 ± 1.4	ND	40 ± 1.6	2.5 ± 0.4	34.5 ± 1.5	7.9 ± 0.9
HN13	6.5 ± 1.1	ND	23.2 ± 1.3	3.2 ± 0.5	15.2 ± 1.1	7.6 ± 0.8
SCC25	4.4 ± 0.6	150.4 ± 0.14	8.8 ± 0.9	0.6 ± 0.2	7.3 ± 0.9	3.6 ± 0.5
UM SCC47	19.2 ± 1.2	89.19 ± 0.02	25.5 ± 1.4	0.4 ± 0.1	13.8 ± 1.4	3.1 ± 0.5
Mean	**11.8**	**ND**	**20.3**	**1.26**	**16.2**	**4.85**

To further assess the potential anti-neoplastic properties of "combi-molecules", we extended the cell viability analysis to a panel of colorectal cancer cell

lines. In this tumor subtype, we analyzed four cell lines: Caco-2, DiFi, HCT-15 and HCT-116. The same concentrations and treatment times used for the head and neck cells were utilized. As shown in the dose response curves of figure 19, all combi-molecules managed to reach the IC_{50}, presenting lower values than geftinibi and chlorambucil alone. In addition, ZR2002 and JS84 again demonstrated a greater reduction in cell viability when compared to JS61.

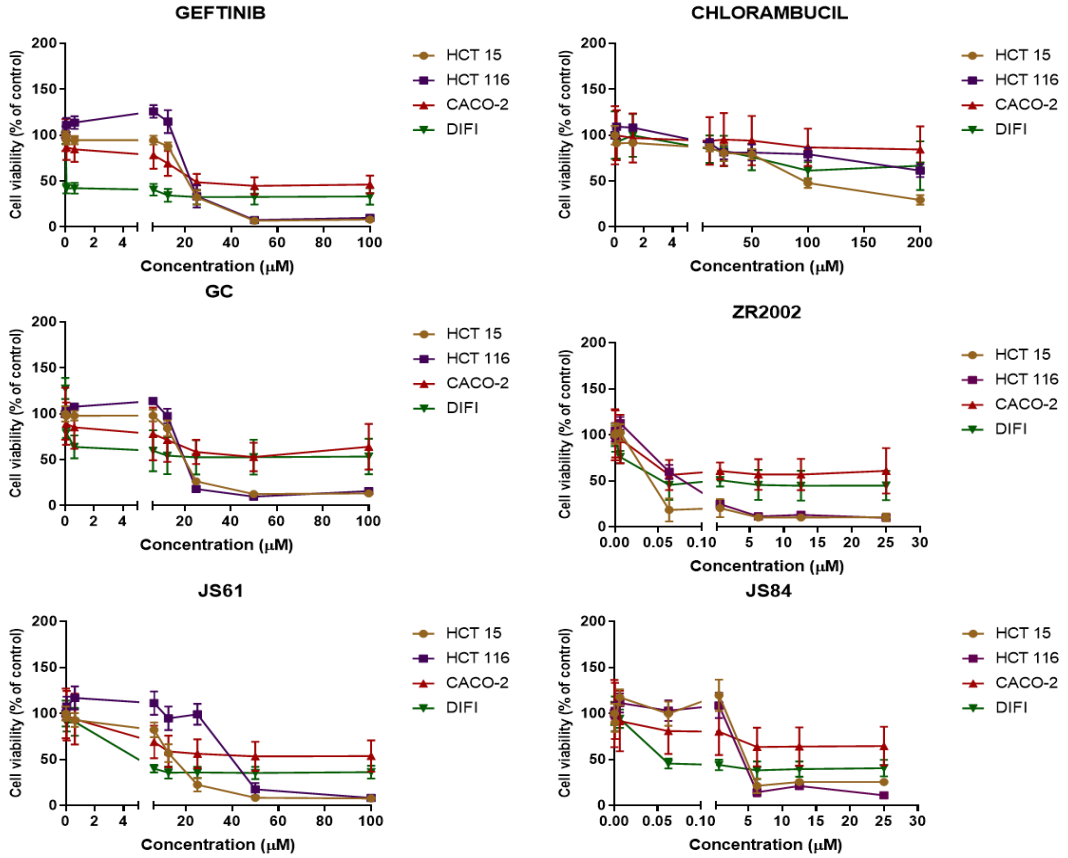

Figure 19-Dose-response curves for combi-molecules and respective controls in the colorectal cancer cell lines.

IC_{50} values for the most resistant cell line to combi-molecules, Caco-2, varied from 8.3 to 61.5 µM. For the DiFi considered the most sensitive, the values ranged from 0.17 to 32.6 µM (Table 6)

Table 7- IC_{50} values for combi-molecules and their respective controls in colorectal cancer cells.

	IC_{50} µM (Mean ± SD)					
	GEFTINIB	**CHLORAMBUCIL**	**G+C**	**ZR2002**	**JS61**	**JS84**
HCT-15	20.6 ± 2.1	105.8	20.2 ± 1.0	0.03 ± 0.0001	12.0 ± 3.2	4.3 ± 0.6
HCT-116	31.2 ± 6.4	ND	23.9 ± 3.12	0.14 ± 0.03	41.0 ± 12.6	3.1 ± 0.7
CACO-2	38.6 ±12.2	ND	61.5 ± 19.5	8.3 ± 2.75	45.0 ± 11.05	26.1 ± 4.11
DIFI	5.36 ± 3.6	ND	32.6 ± 8.3	7.9 ± 1.77	10.8 ± 5.06	0.17 ± 0.02
Mean	**23.8**	**ND**	**34.5**	**4.09**	**27.2**	**8.4**

ND- Not determined ; SD: Standard deviation

4.2.2 Combi-molecules treatment induces the inhibition of EGFR-mediated signaling and increases DNA damage.

In order to understand the mechanisms involved in the reduction of cell viability mediated by combi-molecules treatment, the expression of proteins involved in EGFR signaling and DNA damage were evaluated. For this analysis we used a sensitive cell line (FaDu parental) and a resistant cell line (JHU 28) for the treatment with combi-molecules. The cells were treated for 24 hours with the IC_{50} values determined in the 72-hours viability assay. As shown in figure 20, in JHU28 cells all combi-molecules were able to significantly induce inhibition of the EGFR phosphorylated, similarly to Geftinib, indicating the blocking of receptor activation. However, only ZR2002 and JS84 were able to inhibit downstream EGFR signaling proteins such as AKT. In addition, in relation to DNA damage, only ZR2002 was able to induce PARP cleavage and increase H2AX phosphorylation.

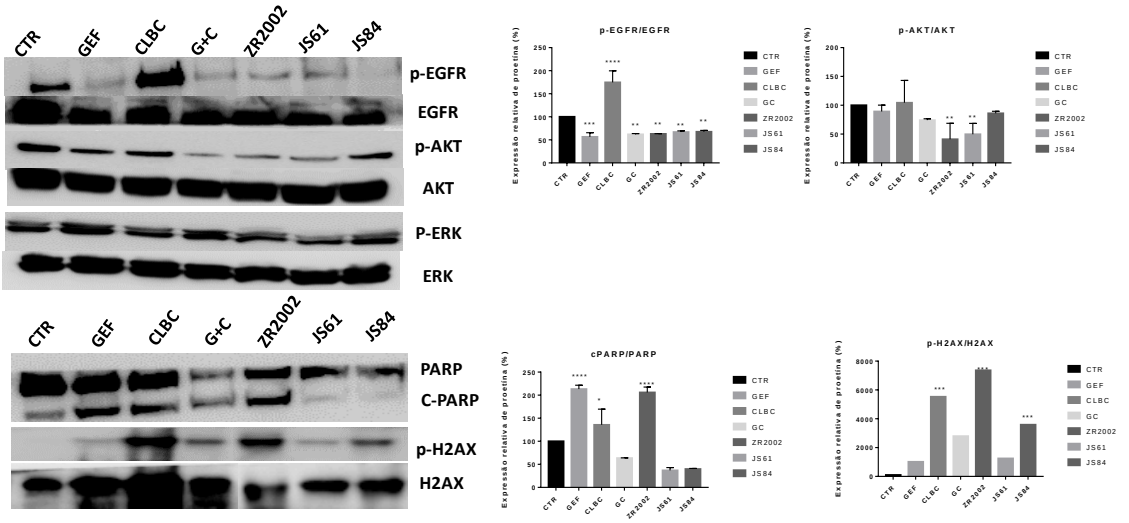

Figure 20-Analysis of EGFR-mediated signaling and DNA damage in the JHU28 (resistant) cells after treatment with the IC50 values of the combi-molecules and their respective controls for 24 hours. **p<0.05 ;***p<0.001.

Similarly, in the sensitive cells, FaDu parental (Figure 21), showed a reduction in the EGFR phosphorylated for all combi-molecules analyzed. However, only ZR2002 and JS84 demonstrated complete pathway block, with concomitant inhibition of the phosphorylated forms of AKT and ERK, differently from what was observed in the resistant cells. In addition, ZR2002 was able to induce PARP cleavage and H2AX phosphorylation levels, thereby indicating DNA damage. Furthermore, JS61 was able to induce phosphorylation of H2AX in the FaDu cells, which was not observed in the JHU28 cells.

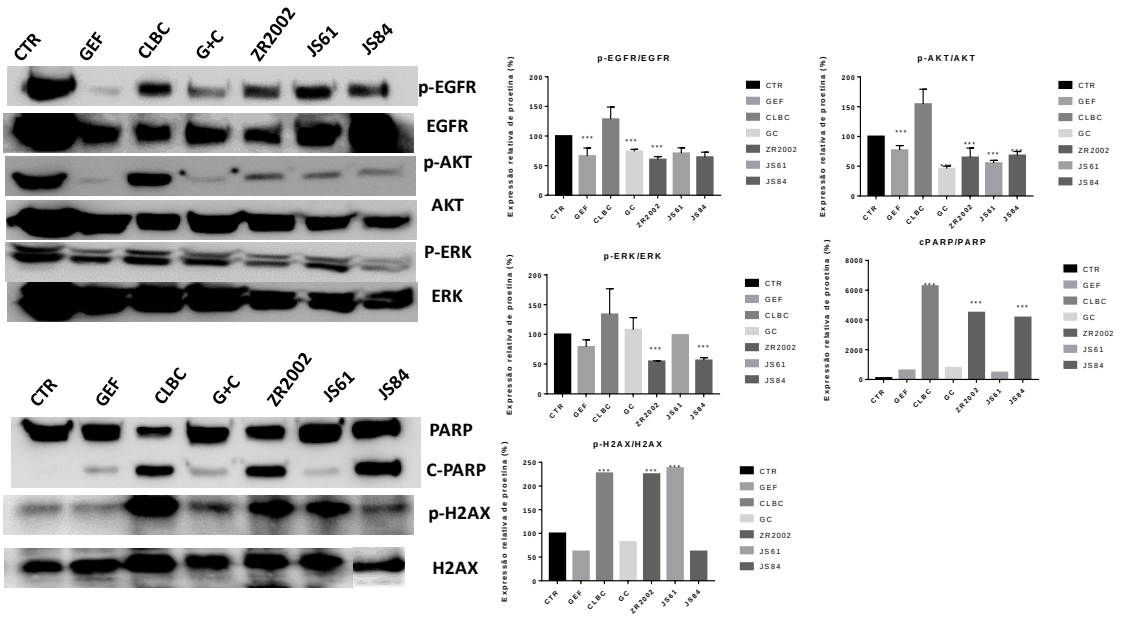

Figure 21-Analysis of EGFR-mediated signaling and DNA damage in FaDu (sensitive) cells after treatment with the IC50 values of the combi-molecules and their respective controls for 24 hours ., .**p<0.05 ;***p<0.001.

For colorectal cancer cells, we analyzed an anti-EGFR resistant cell line (HCT-15) and an anti-EGFR sensitive cell line (DiFi) for the treatment with combi-molecules. The cell treatment conditions were also IC_{50} values determined in the 72-hours viability assay for 24 hours. As shown in figure 22, in DiFi cells all combi-molecules were able to significantly induce inhibition of the EGFR phosphorylated, similarly to geftinib, indicating the blocking of receptor activation. However, only ZR2002 and JS61 were able to inhibit downstream EGFR signaling proteins such as AKT and ERK. In addition, in relation to DNA damage, H2AX phosphorylation and PARP cleavage were weakly induced in DiFi cells after ZR2002 treatment when we compare with DMSO control.

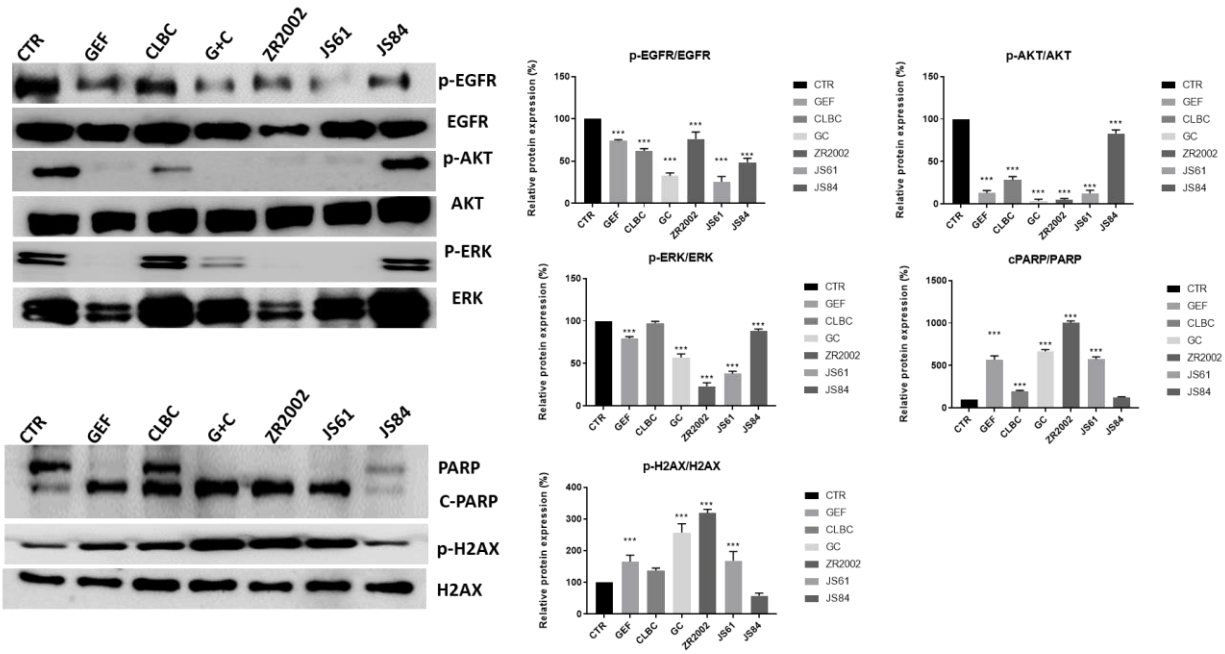

Figure 22-Analysis of EGFR-mediated signaling and DNA damage in DiFi cells after treatment with the IC_{50} values of the combi-molecules and their respective controls for 24 hours. ***p<0.001.

In addition, HCT-15 (Figure 23) cells we observe a strongly inhibition of EGFR phosphorylation upon geftinib, combination between geftinib plus chlorambucil and JS84 treatment. However, only JS61 and JS84 demonstrated EGFR pathway block, with concomitant inhibition of the phosphorylated form of ERK. ZR2002 was able to induce PARP cleavage and H2AX phosphorylation, thereby indicating DNA damage.

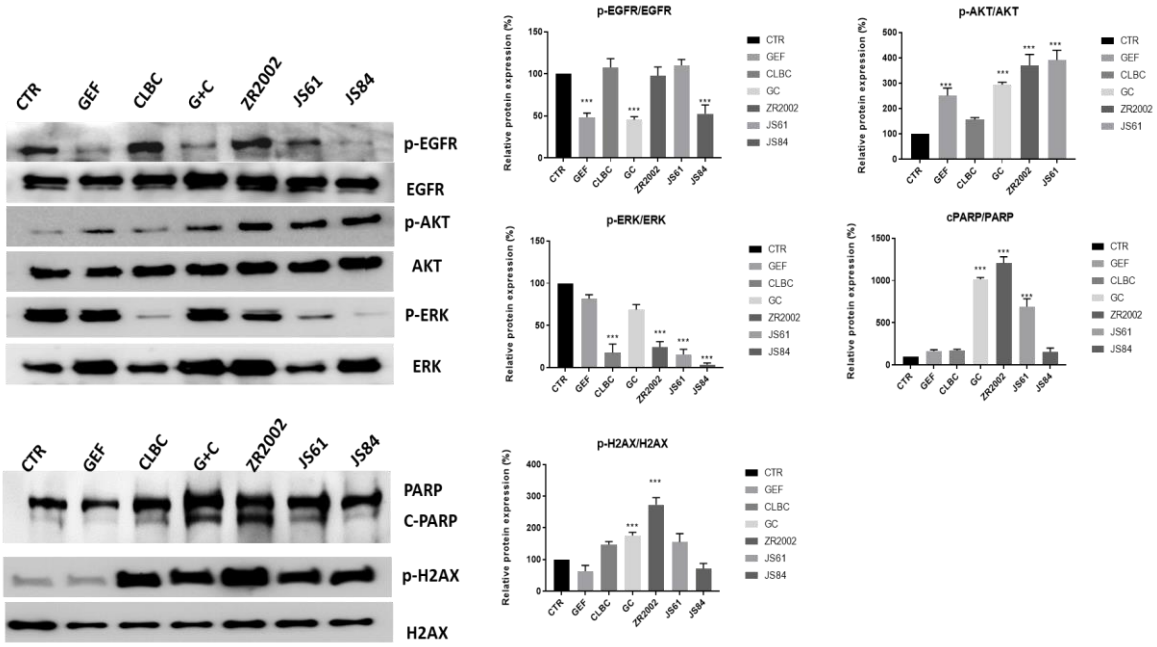

Figure 23-Analysis of EGFR-mediated signaling and DNA damage in HCT-15 cells after treatment with the IC50 values of the combi-molecules and their respective controls for 24 hours. ***p<0.001.

4.2.3 ZR2002 inhibits migration, colony formation and promotes apoptosis in head and neck and colorectal cell lines

After evaluating the role of combi-molecules in inhibiting proliferative signaling mediated by EGFR and promoting damage to DNA, we concluded that among the combi-molecules tested, ZR2002, it demonstrated a greater cytotoxic effect in relation to the other combi-molecules analyzed. To determine if the ZR2002 -induced cell death is an apoptotic response we first examined the PE Annexin V by flow cytometry. The treatment with the IC_{50} values of ZR2002 (0.4 µM-FaDu; 2.5 µM-JHU-28; 0.03 µM-HCT-15; 7.9 µM -DiFi) increased the percentage of cells in late apoptosis by 18.6 % against 3.8 % of the control in the JHU-28 cells. This same result was observed in the FaDu cells, where ZR2002 increased the rate of cells in late apoptosis by 13.2 % against 3.4 % of the control (Figure 24; Table 8).

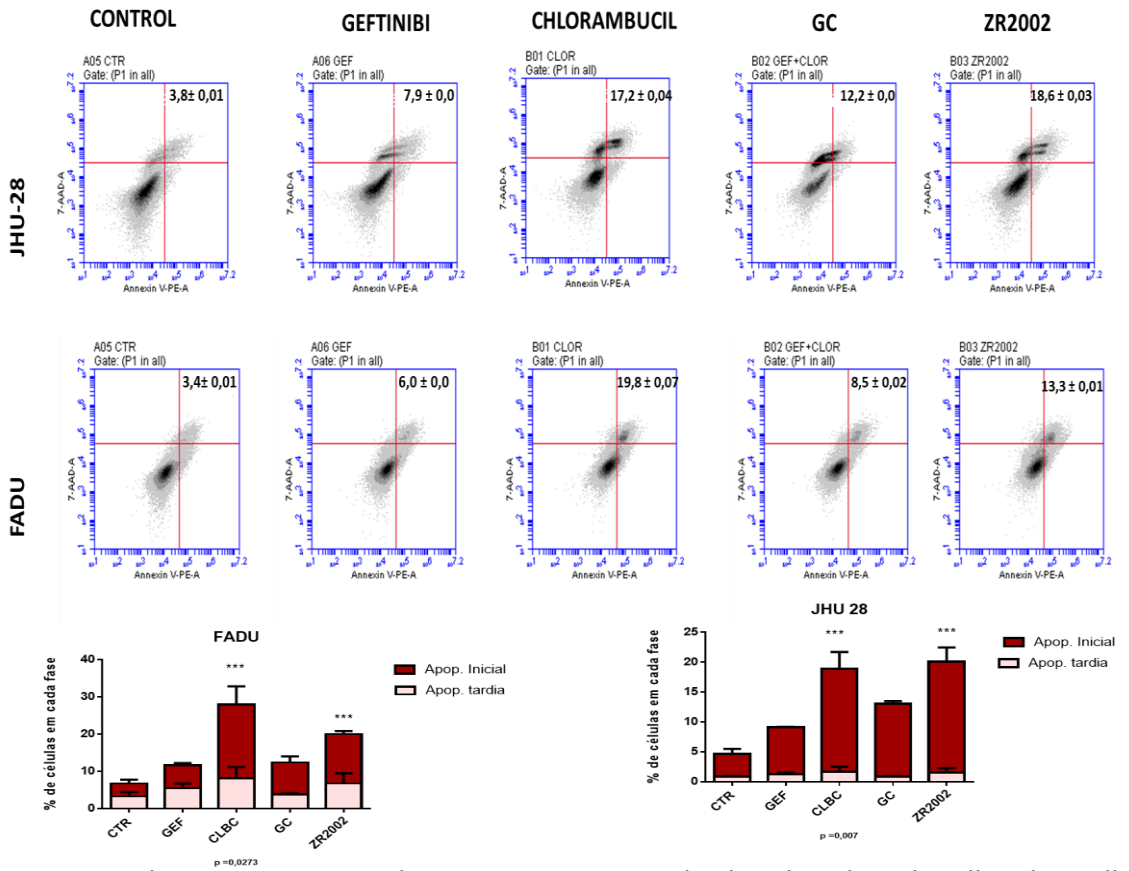

Figure 24-Flow cytometry evaluating apoptosis in the head and neck cells. The cells were treated with the IC50 values of ZR2002 and their respective controls for 24 hours. $p<0.001$.

Table 8- Percentage of apoptotic cells after treatment with ZR2002 and its respective controls

Cell Line	Apoptosis (% ± SD)				
		Viables	**Initial**	**late**	**Non-viables**
JHU28	CTR	91,86 ± 0,03	0,84 ± 0,01	3,82 ± 0,01	3,49 ± 0,02
	GEF	76,57 ± 0,02	1,20 ± 0,00	7,92 ± 0,00	14,3 ± 0,02
	CLOR	65,5 ± 0,09	1,66 ± 0,04	17,2 ± 0,04	15,66 ± 0,04
	GEF+CLOR	60,7 ± 0,06	0,86 ± 0,00	12,2 ± 0,00	26,3 ± 0,07
	ZR2002	60,7 ± 0,05	1,47 ± 0,03	18,6 ± 0,03	19,2 ± 0,02
		Viables	**Initial**	**late**	**Non-viables**
FaDu	CTR	92,6 ± 0,03	3,26 ± 0,02	3,48 ± 0,01	0,66 ± 0,00
	GEF	87,66 ± 0,03	5,47 ± 0,02	6,08 ± 0,00	0,80 ± 0,00
	CLOR	68,3 ± 0,06	8,2 ± 0,04	19,8 ± 0,07	3,81 ± 0,03
	GEF+CLOR	86,4 ± 0,03	3,84 ± 0,00	8,54 ± 0,02	1,27 ± 0,00
	ZR2002	74,4 ± 0,09	10,9 ± 0,02	13,3 ± 0,01	1,45 ± 0,00

To validate these results, we evaluated by western blotting the caspase 3 status upon ZR2002 treatment, as we can see in figure 25, the treatment with ZR2002 strongly increased the cleaved caspase 3 levels in FaDu cells as well as chlorambucil and the combination. However, in JHU-28 cells, that correspond a resistant phenotype, only chlorambucil induces cleaved caspase 3.

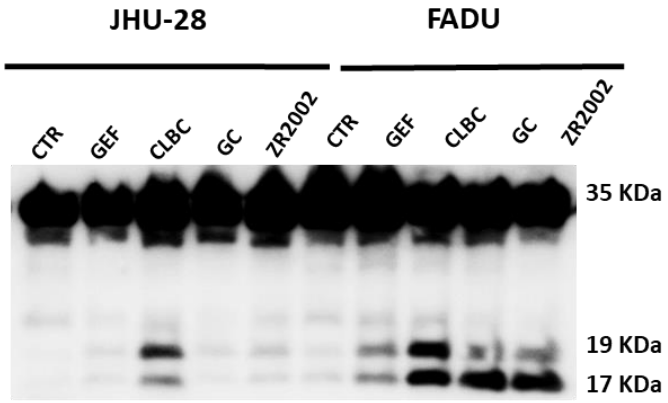

Figure 25-Caspase 3 analysis in JHU-28 and FaDu cells after treatment with the IC_{50} values of the combi-molecules and their respective controls for 24 hours.

Moreover, we extended our analysis using DiFi and HCT-15 cells. ZR2002increased the percentage of cells in late apoptosis by 39 % against 29.4 % of the control in DiFi cells. This same result was observed in the HCT-15 cells, where ZR2002 increased the rate of cells in late apoptosis by 17.6 % against 7.4 % of the control (Figure 26; Table 9).

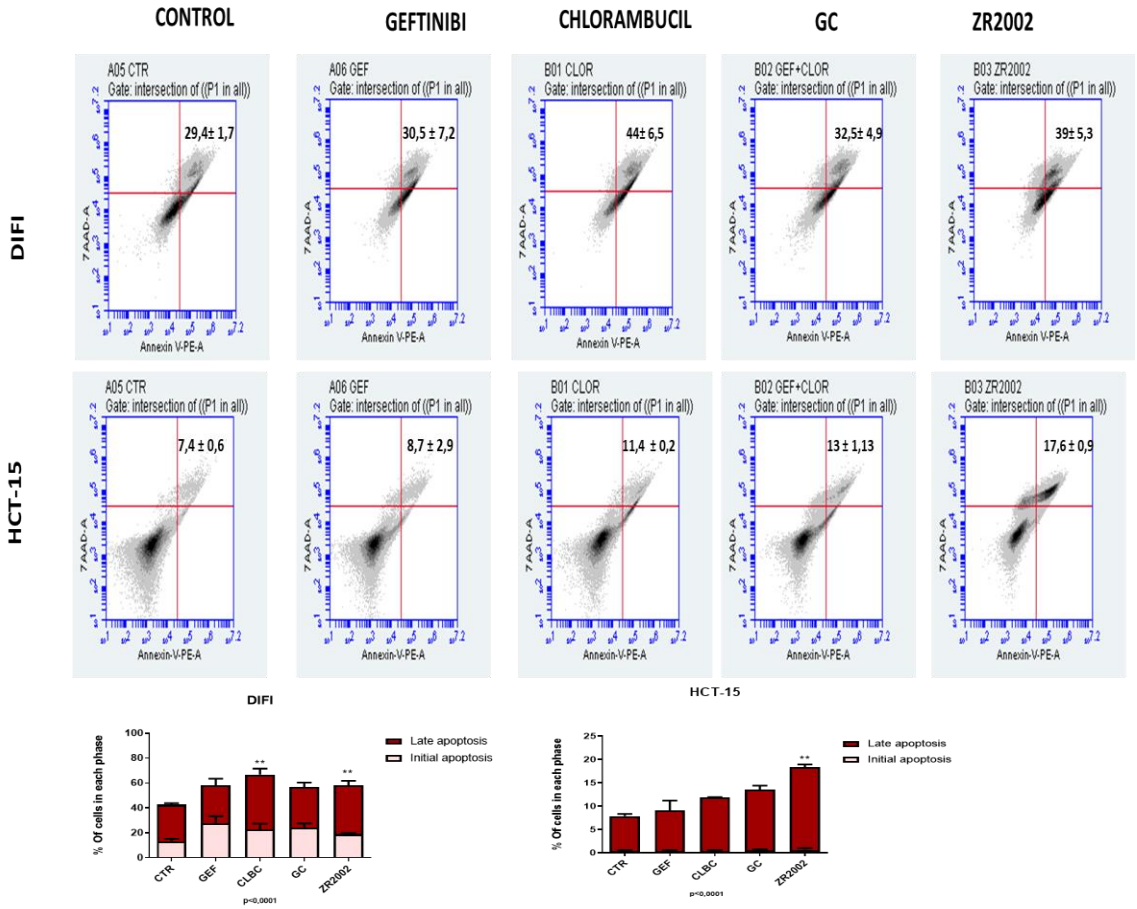

Figure 26-Flow cytometry evaluating apoptosis in the colorectal cancer cells. The cells were treated with the IC50 values of ZR2002 and their respective controls for 24 hours. **p<0.05.

Table 9-Percentage of apoptotic cells in colorectal cancer after treatment with ZR2002 and its respective controls

Linhagem	Apoptosis (% ± SD)				
		Viables	**Initial**	**late**	**Non-viables**
DIFI	CTR	54,5 ± 2,6	13,1 ± 2,9	29,4 ± 1,7	2,9 ± 1,97
	GEF	39,2 ± 15,7	27,6 ± 8,1	30,7 ± 7,2	2,4 ± 0,28
	CLOR	31,9 ± 12,3	22,8 ± 6,4	44,0 ± 6,5	1,2 ± 0,56
	GEF+CLOR	39,4 ± 8,4	24,4± 4,5	32,5 ± 4,9	3,7 ± 0,98
	ZR2002	34,2 ± 6,4	19 ± 1,27	39 ± 5,3	7,7 ± 0,14
		Viables	**Initial**	**late**	**Non-viables**
HCT-15	CTR	88,8 ± 3,4	0,45 ± 0,21	7,45 ± 0,63	2,95 ± 2,61
	GEF	84,8 ± 0,9	0,40 ± 0,28	8,7 ± 2,96	6,10 ± 2,26
	CLOR	84,4 ± 1,6	0,31 ± 0,41	11,4 ± 0,21	3,35 ± 1,9
	GEF+CLOR	78,8 ± 1,2	0,6 ± 0,28	13 ± 1,13	7,55 ± 0,21
	ZR2002	68,2 ± 2,6	0,65 ± 0,49	17,6 ± 0,91	13,4 ± 3,04

We also accessed the cleaved-caspase 3 in DIFI and HCT-15 cells. ZR2002 induces cleaved caspase 3 in DIFI cells, that is an anti-EGFR sensitive cell line, as well as geftinib and the combination between geftinib and chlorambucil. However, in HCT-15 no sign of caspase-3 processing were observed.

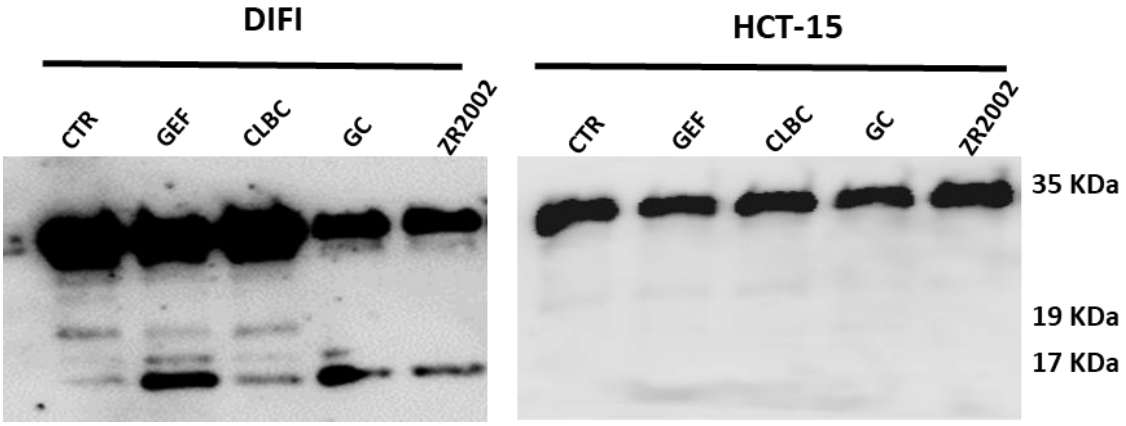

Figure 27- Caspase 3 analysis in DiFi and HCT-15 cells after treatment with the IC_{50} values of the combi-molecules and their respective controls for 24 hours.

Taken together these results suggested that ZR2002 mainly induced apoptotic cell death in head and neck and colorectal cancer cells.

The role of ZR2002 was also evaluated under cell migration. As seen in figure 28, treatment with ZR2002 was able to significantly reduce the migration rates for JHU-28 and FaDu cells.

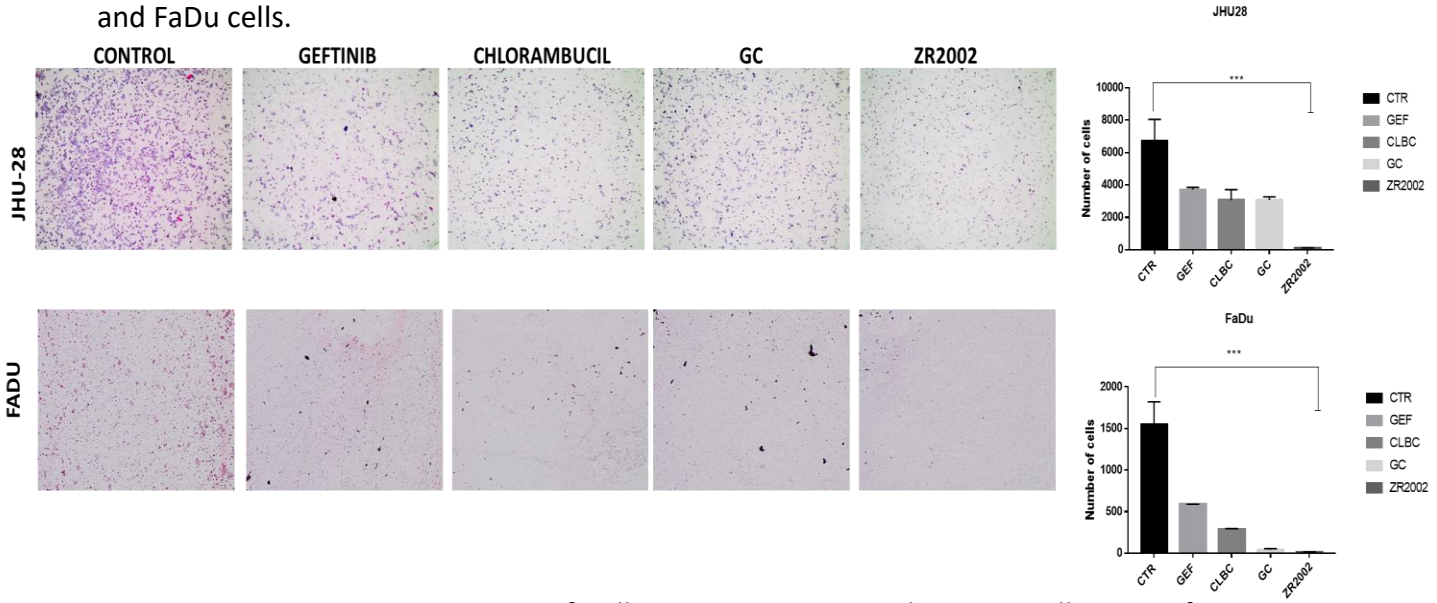

Figure 28-Representative images of cell migration rates in the transwell assay after treatment with ZR2002 and its respective controls in the head and neck cells. The cells

were treated with the IC_{50} values of ZR2002 s and their respective controls for 24 hours.

This same profile of response was observed for colorectal cancer cells. The treatment with ZR2002 was able to promote attenuation of migration, with a significant decrease ($p < 0.05$) in comparison to the control cells (Figure 29).

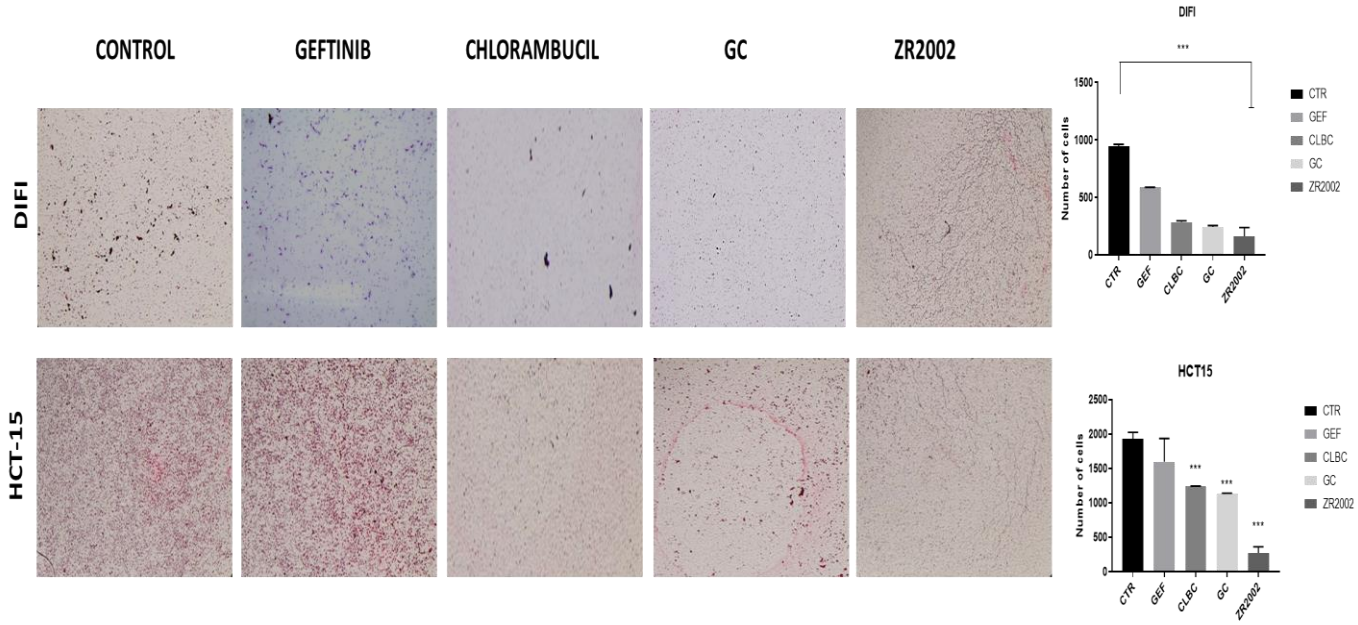

Figure 29-Representative images of cell migration rates in the transwell assay after treatment with ZR2002 and its respective controls in the colorectal cells. The cells were treated with the IC50 values of ZR2002 s and their respective controls for 24 hours. ($p < <0.05$).

Likewise, in the anchorage-dependent colony formation assay, chlorambucil, the combination of geftinibi and chlorambucil and ZR2002 significantly reduced the number of colonies formed in the JHU-28 cells. We emphasize that although chlorambucil and the combination reduce the number of colonies, the IC_{50} values for both are about 10 times higher than for ZR2002 (200 µM, 40 µM and 2.5 µM). Regarding the results in the FaDu cells, since it is a sensitivity model, all compounds tested significantly reduced the number of colonies formed (Figure 30).

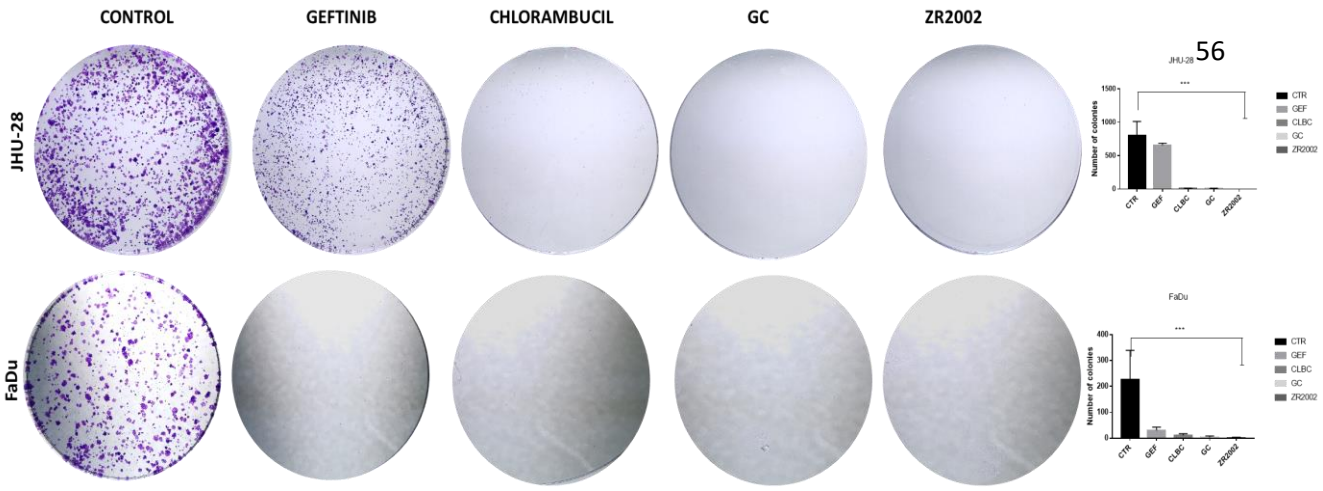

Figure 30- Representative images of colony formation assay, after treatment with ZR2002 and its respective controls in the head and neck lines. The cells were treated with the IC50 values of ZR2002 s and their respective controls for 24 hours. ($p < 0.05$).

Regarding the results in colorectal cells, ZR2002 strongly reduced the number of colonies formed in both cell lines analyzed. Moreover, we highlight that all compounds were able to significantly reduce the number of colonies formed in colorectal cancer cells (Figure 31).

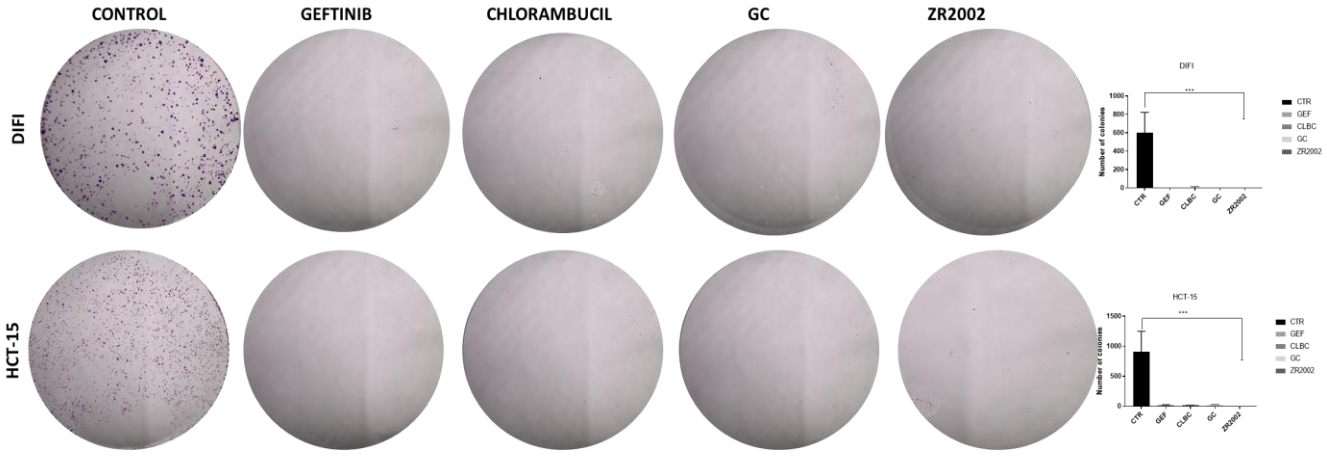

Figure 31-Representative images of colony formation assay, after treatment with ZR2002 and its respective controls in colorectal cancer cells. The cells were treated with the IC50 values of ZR2002 s and their respective controls for 24 hours. ($p < 0.05$).

These results suggest that ZR2002 could represents a new therapeutic approach for head and neck and colorectal tumors that present high EGFR expression rates. rates.

5. DISCUSSION

Targeted therapies are the key to the personalized treatment of cancer patients[103]. Herein, using an in vitro model of HNSCC, we performed a comprehensive evaluation of the molecular profile and biological mechanisms of cetuximab resistance using a long-term cetuximab exposure model. We showed that a cetuximab acquired-resistance model was successfully established and demonstrated that the overexpression of mTOR-PI3K-AKT related genes and the acquired mesenchymal and stem cell signatures might be potentially novel cetuximab-resistance (acquired) biomarkers. Moreover, we highlight the new therapeutical approach named "combi-molecules", inhibiting EGFR and inducing DNA damage, as a new strategy in EGFR overexpressing head and neck and colorectal tumors.

5.1 Identification of Cetuximab acquired resistance mechanisms *in vitro*

Using an *in vitro* model to create a cetuximab resistant cell line by incremental dose exposition, we found 17-fold-higher IC_{50} for the resistant cell line, like the previous study conducted in HNSCC cell lines that showed a 10-fold IC_{50} for cetuximab [104]. We exposed the FaDu cell line for eight months in incremental doses to obtain cetuximab-acquired-resistant cells. Some studies have reported a resistant phenotype in 6 or 7 months at 100 µg/mL and 5µg/mL of cetuximab or even in periods shorter than 15 days [49, 105, 106]. We believe that resistance models based on long exposure times generate a persistent resistance to cetuximab.

We observed several chromosomal numerical aberrations with a gain of chromosomes 3, 7, and 12. Some of these alterations are known to be frequent in HNSCC, such as the gain of chromosome 7, as well as its tetrasomy[89]. Moreover, we observed specific CNA in several gene loci associated with gene overexpression in the cetuximab resistant cells, including *KRAS, RHOA, PTPN11, GTF2H3*, *IKZF1, PIK3R3*, *PLCG2, PDGFD*, and *RASGRF1.* These results suggest that where *KRAS* mutation is a biomarker of cetuximab response in colorectal cancer [107], in HNSCC, *KRAS* amplification may be a predictive marker of cetuximab resistance.

In our study, *RHOA* was the most overexpressed gene in resistant cells. *RHOA* belongs to the Rho GTPases family, which is also involved in the RAS and mTOR-PIK3-AKT signaling and controls all aspects of cellular motility and invasion, including cellular polarity, cytoskeletal organization, and transduction of signals[108, 109]. Recently, Pan and coworkers reported that dysregulation of Rho GTPases, particularly Rho-A, Rho-C, and Rac2, resulted in an aggressive HNSCC phenotype[109]. Furthermore, Rho-A has been described to modulate the EMT by TGF-β and mTOR [110, 111]. EMT is a cellular transformation process in which epithelial cells lose epithelial polarity and intercellular adhesiveness, gaining migratory potential and acquire mesenchymal and stem cell signatures [112]. In the current study, cetuximab-resistant cells showed a morphological change and increased levels of TGF-β, SLUG, and CD44 becoming like to EMT cell activation. We also observed an increase in adhesion rates in FaDu resistant and increased levels of mTOR, and CD44, essential regulators of EMT and metastasis [102, 110, 113]. Overall, this data set reinforces that the EMT transition phenotype and overexpression of Rho-A are involved in HNSCC cetuximab resistance.

Another important therapy resistance mechanism is associated with cancer stem cells (CSCs) [114]. Our study observed a significant difference in mesenchymal stem cell markers and cell surface markers in FaDu resistant cells compared to parental cells such as CD44, ICAM-1, ENG, PD-L1 LAMP1, and LAMP2. CD44 is an important marker of CSC´s in carcinomas, and it plays a role in the mediation of resistance to drug therapy, including anti-EGFR inhibitors [115, 116]. In the HNSCC context, cancer stem cells are responsible for treatment failure in which CD44 has been reported to represent a candidate of resistance marker [117]. Moreover, it has been demonstrated that CD44 regulates EGFR, activating the mTOR-PI3K/Akt signaling pathway[118].

Additionally, in our resistance model, PD-L1 (CD274) amplification/overexpression may involve the adaptive immune resistance to cetuximab. PD-L1 upregulation was associated with a higher risk for nodal metastasis at diagnosis, overall tumor-related death, and recurrence in HNSCC and associated with TKI's resistance in lung cancer[119, 120]. Importantly, it can be suggested that immune-checkpoint blockers, such as pembrolizumab, which targets PD-L1, could activate an immune response and overcome the cetuximab response. Alterations of

the EGFR signaling cascade are known factors influencing cetuximab response [121]. We observed a decreased EGFR phosphorylation in the resistant cells, despite the absence of variation of total EGFR and the upregulation of genes involved in the mTOR/PI3K/AKT pathway. In concordance with our results, Lida et al. showed constitutive activation of the mTOR/PI3K/AKT signaling axis in cetuximab resistant lung cell lines [122]. The upregulation of the mTOR/PI3K/AKT pathway was also reported using UM-SCC-6R cetuximab-resistant cells that demonstrated EGF-independent signaling [106]. On the other hand, it was previously reported that the mTOR/PI3K/AKT pathway's constitutive activation leads to EGFR trafficking[123]. Nuclear EGFR translocation is reported to be related to anti-EGFR therapy resistance[124], so our results corroborate this hypothesis.

As mentioned, the mTOR pathway seems to play a significant role in cetuximab resistance in HNSCC. A recent study associated *MTOR* overexpression in the TKI inhibitors resistance process, demonstrating that stress-induced mutagenesis contributes to adaptive evolution in cancer for drug resistance[125]. Our study found an increase in mTOR levels in whole cellular compartments, including in the membrane, cytoplasm, and mainly in the nucleus of cetuximab-resistant cells. Besides, we also identified an upregulation of genes involved in mTOR signaling, namely *RHOA*, *PIK3R3*, *SKP2*, and a frameshift mutation in *IRS2* that was not present in the parental cell line. IRS2 acts as a protein scaffold that activates the phosphoinositide 3-kinase (PI3K)/AKT/mTOR pathway leading to proliferation and migration[126]. Thus, the inability of IRS2 to respond to negative feedback signals could contribute to higher PI3K/mTOR activity associated with cetuximab resistance in HNSCC. Of note, *IRS2* mutations were recently associated with invasion in pleomorphic invasive lobular carcinoma [127]. Overall, mTOR-PIK3-AKT family members' overexpression could be involved with cetuximab resistance, and combination regimens with drugs that block mTOR may overcome cetuximab resistance in HNSCC.

Interestingly, we also found a *ROS1* variant (c.6341A>G) associated with resistant cells. *ROS1* was previously described as regulated and associated with metastasis to lung and lymph nodes in oral squamous cell carcinoma[128]. Of note, *ROS1* mutations were associated with response to anti-ROS1 inhibitors, such as Lorlatinib in

pancreatic cancer [129].Recently, Davies and coworkers demonstrated a compensatory mechanism of growth control involving ROS and EGFR, where cells resistant to ROS1 inhibition have been resensitized by inhibiting EGFR by a switch between these pathways [130]. Thus, co-targeting of ROS1 and EGFR could potentially offer an effective option to overcome cetuximab resistance.

Regarding the miRNA´s expression we observed that sample processing conditions induced dramatic changes in the expression profile. Cheng et al previously reported a huge variation of miRNA expression with the majority (72%) of detectable miRNAs substantially affected by processing alone. This effect was due to platelet contamination[131]. In an analyze compare plasma and serum from non-ST-elevation myocardial infarction, the authors highlight that plasma and serum exhibit different patterns of circulating miRNA expression and suggest that results from studies with different starting material could not be comparable[132]. Nevertheless, three miRNA´s were conserved between the samples processing: hsa-miR-92a-3p was downregulated in resistant cell line and hsa-miR-155-5p and hsa-miR-23a-3p were upregulated in cetuximab resistant cells. These miRNA´s are involved in focal adhesion, regulation of cytoskeleton MAPK and mTOR signaling.

In summary, this is the first report to describe a deep molecular basis of cetuximab resistance in HNSCC. Our study suggests that the development of cetuximab resistance in HNSCC is a complex mechanism that involves an increased number of genetic aberrations and protein dysregulation. The cetuximab acquired-resistant model was successfully established and demonstrated that the overexpression of the RhoA-mTOR-PIK3-AKT pathway and stem/mesenchymal phenotype are potentially novel biomarkers founded in cetuximab-resistance. Combining regimens between cetuximab and RhoA-mTOR-PIK3-AKT inhibitors appears to be an excellent strategy to overcome cetuximab resistance. The clinical benefit from these molecules' inhibitors should be evaluated in clinical trials, especially in a salvage setting with patients who have acquired resistance to cetuximab.

5.2 Cytotoxic potential of anti-EGFR combi-molecules in head and neck and colorectal cancer

The molecular complexity of cancers and their resistance to anticancer drugs indicate that it is challenge to achieve desirable effects in advanced neoplasms using single drug approaches [133]. Therefore, the multi-targeted concept appears as novel therapeutical approach that provides not only greater therapeutic benefits and improved safety, but also reduces the risk of drug resistance due the activation of compensatory signaling pathways [133, 134135]. Within this context, Dr Jean-Claude, group at McGill University, developed a novel approach termed “combi-targeting” that sought to design compounds named as “combi-molecules” capable of inducing tandem blockade of two divergent biological targets (e.g., EGFR, PARP, MEK, and DNA). Since the studies of hybrid molecules in solids tumors are still scarce, herein, we performed a cytotoxic screening of three different combi-molecules: ZR2002, JS61 and JS84 containing a quinazoline structure, that target EGFR, and a nitrogen (half-)mustard group, able to alkylate DNA against a panel of head and neck and colorectal cancer cell lines harboring different molecular profile, including EGFR expression.

Our results indicated that the alkylating nitrogen mustard chlorambucil did not show great activity in the cells. The clinical EGFR inhibitor gefitinib was extremely potent in the sensitive cells (FaDu and Difi) as reported in the literature[136, 137]. Regarding the equimolar combinations, the IC_{50} values were quite equal to geftinib values alone. These results are in accordance with Rao *et al*, that described this same response profile for equimolar combinations between two different kinases inhibitors *in vitro* [138]. Moreover, all combi-molecules exhibited dose-dependent cytotoxic effect in all cell lines analyzed. The combi-molecule ZR2002 showed superior activity when compared with gefitinib and chlorambucil alone or even between the equimolar combination of both as previously reported in lung cancer[139]. Also, ZR2002 was the first type of combi molecule that it did not depend on hydrolysis to act on its targets, being classified as a "combi molecule type II"[140]. It means that, even with its structure intact, ZR2002 is able to bind to the ATP site of the EGFR and prevent its activation/phosphorylation and also add an alkyl group to the DNA, promoting the

formation of adducts and consequent DNA damage[139] . The combi-molecules JS-84 and JS-61 are also classified as "combi-molecules type II"[139].

Regarding to EGFR signaling inhibition, all combi-molecules powerfully inhibited EGFR compared with the control, and variable results were observed in the downstream signaling. Inhibition of EGFR was associated with clear downregulation of the MAPK and AKT pathways in the head and neck cancer cells for all combi-molecule, mostly for ZR2002. However, in colorectal cancer cells EGFR inhibition lead to inhibition of downstream signaling just for ZR20002 and JS61 in DiFi cells and in MAPK inhibition only for JS61 and JS84 in HCT-15 cells. Taken together, the results suggest a possible contribution of EGFR signaling inhibition to the potency of the combi-molecules in head and neck and colorectal cancer. Our results are in accordance with an previously work that demonstrated the design of hybrid drugs where tyrosine kinase inhibitors (TKI) were conjugated to classical platinum based drugs and demonstrated a strongly kinase inhibition and specificity[141] and also with our previously work that demonstrated strongly EGFR inhibition against lung cancer[139]. Moreover, EGFR signaling inhibition caused by ZR2002 could be explain since ZR2002 it was classified previously as an irreversible inhibitor of EGFR[140].

ZR2002, JS84 and JS61 were reported to alkylated DNA and promote DNA damage in lung cancer [139]. Similarly, our results demonstrated a strongly PARP cleavage and increased levels of phopho-H2AX meanly upon ZR2002 treatment in all cell lines analyzed indicated a strongly DNA damage potency in head and neck and colorectal cells. In this sense, Ma *et al* reported a interesting strategy for overcoming the platinum resistance of triple-negative breast cancer cell lines (TNBC) using hybrid drugs that corresponds to platinum complexes with chlorambucil. These compounds demonstrated higher cytotoxicity than cisplatin on MDA-MB-231 cells, apparently due to enhanced cellular uptake and increased DNA damaged[142] . We also observed increased rates of late apoptosis by flow cytometry and cleaved caspase 3 upon ZR2002 treatment in all cell lines analyzed. Actually, ZR2002 have shown capable of inducing significant levels of cell death by apoptosis in MDA-MB-468 cells[140]. Additionally, Fu *et al*, also demonstrated higher apoptosis rates using pid–polymer hybrid nanoparticles containing cisplatin and afatinib in nasopharyngeal cells[143].

Moreover, these same response profile were obtain in the combination between afatinib and cisplatin in head and neck cells due to afatinib-induced cell cycle arrest, which prevents the repair of cisplatin-induced DNA damage and promotes cell death by apoptosis[144].

Likewise, ZR2002 was able to significantly reduce the cell migration and the anchorage -colony formation in head and neck and colorectal cancer cells. Recently, it was reported that hybrid molecules that target HDAC and EGFR/HER2 pathway reduced cancer cell migration and the number of colonies in human breast cancer cells[145]. Our results suggest that although the monotherapy regimen has shown effective results in recent years, the multi-targeted concept emerged as a new rational therapeutical approach for cancer therapies. Targeting EGFR and DNA damage seems to be a novel therapeutical approach to head and neck and colorectal cancer that express high EGFR levels.

6.CONCLUSION

Taken together, we can conclude that:

- The model of cetuximab acquired resistance that was developed has been validated and represents an *in vitro* tool for analyzing molecular changes resulting from resistance to cetuximab. Preliminary analyzes revealed molecular alterations in important cellular functions and alterations in the gene expression of regulatory pathways of the processes of proliferation, invasion, and metastasis as mTOR and EMT. These findings will be validated in patients with head and neck cancer refractory to cetuximab.

- The new therapeutic approach "combi-molecules", represented in this study by the irreversible inhibitors ZR2002 and JS61 and reversible JS84, demonstrated an efficient antineoplastic action in a panel of head and neck and colorectal cancer cell lines, surpassing the results obtained by the drugs alone or by the equimolar combination between them. These molecules also inhibit important processes in tumor progression, such as the ability to migrate and colony formation, as well as promoting cell death by apoptosis. Therefore, we conclude that the multi-target approach between EGFR inhibitors and alkylating agents can benefit patients with solid tumors. Therefore, the potential of hybrid molecules in solid tumors should be better explored from pre-clinical in vivo trials.

7. PERSPECTIVES/ NEXT STEPS

According to the results of this study, analyzes of the cetuximab resistance model indicated alterations in genes and intracellular pathways that represent candidates for resistance biomarkers. Furthermore, the development of the resistance model enables new experimental approaches. Moreover, our results demonstrated a potential therapeutic application of ZR2002 in the head and neck and colorectal cancer treatment. The findings found in this work will be validated, initially from *in vivo* experiments, to analyze the influence of the microenvironment in our resistance model and the tumor growth under ZR2002 treatment. Moreover, in our resistance model we founded an upregulation of mTOR signaling, the possibility of cetuximab resistance reversal will be also analyzed using mTOR inhibitors.

8. REFERENCES

1. Hanahan D, Weinberg Robert A. *Hallmarks of Cancer: The Next Generation*. **Cell**.144(5):646-74.

2. Sung H, Ferlay J, Siegel RL, Laversanne M, Soerjomataram I, Jemal A, et al. *Global Cancer Statistics 2020: GLOBOCAN Estimates of Incidence and Mortality Worldwide for 36 Cancers in 185 Countries*. **CA Cancer J Clin**. 2021;71(3):209-49.

3. Lee L, Cheung WY, Atkinson E, Krzyzanowska MK. *Impact of comorbidity on chemotherapy use and outcomes in solid tumors: a systematic review*. **J Clin Oncol**. 2011;29(1):106-17.

4. Ferlay J, Shin HR, Bray F, Forman D, Mathers C, Parkin DM. *Estimates of worldwide burden of cancer in 2008: GLOBOCAN 2008*. **Int J Cancer**. 2010;127(12):2893-917

5. Torre LA, Bray F, Siegel RL, Ferlay J, Lortet-Tieulent J, Jemal A. *Global cancer statistics, 2012*. **CA Cancer J Clin**. 2015;65(2):87-108.

6. Sung H, Ferlay J, Siegel RL, Laversanne M, Soerjomataram I, Jemal A, et al. *Global cancer statistics 2020: GLOBOCAN estimates of incidence and mortality worldwide for 36 cancers in 185 countries*. **CA Cancer J Clin**. 2021.

7. Instituto Nacional de Câncer José Alencar Gomes da Silva CGdAE CdPeV. *Estimativa 2016 : incidência de câncer no Brasil.* **Câncer José Alencar Gomes da Silva CGdAE, Coordenação de Prevenção e Vigilância,**.p56.

8. Skulsky SL, O'Sullivan B, McArdle O, Leader M, Roche M, Conlon PJ, et al. *Review of high-risk features of cutaneous squamous cell carcinoma and discrepancies between the American Joint Committee on Cancer and NCCN Clinical Practice Guidelines In Oncology*. **Head Neck**. 2016.

9. Fleming M, Ravula S, Tatishchev SF, Wang HL. *Colorectal carcinoma: Pathologic aspects*. **J Gastrointest Oncol**. 2012;3(3):153-73.

10. Zarogoulidis K, Zarogoulidis P, Darwiche K, Boutsikou E, Machairiotis N, Tsakiridis K, et al. *Treatment of non-small cell lung cancer (NSCLC)*. **J Thorac Dis**. 2013;5 Suppl 4:S389-96.

11. Dal Maso L, Torelli N, Biancotto E, Di Maso M, Gini A, Franchin G, et al. *Combined effect of tobacco smoking and alcohol drinking in the risk of head and neck cancers: a re-analysis of case-control studies using bi-dimensional spline models*. **Eur J Epidemiol**. 2016;31(4):385-93.

12. Shaw R, Beasley N. *Aetiology and risk factors for head and neck cancer: United Kingdom National Multidisciplinary Guidelines*. **J Laryngol Otol**. 2016;130(S2):S9-S12.

13. D'Souza G, Anantharaman D, Gheit T, Abedi-Ardekani B, Beachler DC, Conway DI, et al. *Effect of HPV on head and neck cancer patient survival, by region and tumor site: A comparison of 1362 cases across three continents*. **Oral Oncol**. 2016;62:20-7.

14. Haggar FA, Boushey RP. *Colorectal cancer epidemiology: incidence, mortality, survival, and risk factors*. **Clin Colon Rectal Surg**. 2009;22(4):191-7.

15. Algazi AP, Grandis JR. *Head and neck cancer in 2016: A watershed year for improvements in treatment?* **Nat Rev Clin Oncol**. 2016.

16. Haddad R, Annino D, Tishler RB. *Multidisciplinary approach to cancer treatment: focus on head and neck cancer*. **Dent Clin North Am**. 2008;52(1):1-17, vii.

17. Patel AN, Mehnert JM, Kim S. *Treatment of recurrent metastatic head and neck cancer: focus on cetuximab*. **Clin Med Insights Ear Nose Throat**. 2012;5:1-16.

18. Budach V. *TPF sequential therapy: when and for whom?* **Oncologist**. 2010;15 Suppl 3:13-8.

19. Adams MT, Saltzman B, Perkins JA. *Head and neck lymphatic malformation treatment: a systematic review*. **Otolaryngol Head Neck Surg**. 2012;147(4):627-39.

20. Oksuz DC, Prestwich RJ, Carey B, Wilson S, Senocak MS, Choudhury A, et al. *Recurrence patterns of locally advanced head and neck squamous cell carcinoma after 3D conformal (chemo)-radiotherapy*. **Radiat Oncol**. 2011;6:54.

21. Hammond WA, Swaika A, Mody K. *Pharmacologic resistance in colorectal cancer: a review*. **Ther Adv Med Oncol**. 2016;8(1):57-84.

22. Nedergaard MK, Hedegaard CJ, Poulsen HS. *Targeting the epidermal growth factor receptor in solid tumor malignancies*. **BioDrugs**. 2012;26(2):83-99.

23. Laskin JJ, Sandler AB. *Epidermal growth factor receptor: a promising target in solid tumours*. **Cancer Treat Rev**. 2004;30(1):1-17.

24. Mitchell RA, Luwor RB, Burgess AW. *Epidermal growth factor receptor: Structure-function informing the design of anticancer therapeutics*. **Exp Cell Res**. 2018;371(1):1-19.

25. Kogata N, Zvelebil M, Howard BA. *Neuregulin 3 and erbb signalling networks in embryonic mammary gland development*. **J Mammary Gland Biol Neoplasia**. 2013;18(2):149-54.

26. Eccles SA. *Cell biology of lymphatic metastasis. The potential role of c-erbB oncogene signalling*. **Recent Results Cancer Res**. 2000;157:41-54.

27. Seshacharyulu P, Ponnusamy MP, Haridas D, Jain M, Ganti AK, Batra SK. *Targeting the EGFR signaling pathway in cancer therapy*. **Expert Opin Ther Targets**. 2012;16(1):15-31.

28. Oliveira-Silva RJ, Carolina de Carvalho A, de Souza Viana L, Carvalho AL, Reis RM. *Anti-EGFR Therapy: Strategies in Head and Neck Squamous Cell Carcinoma*. **Recent Pat Anticancer Drug Discov**. 2016;11(2):170-83.

29. Baselga J, Albanell J. *Epithelial growth factor receptor interacting agents*. **Hematol Oncol Clin North Am**. 2002;16(5):1041-63.

30. Smilek P, Neuwirthova J, Jarkovsky J, Dusek L, Rottenberg J, Kostrica R, et al. *Epidermal growth factor receptor (EGFR) expression and mutations in the EGFR signaling pathway in correlation with anti-EGFR therapy in head and neck squamous cell carcinomas*. **Neoplasma**. 2012;59(5):508-15.

31. Fontanini G, De Laurentiis M, Vignati S, Chine S, Lucchi M, Silvestri V, et al. *Evaluation of epidermal growth factor-related growth factors and receptors and of neoangiogenesis in completely resected stage I-IIIA non-small-cell lung cancer: amphiregulin and microvessel count are independent prognostic indicators of survival*. **Clin Cancer Res**. 1998;4(1):241-9.

32. Hong L, Han Y, Brain L. *Epidermal growth factor receptor: an important target in esophageal cancer*. **Expert Opin Ther Targets**. 2013;17(10):1179-85.

33. Petrelli A, Giordano S. *From single- to multi-target drugs in cancer therapy: when aspecificity becomes an advantage*. **Curr Med Chem**. 2008;15(5):422-32.

34. Montal R, Oliva M, Taberna M, De Avila L, Rovira A, Cos M, et al. *Residual neck disease management in squamous-cell carcinoma of the head and neck treated with radiotherapy plus cetuximab*. **Clin Transl Oncol**. 2016;18(11):1140-6.

35. Bonner JA, Harari PM, Giralt J, Azarnia N, Shin DM, Cohen RB, et al. *Radiotherapy plus cetuximab for squamous-cell carcinoma of the head and neck*. **N Engl J Med**. 2006;354(6):567-78.

36. Bou-Assaly W, Mukherji S. *Cetuximab (erbitux)*. **AJNR Am J Neuroradiol**. 2010;31(4):626-7.

37. Niu X, Hu C, Kong L. *Experience with combination of cetuximab plus intensity-modulated radiotherapy with or without chemotherapy for locoregionally advanced nasopharyngeal carcinoma*. **J Cancer Res Clin Oncol**. 2013;139(6):1063-71.

38. Bonner JA, Harari PM, Giralt J, Cohen RB, Jones CU, Sur RK, et al. *Radiotherapy plus cetuximab for locoregionally advanced head and neck cancer: 5-year survival data from a phase 3 randomised trial, and relation between cetuximab-induced rash and survival*. **Lancet Oncol**. 2010;11(1):21-8.

39. Huang J, Zhang J, Shi C, Liu L, Wei Y. *Survival, recurrence and toxicity of HNSCC in comparison of a radiotherapy combination with cisplatin versus cetuximab: a meta-analysis*. **BMC Cancer**. 2016;16:689.

40. Rebucci M, Peixoto P, Dewitte A, Wattez N, De Nuncques MA, Rezvoy N, et al. *Mechanisms underlying resistance to cetuximab in the HNSCC cell line: role of AKT inhibition in bypassing this resistance*. **Int J Oncol**. 2011;38(1):189-200.

41. Bardelli A, Siena S. *Molecular mechanisms of resistance to cetuximab and panitumumab in colorectal cancer*. **J Clin Oncol**. 2010;28(7):1254-61.

42. Brand TM, Iida M, Wheeler DL. *Molecular mechanisms of resistance to the EGFR monoclonal antibody cetuximab*. **Cancer Biol Ther**. 2011;11(9):777-92.

43. Boeckx C, Blockx L, de Beeck KO, Limame R, Camp GV, Peeters M, et al. *Establishment and characterization of cetuximab resistant head and neck squamous cell carcinoma cell lines: focus on the contribution of the AP-1 transcription factor*. **Am J Cancer Res**. 2015;5(6):1921-38.

44. Stransky N, Egloff AM, Tward AD, Kostic AD, Cibulskis K, Sivachenko A, et al. *The mutational landscape of head and neck squamous cell carcinoma*. **Science**. 2011;333(6046):1157-60.

45. Cancer Genome Atlas N. *Comprehensive genomic characterization of head and neck squamous cell carcinomas*. **Nature**. 2015;517(7536):576-82.

46. Rampias T, Giagini A, Siolos S, Matsuzaki H, Sasaki C, Scorilas A, et al. *RAS/PI3K crosstalk and cetuximab resistance in head and neck squamous cell carcinoma*. **Clin Cancer Res**. 2014;20(11):2933-46.

47. Jedlinski A, Ansell A, Johansson AC, Roberg K. *EGFR status and EGFR ligand expression influence the treatment response of head and neck cancer cell lines*. **J Oral Pathol Med**. 2013;42(1):26-36.

48. Rowland MA, Greenbaum JM, Deeds EJ. *Crosstalk and the evolvability of intracellular communication*. **Nat Commun**. 2017;8:16009.

49. Logue JS, Morrison DK. *Complexity in the signaling network: insights from the use of targeted inhibitors in cancer therapy*. **Genes Dev**. 2012;26(7):641-50.

50. Lu JJ, Pan W, Hu YJ, Wang YT. *Multi-target drugs: the trend of drug research and development*. **PLoS One**. 2012;7(6):e40262.

51. Matheson SL, Brahimi F, Jean-Claude BJ. *The combi-targeting concept: intracellular fragmentation of the binary epidermal growth factor (EGFR)/DNA targeting "combi-triazene" SMA41*. **Biochemical Pharmacology**. 2004;67(6):1131-8.

52. Chauhan M, Sharma G, Joshi G, Kumar R. *Epidermal Growth Factor Receptor (EGFR) and its Cross-Talks with Topoisomerases: Challenges and Opportunities for Multi-Target Anticancer Drugs*. **Curr Pharm Des**. 2016;22(21):3226-36.

53. Larroque-Lombard AL, Todorova M, Golabi N, Williams C, Jean-Claude BJ. *Synthesis and uptake of fluorescence-labeled Combi-molecules by P-glycoprotein-proficient and -deficient uterine sarcoma cells MES-SA and MES-SA/DX5*. **J Med Chem**. 2010;53(5):2104-13.

54. Rachid Z, Brahimi F, Domarkas J, Jean-Claude BJ. *Synthesis of half-mustard combi-molecules with fluorescence properties: correlation with EGFR status*. **Bioorg Med Chem Lett**. 2005;15(4):1135-8.

55. Barchechath S, Williams C, Saade K, Lauwagie S, Jean-Claude B. *Rational design of multitargeted tyrosine kinase inhibitors: a novel approach*. **Chem Biol Drug Des**. 2009;73(4):380-7

56. MacPhee M, Rachid Z, Todorova M, Qiu Q, Belinsky G, Jean-Claude BJ. *Characterization of the potency of epidermal growth factor (EGFR)-DNA targeting combi-molecules containing a hydrolabile carbamate at the 3-position of the triazene chain*. **Invest New Drugs**. 2011;29(5):833-45.

57. Rachid Z, Macphee M, Williams C, Todorova M, Jean-Claude BJ. *Design and synthesis of new stabilized combi-triazenes for targeting solid tumors expressing the epidermal growth factor receptor (EGFR) or its closest homologue HER2*. **Bioorg Med Chem Lett**. 2009;19(18):5505-9.

58. Benafif S, Hall M. *An update on PARP inhibitors for the treatment of cancer*. **Onco Targets Ther**. 2015;8:519-28.

59. Yacoub A, Park JS, Qiao L, Dent P, Hagan MP. *MAPK dependence of DNA damage repair: ionizing radiation and the induction of expression of the DNA repair genes XRCC1 and ERCC1 in DU145 human prostate carcinoma cells in a MEK1/2 dependent fashion*. **Int J Radiat Biol**. 2001;77(10):1067-78.

60. Yen L, Nie ZR, You XL, Richard S, Langton-Webster BC, Alaoui-Jamali MA. *Regulation of cellular response to cisplatin-induced DNA damage and DNA repair in cells overexpressing p185(erbB-2) is dependent on the ras signaling pathway*. **Oncogene**. 1997;14(15):1827-35.

61. Gjerset RA, Lebedeva S, Haghighi A, Turla ST, Mercola D. *Inhibition of the Jun kinase pathway blocks DNA repair, enhances p53-mediated apoptosis and promotes gene amplification*. **Cell Growth Differ**. 1999;10(8):545-54.

62. Banerjee R, Rachid Z, McNamee J, Jean-Claude BJ. *Synthesis of a prodrug designed to release multiple inhibitors of the epidermal growth factor receptor tyrosine kinase and an alkylating agent: a novel tumor targeting concept*. **J Med Chem**. 2003;46(25):5546-51.

63. Zanchi C, Zuco V, Lanzi C, Supino R, Zunino F. *Modulation of survival signaling pathways and persistence of the genotoxic stress as a basis for the synergistic interaction between the atypical retinoid ST1926 and the epidermal growth factor receptor inhibitor ZD1839*. **Cancer Res**. 2005;65(6):2364-72.

64. Goodfellow E, Senhaji Mouhri Z, Williams C, Jean-Claude BJ. *Design, synthesis and biological activity of novel molecules designed to target PARP and DNA*. **Bioorg Med Chem Lett**. 2017;27(3):688-94.

65. Banerjee R, Huang Y, Qiu Q, McNamee JP, Belinsky G, Jean-Claude BJ. *The combi-targeting concept: mechanism of action of the pleiotropic combi-molecule RB24 and discovery of a novel cell signaling-based combination principle*. **Cell Signal**. 2011;23(4):630-40.

66. Al-Safadi S, Domarkas J, Han Y, Brahimi F, Jean-Claude BJ. *Enhancement of the cytotoxic potential of the mixed EGFR and DNA-targeting 'combi-molecule' ZRBA1 against human solid tumour cells by a bis-quinazoline-based drug design approach*. **Anticancer Drugs**. 2012;23(5):483-93.

67. Sharifi Z, Abdulkarim B, Meehan B, Rak J, Daniel P, Schmitt J, et al. *Antitumor Activity of a Binary EGFR/DNA Targeting Strategy Overcomes Resistance of Glioblastoma Stem cells to Temozolomide*. **Clin Cancer Res**. 2019.

68. Dirks WG, Faehnrich S, Estella IA, Drexler HG. *Short tandem repeat DNA typing provides an international reference standard for authentication of human cell lines*. **ALTEX**. 2005;22(2):103-9.

69. Schmitt J, Goodfellow E, Huang S, Williams C, Gomes INF, Rosa MN, et al. *Comparative analysis of the dual EGFR-DNA targeting and growth inhibitory properties of 6-mono-alkylamino- and 6,6-dialkylaminoquinazoline-based type II combi-molecules*. **Eur J Med Chem**. 2020;192:112185.

70. Geiss GK, Bumgarner RE, Birditt B, Dahl T, Dowidar N, Dunaway DL, et al. *Direct multiplexed measurement of gene expression with color-coded probe pairs*. **Nat Biotechnol**. 2008;26(3):317-25.

71. Ahn S, Hong M, Van Vrancken M, Lyou YJ, Kim ST, Park SH, et al. *A nCounter CNV Assay to Detect HER2 Amplification: A Correlation Study with Immunohistochemistry and In Situ Hybridization in Advanced Gastric Cancer*. **Mol Diagn Ther**. 2016;20(4):375-83.

72. Kozomara A, Griffiths-Jones S. *miRBase: annotating high confidence microRNAs using deep sequencing data*. **Nucleic Acids Res**. 2014;42(Database issue):D68-73.

73. Shannon P, Markiel A, Ozier O, Baliga NS, Wang JT, Ramage D, et al. *Cytoscape: a software environment for integrated models of biomolecular interaction networks*. **Genome Res**. 2003;13(11):2498-504.

74. Li H, Durbin R. *Fast and accurate long-read alignment with Burrows-Wheeler transform*. **Bioinformatics**. 2010;26(5):589-95.

75. Koboldt DC, Larson DE, Wilson RK. *Using VarScan 2 for Germline Variant Calling and Somatic Mutation Detection*. **Curr Protoc Bioinformatics**. 2013;44:15 4 1-7.

76. Forbes SA, Beare D, Boutselakis H, Bamford S, Bindal N, Tate J, et al. *COSMIC: somatic cancer genetics at high-resolution*. **Nucleic Acids Res**. 2017;45(D1):D777-D83.

77. Sherry ST, Ward MH, Kholodov M, Baker J, Phan L, Smigielski EM, et al. *dbSNP: the NCBI database of genetic variation*. **Nucleic Acids Res**. 2001;29(1):308-11.

78. McLaren W, Gil L, Hunt SE, Riat HS, Ritchie GR, Thormann A, et al. *The Ensembl Variant Effect Predictor*. **Genome Biol**. 2016;17(1):122.

79. Genomes Project C, Auton A, Brooks LD, Durbin RM, Garrison EP, Kang HM, et al. *A global reference for human genetic variation*. **Nature**. 2015;526(7571):68-74.

80. Lek M, Karczewski KJ, Minikel EV, Samocha KE, Banks E, Fennell T, et al. *Analysis of protein-coding genetic variation in 60,706 humans*. **Nature**. 2016;536(7616):285-91.

81. Robinson JT, Thorvaldsdottir H, Winckler W, Guttman M, Lander ES, Getz G, et al. *Integrative genomics viewer*. **Nat Biotechnol**. 2011;29(1):24-6.

82. Gehring JS, Fischer B, Lawrence M, Huber W. *SomaticSignatures: inferring mutational signatures from single-nucleotide variants*. **Bioinformatics**. 2015;31(22):3673-5.

83. Singchat W, Hitakomate E, Rerkarmnuaychoke B, Suntronpong A, Fu B, Bodhisuwan W, et al. *Genomic Alteration in Head and Neck Squamous Cell Carcinoma (HNSCC) Cell Lines Inferred from Karyotyping, Molecular Cytogenetics, and Array Comparative Genomic Hybridization*. **PLoS One**. 2016;11(8):e0160901.

84. Sumner AT. *A simple technique for demonstrating centromeric heterochromatin*. **Exp Cell Res**. 1972;75(1):304-6.

85. Suomela S, Elomaa O, Skoog T, Ala-aho R, Jeskanen L, Parssinen J, et al. *CCHCR1 is up-regulated in skin cancer and associated with EGFR expression*. **PLoS One**. 2009;4(6):e6030.

86. Walmsley GG, Atashroo DA, Maan ZN, Hu MS, Zielins ER, Tsai JM, et al. *High-Throughput Screening of Surface Marker Expression on Undifferentiated and Differentiated Human Adipose-Derived Stromal Cells*. **Tissue Eng Part A**. 2015;21(15-16):2281-91.

87. Salo T, Sutinen M, Hoque Apu E, Sundquist E, Cervigne NK, de Oliveira CE, et al. *A novel human leiomyoma tissue derived matrix for cell culture studies*. **BMC Cancer**. 2015;15:981.

88. Martinho O, Granja S, Jaraquemada T, Caeiro C, Miranda-Goncalves V, Honavar M, et al. *Downregulation of RKIP is associated with poor outcome and malignant progression in gliomas*. **PLoS One**. 2012;7(1):e30769.

89. Geissmann Q. *OpenCFU, a new free and open-source software to count cell colonies and other circular objects*. **PLoS One**. 2013;8(2):e54072.

90. Roche J. *The Epithelial-to-Mesenchymal Transition in Cancer*. **Cancers (Basel)**. 2018;10(2).

91. Cheng KY, Hao M. *Mammalian Target of Rapamycin (mTOR) Regulates Transforming Growth Factor-beta1 (TGF-beta1)-Induced Epithelial-Mesenchymal Transition via Decreased Pyruvate Kinase M2 (PKM2) Expression in Cervical Cancer Cells*. **Med Sci Monit**. 2017;23:2017-28.

92. Krzyszczyk P, Acevedo A, Davidoff EJ, Timmins LM, Marrero-Berrios I, Patel M, et al. *The growing role of precision and personalized medicine for cancer treatment*. **Technology (Singap World Sci)**. 2018;6(3-4):79-100.

93. Benavente S, Huang S, Armstrong EA, Chi A, Hsu KT, Wheeler DL, et al. *Establishment and characterization of a model of acquired resistance to epidermal growth factor receptor targeting agents in human cancer cells*. **Clin Cancer Res**. 2009;15(5):1585-92.

94. De Pauw I, Lardon F, Van den Bossche J, Baysal H, Pauwels P, Peeters M, et al. *Overcoming Intrinsic and Acquired Cetuximab Resistance in RAS Wild-Type Colorectal*

Cancer: An In Vitro Study on the Expression of HER Receptors and the Potential of Afatinib. **Cancers (Basel)**. 2019;11(1).

95. Willey CD, Anderson JC, Trummell HQ, Naji F, de Wijn R, Yang ES, et al. *Differential escape mechanisms in cetuximab-resistant head and neck cancer cells*. **Biochem Biophys Res Commun**. 2019;517(1):36-42.

96. Lievre A, Bachet JB, Le Corre D, Boige V, Landi B, Emile JF, et al. *KRAS mutation status is predictive of response to cetuximab therapy in colorectal cancer*. **Cancer Res**. 2006;66(8):3992-5.

97. Li H, Peyrollier K, Kilic G, Brakebusch C. *Rho GTPases and cancer*. **Biofactors**. 2014;40(2):226-35.

98. Pan Q, Bao LW, Teknos TN, Merajver SD. *Targeted disruption of protein kinase C epsilon reduces cell invasion and motility through inactivation of RhoA and RhoC GTPases in head and neck squamous cell carcinoma*. **Cancer Res**. 2006;66(19):9379-84.

99. Gulhati P, Bowen KA, Liu J, Stevens PD, Rychahou PG, Chen M, et al. *mTORC1 and mTORC2 regulate EMT, motility, and metastasis of colorectal cancer via RhoA and Rac1 signaling pathways*. **Cancer Res**. 2011;71(9):3246-56.

100. Bhowmick NA, Ghiassi M, Bakin A, Aakre M, Lundquist CA, Engel ME, et al. *Transforming growth factor-beta1 mediates epithelial to mesenchymal transdifferentiation through a RhoA-dependent mechanism*. **Mol Biol Cell**. 2001;12(1):27-36.

101. Kalluri R, Weinberg RA. *The basics of epithelial-mesenchymal transition*. **J Clin Invest**. 2009;119(6):1420-8.

102. Lamouille S, Connolly E, Smyth JW, Akhurst RJ, Derynck R. *TGF-beta-induced activation of mTOR complex 2 drives epithelial-mesenchymal transition and cell invasion*. **J Cell Sci**. 2012;125(Pt 5):1259-73.

103. Prieto-Vila M, Takahashi RU, Usuba W, Kohama I, Ochiya T. *Drug Resistance Driven by Cancer Stem Cells and Their Niche*. **Int J Mol Sci**. 2017;18(12).

104. Thapa R, Wilson GD. *The Importance of CD44 as a Stem Cell Biomarker and Therapeutic Target in Cancer*. **Stem Cells Int**. 2016;2016:2087204.

105. Suda K, Murakami I, Yu H, Kim J, Tan AC, Mizuuchi H, et al. *CD44 Facilitates Epithelial-to-Mesenchymal Transition Phenotypic Change at Acquisition of Resistance to EGFR Kinase Inhibitors in Lung Cancer*. **Mol Cancer Ther**. 2018;17(10):2257-65.

106. Trapasso S, Allegra E. *Role of CD44 as a marker of cancer stem cells in head and neck cancer*. **Biologics**. 2012;6:379-83.

107. Xu H, Tian Y, Yuan X, Wu H, Liu Q, Pestell RG, et al. *The role of CD44 in epithelial-mesenchymal transition and cancer development*. **Onco Targets Ther**. 2015;8:3783-92.

108. Straub M, Drecoll E, Pfarr N, Weichert W, Langer R, Hapfelmeier A, et al. *CD274/PD-L1 gene amplification and PD-L1 protein expression are common events in squamous cell carcinoma of the oral cavity*. **Oncotarget**. 2016;7(11):12024-34.

109. Jiang L, Guo F, Liu X, Li X, Qin Q, Shu P, et al. *Continuous targeted kinase inhibitors treatment induces upregulation of PD-L1 in resistant NSCLC*. **Sci Rep**. 2019;9(1):3705.

110. Yonesaka K, Zejnullahu K, Okamoto I, Satoh T, Cappuzzo F, Souglakos J, et al. *Activation of ERBB2 signaling causes resistance to the EGFR-directed therapeutic antibody cetuximab*. **Sci Transl Med**. 2011;3(99):99ra86.

111. Iida M, Brand TM, Starr MM, Huppert EJ, Luthar N, Bahrar H, et al. *Overcoming acquired resistance to cetuximab by dual targeting HER family receptors with antibody-based therapy*. **Mol Cancer**. 2014;13:242.

112. Er EE, Mendoza MC, Mackey AM, Rameh LE, Blenis J. *AKT facilitates EGFR trafficking and degradation by phosphorylating and activating PIKfyve*. **Sci Signal**. 2013;6(279):ra45.

113. Li C, Iida M, Dunn EF, Ghia AJ, Wheeler DL. *Nuclear EGFR contributes to acquired resistance to cetuximab*. **Oncogene**. 2009;28(43):3801-13.

114. Cipponi A, Goode DL, Bedo J, McCabe MJ, Pajic M, Croucher DR, et al. *MTOR signaling orchestrates stress-induced mutagenesis, facilitating adaptive evolution in cancer*. **Science**. 2020;368(6495):1127-31.

115. Bray SM, Lee J, Kim ST, Hur JY, Ebert PJ, Calley JN, et al. *Genomic characterization of intrinsic and acquired resistance to cetuximab in colorectal cancer patients*. **Sci Rep**. 2019;9(1):15365.

116. Zhu S, Ward BM, Yu J, Matthew-Onabanjo AN, Janusis J, Hsieh CC, et al. *IRS2 mutations linked to invasion in pleomorphic invasive lobular carcinoma*. **JCI Insight**. 2018;3(8).

117. Shih CH, Chang YJ, Huang WC, Jang TH, Kung HJ, Wang WC, et al. *EZH2-mediated upregulation of ROS1 oncogene promotes oral cancer metastasis*. **Oncogene**. 2017;36(47):6542-54.

118. Velthaus JL, Iglauer P, Simon R, Bokemeyer C, Bannas P, Beumer N, et al. *Lorlatinib Induces Durable Disease Stabilization in a Pancreatic Cancer Patient with a ROS1 p.L1950F Mutation: Case Report*. **Oncol Res Treat**. 2021:1-7.

119. Davies KD, Mahale S, Astling DP, Aisner DL, Le AT, Hinz TK, et al. *Resistance to ROS1 inhibition mediated by EGFR pathway activation in non-small cell lung cancer*. **PLoS One**. 2013;8(12):e82236.

120. Cheng HH, Yi HS, Kim Y, Kroh EM, Chien JW, Eaton KD, et al. *Plasma processing conditions substantially influence circulating microRNA biomarker levels*. **PLoS One**. 2013;8(6):e64795.

121. Mompeon A, Ortega-Paz L, Vidal-Gomez X, Costa TJ, Perez-Cremades D, Garcia-Blas S, et al. *Disparate miRNA expression in serum and plasma of patients with acute myocardial infarction: a systematic and paired comparative analysis*. **Sci Rep**. 2020;10(1):5373

122. Szumilak M, Wiktorowska-Owczarek A, Stanczak A. *Hybrid Drugs-A Strategy for Overcoming Anticancer Drug Resistance?* **Molecules**. 2021;26(9).

123. Hopkins AL. *Network pharmacology: the next paradigm in drug discovery*. **Nat Chem Biol**. 2008;4(11):682-90.

124. Delou JMA, Souza ASO, Souza LCM, Borges HL. *Highlights in Resistance Mechanism Pathways for Combination Therapy*. **Cells**. 2019;8(9).

125. Li Z, Liao J, Yang Z, Choi EY, Lapidus RG, Liu X, et al. *Co-targeting EGFR and IKKbeta/NF-kappaB signalling pathways in head and neck squamous cell carcinoma: a potential novel therapy for head and neck squamous cell cancer*. **Br J Cancer**. 2019;120(3):306-16.

126. Lu Y, Liang K, Li X, Fan Z. *Responses of cancer cells with wild-type or tyrosine kinase domain-mutated epidermal growth factor receptor (EGFR) to EGFR-targeted therapy are linked to downregulation of hypoxia-inducible factor-1alpha*. **Mol Cancer**. 2007;6:63.

127. Rao S, Thibault B, Peyrard L, Larroque-Lombard AL, Rupp M, Thauvin C, et al. *Quantitative Analysis of the Potency of Equimolar Two-Drug Combinations and Combi-Molecules Involving Kinase Inhibitors In Vitro: The Concept of Balanced Targeting*. **Int J Mol Sci**. 2021;22(17).

128. Brahimi F, Rachid Z, Qiu Q, McNamee JP, Li YJ, Tari AM, et al. *Multiple mechanisms of action of ZR2002 in human breast cancer cells: a novel combi-molecule designed to block signaling mediated by the ERB family of oncogenes and to damage genomic DNA*. **Int J Cancer**. 2004;112(3):484-91.

129. Wei Y, Poon DC, Fei R, Lam AS, Au-Yeung SC, To KK. *A platinum-based hybrid drug design approach to circumvent acquired resistance to molecular targeted tyrosine kinase inhibitors*. **Sci Rep**. 2016;6:25363.

130. Ma ZY, Wang DB, Song XQ, Wu YG, Chen Q, Zhao CL, et al. *Chlorambucil-conjugated platinum(IV) prodrugs to treat triple-negative breast cancer in vitro and in vivo*. **Eur J Med Chem**. 2018;157:1292-9.

131. Fu D, Li C, Huang Y. *Lipid-Polymer Hybrid Nanoparticle-Based Combination Treatment with Cisplatin and EGFR/HER2 Receptor-Targeting Afatinib to Enhance the Treatment of Nasopharyngeal Carcinoma*. **Onco Targets Ther**. 2021;14:2449-61.

132. Longton E, Schmit K, Fransolet M, Clement F, Michiels C. *Appropriate Sequence for Afatinib and Cisplatin Combination Improves Anticancer Activity in Head and Neck Squamous Cell Carcinoma*. **Front Oncol**. 2018;8:432.

133. Lai CJ, Bao R, Tao X, Wang J, Atoyan R, Qu H, et al. *CUDC-101, a multitargeted inhibitor of histone deacetylase, epidermal growth factor receptor, and human epidermal growth factor receptor 2, exerts potent anticancer activity*. **Cancer Res**. 2010;70(9):3647-56.

134. Cramer JD, Burtness B, Le QT, Ferris RL. *The changing therapeutic landscape of head and neck cancer*. **Nat Rev Clin Oncol**. 2019;16(11):669-83.

135. Alsahafi E, Begg K, Amelio I, Raulf N, Lucarelli P, Sauter T, et al. *Clinical update on head and neck cancer: molecular biology and ongoing challenges*. **Cell Death Dis**. 2019;10(8):540.

136. Leemans CR, Snijders PJF, Brakenhoff RH. *The molecular landscape of head and neck cancer*. **Nat Rev Cancer**. 2018;18(5):269-82.

137. de Carvalho AC, Perdomo S, Dos Santos W, Fernandes GC, de Jesus LM, Carvalho RS, et al. *Impact of genetic variants in clinical outcome of a cohort of patients with oropharyngeal squamous cell carcinoma*. **Sci Rep**. 2020;10(1):9970.

138. Brand TM, Iida M, Luthar N, Starr MM, Huppert EJ, Wheeler DL. *Corrigendum to: "Nuclear EGFR as a molecular target in cancer" [Radiother Oncol 108 (2013) 370-77]*. **Radiother Oncol**. 2019;130:195.

139. Moreira J, Tobias A, O'Brien MP, Agulnik M. *Targeted Therapy in Head and Neck Cancer: An Update on Current Clinical Developments in Epidermal Growth Factor Receptor-Targeted Therapy and Immunotherapies*. **Drugs**. 2017;77(8):843-57.

140. Azoury SC, Gilmore RC, Shukla V. *Molecularly targeted agents and immunotherapy for the treatment of head and neck squamous cell cancer (HNSCC)*. **Discov Med**. 2016;21(118):507-16.

141. Vermorken JB, Trigo J, Hitt R, Koralewski P, Diaz-Rubio E, Rolland F, et al. *Open-Label, Uncontrolled, Multicenter Phase II Study to Evaluate the Efficacy and Toxicity of Cetuximab As a Single Agent in Patients With Recurrent and/or Metastatic Squamous Cell Carcinoma of the Head and Neck Who Failed to Respond to Platinum-Based Therapy*. 2007;25(16):2171-7.

142. Vermorken JB, Mesia R, Rivera F, Remenar E, Kawecki A, Rottey S, et al. *Platinum-based chemotherapy plus cetuximab in head and neck cancer*. **N Engl J Med**. 2008;359(11):1116-27.

143. Mehra R, Cohen RB, Burtness BA. *The role of cetuximab for the treatment of squamous cell carcinoma of the head and neck*. **Clin Adv Hematol Oncol**. 2008;6(10):742-50.

144. Tamborero D, Rubio-Perez C, Deu-Pons J, Schroeder MP, Vivancos A, Rovira A, et al. *Cancer Genome Interpreter annotates the biological and clinical relevance of tumor alterations*. **Genome Med**. 2018;10(1):25.

145. Szklarczyk D, Gable AL, Lyon D, Junge A, Wyder S, Huerta-Cepas J, et al. *STRING v11: protein-protein association networks with increased coverage, supporting functional discovery in genome-wide experimental datasets*. **Nucleic Acids Res**. 2019;47(D1):D607-D13.

146. D'Amato V, Rosa R, D'Amato C, Formisano L, Marciano R, Nappi L, et al. *The dual PI3K/mTOR inhibitor PKI-587 enhances sensitivity to cetuximab in EGFR-resistant human head and neck cancer models*. **Br J Cancer**. 2014;110(12):2887-95.

147. Liu X, Fan D. *The epithelial-mesenchymal transition and cancer stem cells: functional and mechanistic links*. **Curr Pharm Des**. 2015;21(10):1279-91.

148. Byeon HK, Ku M, Yang J. *Beyond EGFR inhibition: multilateral combat strategies to stop the progression of head and neck cancer*. **Exp Mol Med**. 2019;51(1):1-14.

149. Silva-Oliveira RJ, Melendez M, Martinho O, Zanon MF, de Souza Viana L, Carvalho AL, et al. *AKT can modulate the in vitro response of HNSCC cells to irreversible EGFR inhibitors*. **Oncotarget**. 2017;8(32):53288-301.

150. Rosa MN, Evangelista AF, Leal LF, De Oliveira CM, Silva VAO, Munari CC, et al. *Establishment, molecular and biological characterization of HCB-514: a novel human cervical cancer cell line*. **Sci Rep**. 2019;9(1):1913.

151. Waggott D, Chu K, Yin S, Wouters BG, Liu FF, Boutros PC. *NanoStringNorm: an extensible R package for the pre-processing of NanoString mRNA and miRNA data*. **Bioinformatics**. 2012;28(11):1546-8.

152. Gu Z, Eils R, Schlesner M. *Complex heatmaps reveal patterns and correlations in multidimensional genomic data*. **Bioinformatics**. 2016;32(18):2847-9.

153. Vicente A, Crovador CS, Macedo G, Scapulatempo-Neto C, Reis RM, Vazquez VL. *Mutational Profile of Driver Genes in Brazilian Melanomas*. **J Glob Oncol**. 2019;5:1-14.

154. Martinho O, Silva-Oliveira R, Miranda-Goncalves V, Clara C, Almeida JR, Carvalho AL, et al. *In Vitro and In Vivo Analysis of RTK Inhibitor Efficacy and Identification of Its Novel Targets in Glioblastomas*. **Transl Oncol**. 2013;6(2):187-96.

9. APPENDIXES

APPENDIX I – MANUSCRIPT SUBMITTED TO SCIENTIFIC REPORTS

Comprehensive molecular landscape of cetuximab resistance in head and neck cancer cell lines

Izabela Natalia Faria Gomes[1ŧ], Renato José da Silva Oliveira[1,2ŧ], Luciane Sussuchi da Silva[1], Olga Martinho[4], Adriane Feijó Evangelista[1], André van Helvoort Lengert[1], Letícia Ferro Leal[1,2], Viviane Aline Oliveira Silva[1], Stéphanie Piancenti dos Santos[3], Flávia Caroline Nascimento[3], André Lopes Carvalho[1], Rui Manuel Reis [1, 4, 5*]

[1] Molecular Oncology Research Center, Barretos Cancer Hospital, Barretos 14784-400, Brazil;

[2]Barretos School of Medicine Dr. Paulo Prata - FACISB, Barretos, Brazil

[3] Laboratory of Molecular Diagnosis, Barretos Cancer Hospital, Barretos, 14784-400, Brazil

[4] Life and Health Sciences Research Institute (ICVS), Medical School, University of Minho, Braga 4710-057, Portugal;

[5] 3ICVS/3B's-PT Government Associate Laboratory, Braga 4710-057, Portugal.

ŧThese authors contributed equally to this work.

***Corresponding author**

Rui Manuel Reis, Ph.D.,

Molecular Oncology Research Center, Barretos Cancer Hospital

Antenor Duarte Villela, 1331, Zip Code: 14784 400, Barretos, São Paulo, Brazil

Phone/Fax: +55 173 321 6600; E-mail: rui.reis@hcancerbarretos.com.br

Abstract

Cetuximab is the sole anti-EGFR monoclonal antibody FDA approved to treat head and neck squamous cell carcinoma (HNSCC). However, no predictive biomarkers of

cetuximab response are known for HNSCC. Herein, we address the molecular mechanisms underlying cetuximab resistance in an *in vitro* model. We established a cetuximab resistant model (FaDu), using increased cetuximab concentrations for more than eight months. The resistance and parental cells were evaluated for cell viability, clonogenic, migration, and adhesion assays. The protein expression profile was analyzed by western blot and human cell surface panel by lyoplate. The mutational profile, karyotype analysis, and copy number alterations (CNA) were analyzed using whole-exome sequencing (WES) and the NanoString platform. FaDu resistant clones exhibited at least 2-fold higher IC_{50} compared to the parental cell line. WES showed relevant mutations in several cancer-related genes, and the comparative mRNA expression analysis showed 36 differentially expressed genes associated with EGFR tyrosine kinase inhibitors resistance, RAS, MAPK, and mTOR signaling. Importantly, we observed that overexpression of KRAS, RhoA, and CD44, as well as upregulation of epithelial–mesenchymal transition (EMT) and stem cell mechanisms, were associated with cetuximab resistance. Protein analysis revealed EGFR phosphorylation inhibition and mTOR increase in resistant cells. Moreover, the resistant cell line demonstrated an aggressive phenotype with a significant increase in adhesion, the number of colonies, and migration rates. Overall, we identified several molecular alterations in the cetuximab resistant cell line that may constitute novel biomarkers of cetuximab response and indicate new strategies to overcome anti-EGFR resistance in HNSCC.

Keywords: EGFR, Cetuximab, Drug resistance; Head and Neck tumors, biomarkers, in vitro, pre-clinical

APPENDIX II (Article published in Journal of Medicinal Chemistry that correspond to sandwich period at MCGill University)

European Journal of Medicinal Chemistry 192 (2020) 112185

Contents lists available at ScienceDirect

European Journal of Medicinal Chemistry

journal homepage: http://www.elsevier.com/locate/ejmech

Research paper

Comparative analysis of the dual EGFR-DNA targeting and growth inhibitory properties of 6-mono-alkylamino- and 6,6-dialkylaminoquinazoline-based type II combi-molecules

Julie Schmitt [a], Elliot Goodfellow [a], Shanlong Huang [a], Christopher Williams [b], Izabela N.F. Gomes [d], Marcela N. Rosa [d], Rui M. Reis [d, e, f], Richard Yang [a], Hatem M. Titi [c], Bertrand J. Jean-Claude [a, *]

[a] Cancer Drug Research Laboratory, Department of Medicine, Division of Medical Oncology, The Research Institute of the McGill University Health Center/Glen Hospital, Montreal, QC, H4A 3J1, Canada
[b] Scientific Support, Chemical Computing Group Inc., Montreal, QC, H3A 2R7, Canada
[c] Department of Chemistry, McGill University, Montreal, QC, H3A 2K6, Canada
[d] Molecular Oncology Research Center, Barretos Cancer Hospital, Barretos, SP, Brazil
[e] Life and Health Sciences Research Institute (ICVS), Medical School, University of Minho, Braga, Portugal
[f] ICVS/3B's-PT Government Associate Laboratory, Braga/Guimarães, Portugal

ARTICLE INFO

Article history:
Received 19 December 2019
Received in revised form
12 February 2020
Accepted 23 February 2020
Available online 26 February 2020

Keywords:
Combi-molecule
Epidermal growth factor receptor (EGFR)
DNA damaging agent
Non-small cell lung cancer (NSCLC)

ABSTRACT

Over the past decade, we described a novel tumour targeted approach that sought to design "combi-molecules" to hit two distinct targets in tumour cells. Here, to generate small combi-molecules with strong DNA damaging potential while retaining EGFR inhibitory potency, we developed the first synthetic strategy to access the 6-N, N-disubstituted quinazoline scaffold and designed **JS61** to possess a nitrogen mustard function directly attached to the 6-position of the quinazoline ring. We compared its biological activity with that of structures containing either a hemi mustard or a non-alkylating substituent. Surprisingly, the results showed that **JS61**, while capable of inducing strong DNA damage, exhibited moderate EGFR inhibitory potency. In contrast, "combi-molecules" with no bulky substituent at the N-6 position (e.g. **ZR2002** and **JS84**) showed stronger EGFR and growth inhibitory potency than **JS61** in a panel of lung cancer cells. To rationalize these results, X-ray crystallography and molecular modeling studies were undertaken, and the data obtained indicated that bulkiness of the 6-N,N-disubstituted moieties hinder its binding to the ATP site and affects binding reversibility.

1. Introduction

The epidermal growth factor receptor (EGFR) is known to be overexpressed in a wide variety of human cancers including non-small cell lung carcinoma (NSCLC) for which this overexpression has been associated with poor prognosis [1–4]. Significant advances in the biological understanding of EGFR expression and its mutational status have led to the design of several inhibitors. A large variety of first-class EGFR inhibitors have been developed such as gefitinib (**1**), which has been used in advanced NSCLC patients (Fig. 1) [5–7]. However, acquired resistance to these inhibitors is frequently developed, leading to the design of second and third generation of EGFR inhibitors. These include afatinib (**2**) (2nd generation) and osimertinib (**3**) (3rd generation) [8–10]. However, acquired resistance still arises rapidly, generally over a period of 9–13 months [11–13].

Another approach to enhance the potency of EGFR inhibitor-based treatment consists of its combination with cytotoxic agents. Indeed, several studies showed that the combination of an inhibitor of EGFR and a DNA damaging agent induced either additive or synergistic growth inhibitory effects [14]. However, one of the major challenges of combination therapy is the risk of additive toxicity associated with the deleterious effects of each individual drug. To circumvent these problems, we developed a novel drug design approach termed "combi-targeting" that seeks to reduce the pharmacotoxicity of multiple antitumour mechanisms to that of a

* Corresponding author.
E-mail address: bertrandj.jean-claude@mcgill.ca (B.J. Jean-Claude).

https://doi.org/10.1016/j.ejmech.2020.112185
0223-5234/

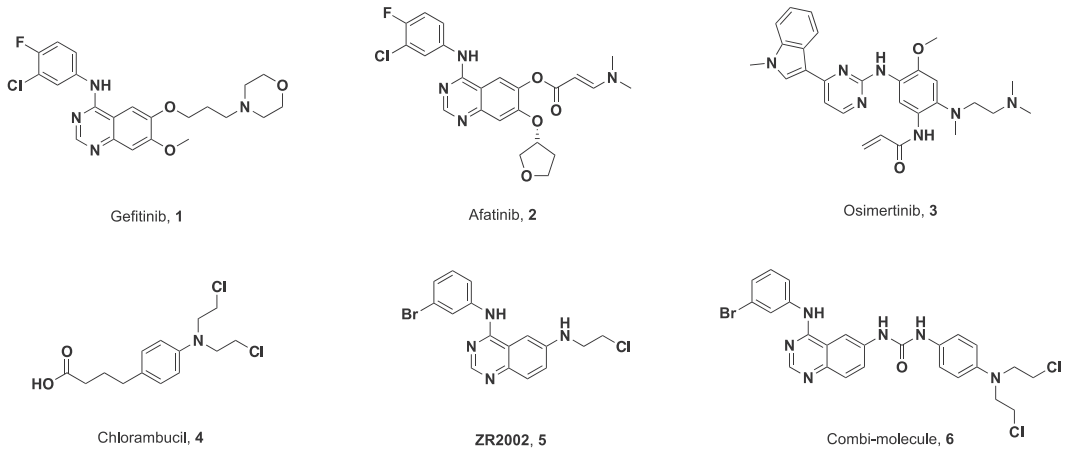

Fig. 1. Selected EGFR inhibitors **1**–**3**, the nitrogen mustard chlorambucil **4** and the combi molecules **ZR2002** (**5**) and **6** that target EGFR and DNA.

single drug. The proof-of-concept of this approach has already been confirmed in our laboratory [15–24]. We classified these "combi-molecules" in different types according to their mechanism of action. As depicted in Fig. 2, type I combi-molecule (EGFR-DNA) is designed as a single agent that, intact, can act exclusively on EGFR. Hydrolysis under physiological conditions allows the activation of the second targeting arm and the subsequent release of both bioactive species, whereupon they can act independently on both their targets EGFR and DNA. Type II combi-molecules are systems that cannot undergo hydrolysis and the single molecule can act only on one of its respective targets. Finally, a type III combi-molecule; **AL776**, has been designed which acts as a hybrid between type I and type II, but is not described here [25]. Regardless of the combi-molecule type, these combi-molecules have shown superior potency and/or reduced toxicity when compared with traditional combinations that compose these molecules, indicating the potential therapeutic benefit of the whole being greater than the sum of its parts. However, the synthesis of multifunctional molecular systems capable of reacting with or binding to the target, and ultimately overcoming drug resistance is a real challenge. Indeed, these systems must maintain strong binding affinity for their desired targets, have sufficient solubility for biological applications and be of appropriate size for diffusion through the cell membrane.

ZR2002 (**5**) was the first type II combi-molecule designed to inhibit EGFR while inducing DNA damage through its 2-chloroethylamino moiety (Fig. 1, compound **5**) [23]. Previous work on this molecule has shown that it can target either EGFR with its inhibitory scaffold or DNA with its 2-chloroethyl function, however a single molecule cannot effect both at the same time (Fig. 2). We have recently achieved a key step in its pre-clinical development by demonstrating that **ZR2002** was able to increase

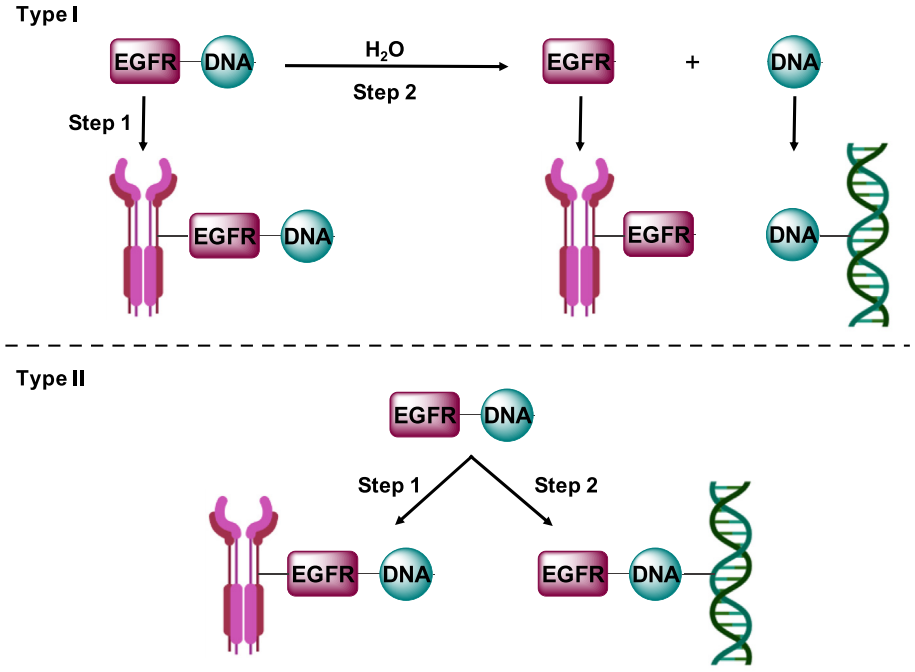

Fig. 2. Type I combi-molecule can inhibit EGFR as an intact molecule (step 1) or can be hydrolyzed to release the two moieties: an EGFR inhibitor + a DNA damaging species (step 2). The type II combi-molecule is capable of targeting either EGFR or DNA as one intact molecule (steps 1 and 2). The word "EGFR" within the rectangle represents an EGFR inhibitory moiety and within the circle, "DNA", the DNA damaging function.

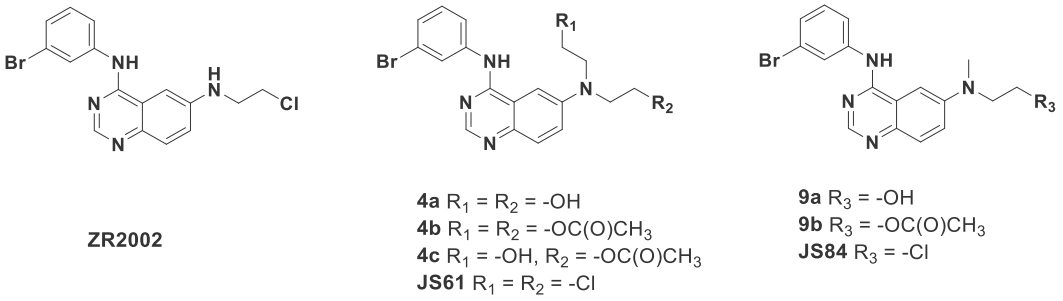

Chart 1. Chemical structures of synthesized N-6-mono- and disubstituted analogues.

overall survival of mice intracranially injected with glioblastoma mesenchymal stem cells harboring temozolomide resistance [26].

In order to enhance the lipophilicity of the drug as well as DNA alkylating potential, we designed and synthesized **JS61** (Chart 1), a type II combi-molecule carrying an additional chloroethyl group on the nitrogen, leading to a highly reactive aromatic nitrogen mustard moiety. We and others have already studied N-mustard-quinazoline molecules (Fig. 1, compound **6**) [21,27–29]. However, these molecules were only achieved through coupling with a linker between the nitrogen mustard and the quinazoline moieties. Furthermore, the addition of a lipophilic chloroethyl group was expected to enhance its lipophilicity without significantly increasing its molecular weight (<500 MW), a property that may be attractive for penetration through the blood brain barrier and potential indication for the therapy of advanced brain tumours.

Herein, for the first time, the synthesis and the biological activity of the first prototype of 6,6-dialkylaminoquinazoline **JS61**, a combi-molecule with a nitrogen mustard directly grafted on the quinazoline scaffold, is described. Further, we challenged its activity by replacing the chloroethyl group(s) with various non alkylating moieties such as methyl (**JS84**), hydroxyethyl and acetoxyethyl (Chart 1) and compared their EGFR binding affinity and growth inhibitory potencies with those of **ZR2002**. To rationalize the results, we performed molecular modeling and X-ray diffraction analyses of the N-disubstituted combi-molecules **JS61**, **JS84** and the N-monosubstituted **ZR2002**.

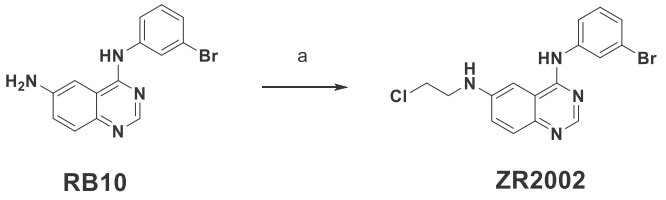

Scheme 2. One-step synthesis of **ZR2002** from a 6-aminoquinazoline[a]
[a] Reagents and conditions: (a) 2-chloroacetaldehyde 50% in water, HCl, $NaBH_3CN$, MeOH, rt, overnight, 86%.

2. Results and discussion

2.1. Chemistry

As previously reported, synthetic strategies involving direct alkylation of the aminoquinazoline or formation of the unstable chloroethyl triazeno-quinazoline to form **ZR2002** were tedious [22,30]. Herein, we describe for the first time a new synthetic pathway that allows the facile synthesis of 6-N,N-disubstituted aminoquinazoline in good yield. Although more recent generations of EGFR inhibitors (e.g. osimertinib, Fig. 1, molecule **3**) showed unique potency against resistant EGFR mutants, we chose to establish our model with the 1st generation of quinazoline

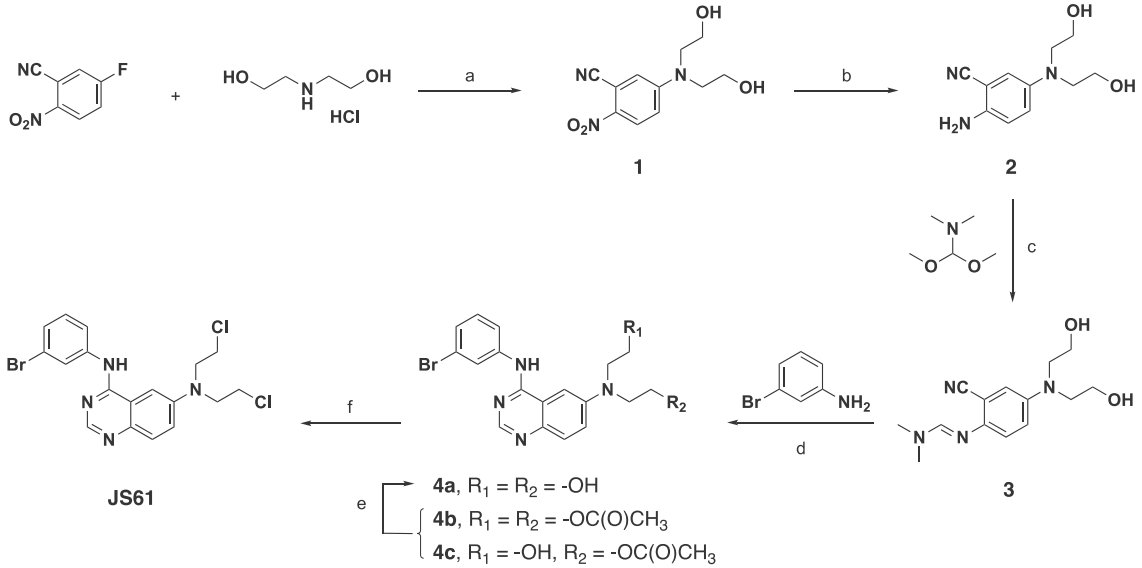

Scheme 1. Synthesis of Compound **JS61**[aa] Reagents and conditions: (a) Cs_2CO_3, DMSO, 100 °C, overnight, 82%; (b) Fe, AcOH, EtOH/H_2O, 100 °C, 2 h, 86%; (c) DMF-dimethylacetal, 110 °C, 1.5 h, 75%; (d) 3-bromoaniline, AcOH, 110 °C, 1 h, **4a** (35%), **4b** (16%) and **4c** (40%); (e) NaOH, MeOH, 3 h, quant. (f) $POCl_3$, 110 °C, 2 h, 75%.

Table 1
Growth inhibition potency of the various analogues against lung cancer cells.

Compound	R_1	R_2	IC_{50} (μM)[a]		
			H1975	PC-9	A549
4a	-OH	-OH	18.05 ± 0.57	0.070 ± 0.012	46.65 ± 1.94
4b	-OAc	-OAc	20.25 ± 1.94	0.130 ± 0.020	52.61 ± 3.24
4c	-OH	-OAc	16.03 ± 0.92	0.086 ± 0.013	48.03 ± 1.08
JS61	-Cl	-Cl	6.07 ± 0.81	0.203 ± 0.049	6.51 ± 1.51
9a	-OH	/	11.31 ± 1.58	0.103 ± 0.022	34.54 ± 3.01
9b	-OAc	/	9.40 ± 1.99	0.098 ± 0.019	30.50 ± 1.57
JS84	-Cl	/	2.81 ± 0.45	0.210 ± 0.050	3.16 ± 0.51
ZR2002			0.48 ± 0.03	0.090 ± 0.020	2.06 ± 0.29
Gefitinib			4.81 ± 0.58	0.017 ± 0.002	15.79 ± 0.70
Chlorambucil			28.16 ± 2.06	7.170 ± 0.430	24.47 ± 1.28
Chlorambucil + Gefitinib[b]			5.98 ± 1.26	0.017 ± 0.002	12.65 ± 0.90

[a] Values represent means and SEM from three independent experiments.
[b] Equimolar combination of chlorambucil and gefitinib.

inhibitor due to its low molecular weight that allowed us to keep a cell penetrable size of the combi-molecule. Furthermore, the EGFR targeting DNA damaging combi-molecules with their unique properties put them in a separate class from traditional clinical inhibitors, targeting EGFR exclusively. According to previous work, this structure is highly tolerant of bulky substituents at the N-6 position since the latter is located at the entrance of the ATP binding pocket of the receptor [25,31]. In the past, we and others showed that the 3′-bromo-substituent was more effective than its methyl and chloro counterparts [22,32]. Therefore, we chose to focus the study on 3′-bromo analogues exclusively. As mentioned earlier, direct alkylation of aminoquinazoline is challenging and our previously described method involving the metastable triazenoquinazoline does not lend itself to the synthesis of disubstituted amino analogues. Therefore, we designed a total synthesis starting from the construction of the quinazoline ring. Briefly, as

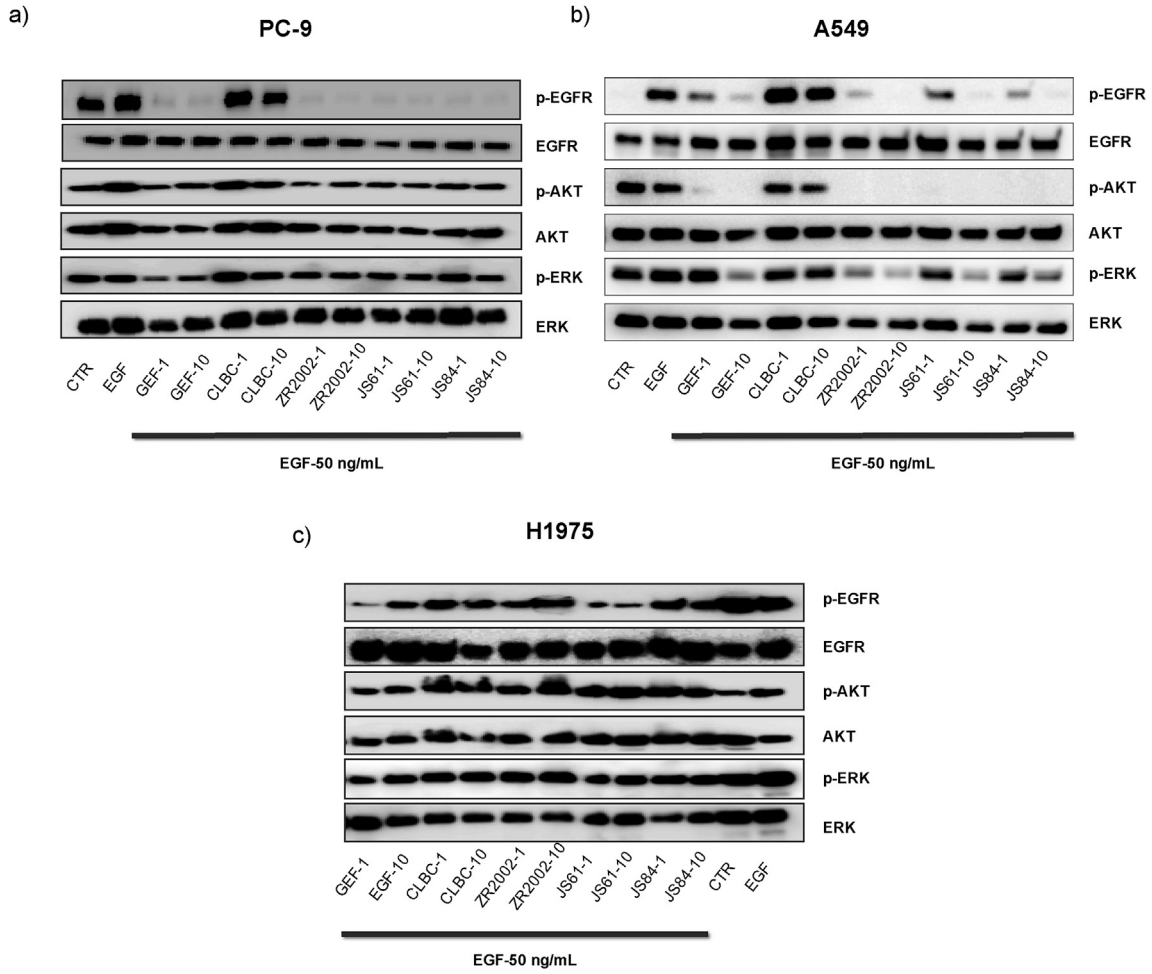

Fig. 3. Inhibition of EGFR signaling by chlorambucil and quinazoline-based compounds in a) PC-9, b) A549 and c) H1975 cell lines. The cells were treated with 1 and 10 μM for 2 h and followed by EGF (50 ng/mL) stimulation. CTR: Control, GEF: gefitinib, CLBC: chlorambucil.

depicted in Schemes 1 and 2, commercially available 5-fluoro-2-nitrobenzonitrile was treated with diethanolamine in DMSO in the presence of Cs_2CO_3 to give **1**, the nitro group of which was reduced in an iron-catalyzed reaction to afford **2**. Compound **2** was subsequently condensed with DMF-dimethyl acetal to give amidine **3**, which was cyclized in the presence of 3-bromoaniline under reflux in acetic acid to afford a mixture of acetylated and hydroxyethyl compounds (Scheme 1). Separation of the mixture with several silica gel column purifications led to compounds **4a-c** as pure yellow powders. The acetate function(s) from compounds **4b** and **4c** were deprotected in a mixture of NaOH in methanol, leading to compound **4a** in quantitative yield. Finally, chlorination of compound **4a** under reflux in $POCl_3$ for 2 h gave the desired combi-molecule **JS61** in 75% yield. The structure of **JS61** was confirmed by ^1H, ^{13}C NMR, high-resolution mass spectrometry and X-ray crystallography.

The methyl group of **JS84** was introduced in a similar fashion, as depicted in Supporting Information (Fig. S1) and its structure confirmed by ^1H, ^{13}C NMR, high-resolution mass spectrometry and X-ray crystallography. Previous work toward the synthesis of **ZR2002** using the formation of a triazene intermediate led to a complex mixture of compounds that require tedious purifications, leading to low yield (27%) [22]. Therefore we revised the synthesis using a reductive amination approach as shown in Scheme 2. Briefly, **RB10** obtained from a previously described method [32] was stirred overnight in a mixture of 2-chloroacetaldehyde and $NaBH_3CN$ to afford **ZR2002** in good yield (84%).

2.2. Biological evaluation

As EGFR inhibitors are indicated for lung cancer, we chose to evaluate the biological response and mechanisms of action of our compounds in a panel of lung cancer cell lines harboring wild type and mutant forms of EGFR (Table 1). The cell lines PC-9 (EGFR mutant, KRAS wildtype, gefitinib sensitive), A549 (EGFR wildtype, KRAS mutant, gefitinib resistant) and H1975 (EGFR mutations L858R/T790 M, KRAS wildtype, gefitinib resistant) were used [33,34]. In our panel, the strong alkylating nitrogen mustard chlorambucil was moderately active. The clinical EGFR inhibitor gefitinib was extremely potent in the PC9 sensitive cells (IC_{50} = 17 nM) and moderately active in H1975 and A549 as reported in the literature [35,36]. For all the EGFR targeting molecules, the IC_{50} values in PC9 cells were in the sub-micromolar range (IC_{50} < 0.21 μM), independent of groups R_1 and R_2. In this cell line, none of our combi-molecules showed superior activity when compared with gefitinib. However, in the resistant and wild type cells (H1975 and A549), **ZR2002** and the disubstituted **JS84** showed 2- to 10-fold stronger potency than gefitinib and the gefitinib + chlorambucil combination. Finally, the mustard-linked analogue **JS61** showed superior potency when compared with gefitinib or gefitinib + chlorambucil in only one cell line (A549).

To determine whether the haloalkyl group presents a cell-killing advantage, we compared the ethylhydroxy and the ethyl acetate analogues against their chloro counterparts. The results showed that all the chloroalkyl compounds, including **JS84** and **JS61**, were 3- to 11-fold more potent than their hydroxy/acetate counterparts **4a-c**, **9a** and **9b**, suggesting that their alkylating functions contributed to their biological activity. Interestingly, despite the strong alkylating potency of the mustard group grafted onto **JS61**, it was less potent than its two half-mustard carrying counterparts, combi-molecules **JS84** and **ZR2002**.

In order to infer on the role of EGFR inhibition on cellular response to the various analogues, we characterized the EGFR pathways following exposure to **ZR2002**, **JS84** and **JS61** in comparison with gefitinib and chlorambucil (Fig. 3). In mutant PC9 cells and wild type expressing A549 cells, all quinazoline-based compounds strongly inhibited EGFR (Fig. 3a and b). By contrast, in the resistant cell line H1975, only **JS61** was able to block EGFR phosphorylation (Fig. 3c). As expected, chlorambucil did not inhibit EGFR phosphorylation.

Regarding downstream signaling, the effect varied between cell lines. Inhibition of EGFR was associated with clear downregulation of the MAPK and Akt pathways in the wild type expressing cells A549 and moderately in PC9 cells for all quinazoline-based compounds. Strikingly, inhibition of EGFR phosphorylation by **JS61**, the only compound capable of inhibiting EGFR in H1975 cell line did not translate into blockade of downstream signaling. The results suggest a possible contribution of EGFR signaling inhibition to the potency of the combi-molecules in A549 cells and PC9. For the resistant H1975 cells, cell killing by all the compounds may be mediated through mechanisms other than EGFR inhibition.

2.3. DNA damaging potential

2.3.1. In vitro alkylation

Nitrogen-mustards are known to react mainly with the N^7 position of guanine and the N^3 position of adenine in DNA through the formation of a reactive aziridinium ion [37]. To assess the DNA damaging potential of the combi-molecules, we first evaluated the reactivity of **ZR2002**, **JS84** and **JS61** *in vitro* using a direct chemical reaction with calf thymus DNA under physiological conditions (Scheme 3) [38].

As depicted in the LC-HRMS profile (Fig. 4), the hydrolytic compound **ZR2002OH** was found for the reaction of **ZR2002** with calf thymus DNA, resulting perhaps from the hydrolysis of the aziridinium ion intermediate. This hydrolytic compound was equally found for both **JS84** and **JS61** (see Supporting Information).

Importantly, we detected the guanine and the adenine alkylated adducts **ZR2002N7Guanine** and **ZR2002N3Adenine**, indicating that **ZR2002** indeed has DNA alkylating potential. The depurination observed for the different products has previously been reported, resulting from the instability of the purine following alkylation [39]. Again, these adducts were equally observed for **JS84** and **JS61**, indicating the presence of DNA alkylating potential as well. Although **JS61** has been designed to be capable of performing cross-links, the observation of the double alkylation product was not observed, possibly due to an undetectable concentration of this adduct in the reaction mixture.

2.3.2. Whole cell alkaline Comet Assay

To assess the DNA damaging potential of the molecules in cells, the whole cell alkaline Comet assay was used [23]. We selected A549 in which blockade of EGFR led to clear inhibition of downstream signaling and where all combi-molecules showed a net difference when compared to the corresponding 2-drug combinations (Fig. 5). As expected, gefitinib did not induce DNA damage [40]. By contrast, all the hemi and full mustard compounds induced significant DNA damage at concentrations in the range of IC_{50} values for growth inhibition, indicating a potential contribution of DNA damage to the overall growth inhibitory activity. Importantly, **JS61** was able to induce more damage than its hemi-mustard counterparts and chlorambucil, indicating that our approach has indeed led to a combi-molecule with enhanced DNA damaging potential.

2.4. Reversibility of EGFR inhibitory potency

2.4.1. Reversible binding

We first evaluated EGFR inhibitory potency of **JS61** in a kinase assay as shown in Table 2. Surprisingly, its activity was in the

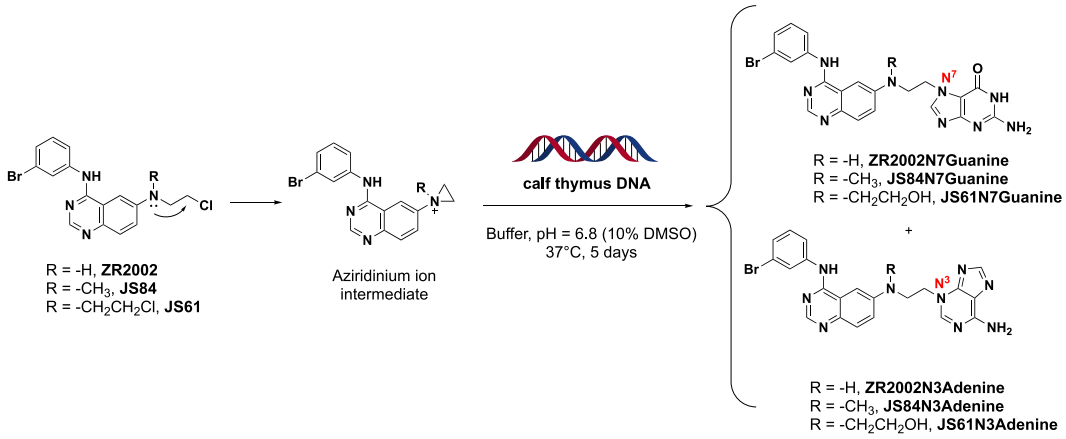

Scheme 3. Reaction of combi-molecules ZR2002, JS84 and JS61 with calf thymus DNA under physiological conditions and corresponding products observed by LC-HRMS.

micromolar range, indicating a 2-fold weaker potency than **JS84** and 100-fold less than the mono-substituted **ZR2002**. Likewise, in a kinase profiling assay involving multiple mutant forms of EGFR, **ZR2002** collectively exhibited stronger inhibitory potency than its di-substituted counterpart **JS61** (see Supporting Information).

In order to understand the differences between the EGFR inhibitory activity of **ZR2002**, **JS61** and **JS84**, we performed a molecular modeling study using MOE software. In Fig. 5, the unbound ligand conformational ensembles of **ZR2002** (green), **JS61** (orange) and **JS84** (cyan) are superimposed on their quinazoline cores and the ensembles are shown both free in space and overlaid in the EGFR binding pocket (PDB code 2ITY). The ensembles overlaid in the EGFR pocket clearly show that all the ligands exhibit some conformations that penetrate the Van Der Waals (VDW) binding surface and thus would clash with the EGFR pocket. Further visual comparison suggests that a higher proportion of the **JS61** conformational ensembles would clash with the binding pocket as compared to the **ZR2002** or **JS84** ensembles. This may suggest that the loss of EGFR activity of **JS61** as compared with **ZR2002** arises from a decrease in the amount of co-planarity between the quinazoline ring and the 6-position substituent. Compounds **ZR2002** and **JS84** both have a small substituent on the N- at position 6 (-H and $-CH_3$ respectively) which allows for low-energy in-plane conformations of the chloroethyl group, which easily fit into the EGFR binding pocket. In contrast, the N-substituents in **JS61** are both large chloroethyl groups and consequently do not allow for low-energy in-plane conformations. As a result, compound **JS61** binds more poorly than **ZR2002** or **JS84** to EGFR because it experiences more conformational restriction upon binding (Fig. 6).

2.4.2. *Irreversible inhibition*

Previous work with **ZR2002** demonstrated that it is an irreversible inhibitor of EGFR. This property was presumed to arise from the ability of its chloroethyl moiety to alkylate the thiol group of the cysteine 773 residue in the ATP binding site of EGFR [23]. Thus, the addition of a chloroethyl group that led to **JS61** prompted us to investigate the reversibility of the latter compound. Thus, a washout western blot experiment was performed to evaluate the recovery of the EGFR phosphorylation in A549 (Fig. 7). This assay was performed as described previously [24,41]. In the washout experiments, cells were washed with drug-free media several times after 2h incubation. **ZR2002** and **JS61** were able to sustain the inhibition after washout, indicating irreversible binding of these compounds to EGFR. Surprisingly, the activity of **JS84** was not, despite its chloroethyl group, indicating a reversible binding mechanism. To rationalize this result, we crystallized and solved

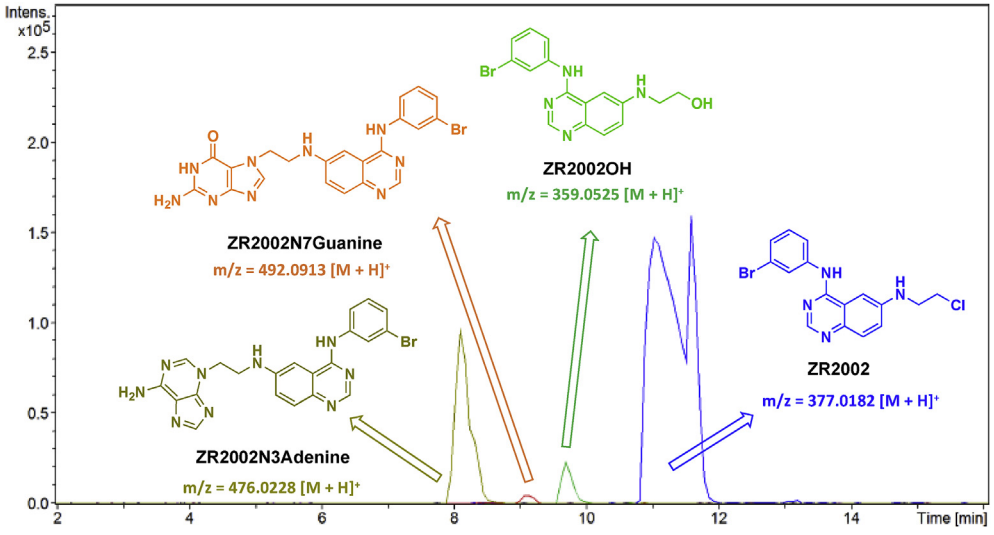

Fig. 4. Observed ion extracted chromatograms for the reaction of **ZR2002** with calf thymus DNA in potassium phosphate buffer, pH = 6.85 (10% DMSO) at 37 °C for 5 days.

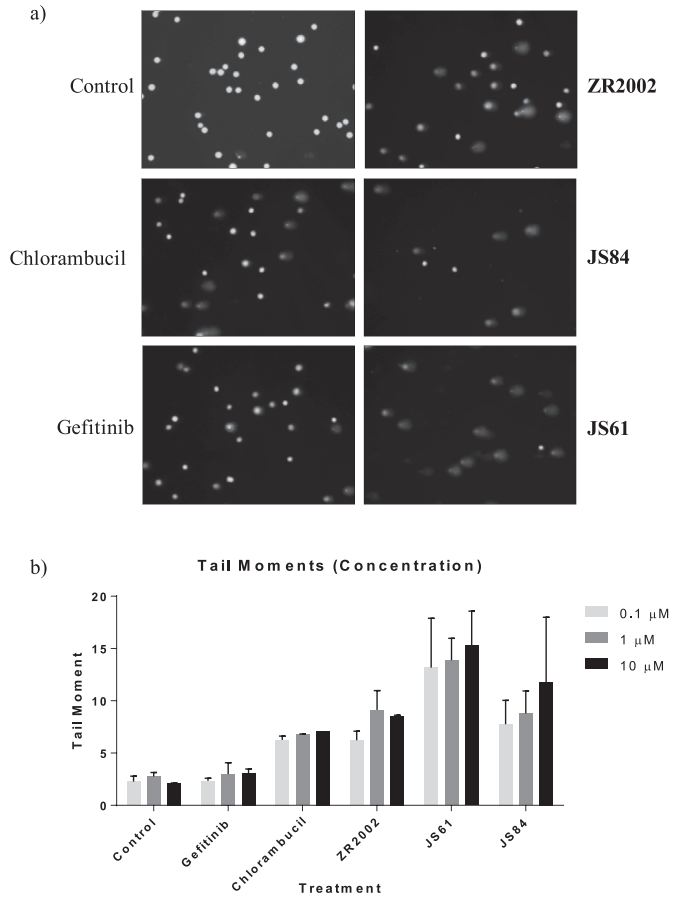

Fig. 5. a) Photographic representations of comets induced by chlorambucil, gefitinib, **ZR2002**, **JS84** and **JS61** at 0.1 μM in A549 cells with 2 h of treatment. b) Quantitative analysis of comet tails induced at 0.1 μM, 1 μM and 10 μM in A549 cells with 2 h of treatment.

the crystal structures of the three compounds **ZR2002**, **JS84** and **JS61** (Fig. 8). Given that the mechanism of irreversibility is based on the positioning of the chloroethyl group with respect to the cysteine residue of the ATP binding pocket of EGFR, attention was focused on the orientation of the latter group in the crystal structure. Interestingly, each of these three compounds assumes a distinct conformation (Fig. 9). One of the chloroethyl group of **JS61** adopted an orientation similar to that of **ZR2002**. By contrast, in **JS84**, the chloroethyl group is pointed in an opposite direction when compared with the other two structures.

To explain why **ZR2002** and **JS61** can form a covalent bond with EGFR while **JS84** does not, PDB crystal structures of EGFR inhibitors covalently bound to Cys773 (PDB codes 2J5E, 2J5F, 4LQM and 4LRM) were used to examine the conformations of the reactive side chain covalently bound to Cys773. Overlaying the four PDB complexes on the hinge residues (Fig. 10) shows that all the reactive chains adopt an orientation pointing towards the reactive Cys773 residue, with a C6–C7–N–C torsion angle < ±90°. Molecular modeling was used to create *in-situ* models of complexes where the reactive chain is pointing away from Cys773. These models suggest that ligand conformations where the reactive chain is pointing away from Cys773 (C6–C7–N–C torsion angle > ±90°) are far less likely to react with Cys773 than ligand positions where the reactive tail points towards Cys773 (C6–C7–N–C torsion angle < ±90°). Thus, ligands where the reactive chain points towards Cys773 (C6–C7–N–C torsion angle < ±90°) can react with Cys773 and bind irreversibly, whereas ligand poses where the reactive chain points away from Cys773 (C6–C7–N–C torsion angle > ±90°) cannot react with Cys773, and only bind reversibly.

Table 2
EGFR binding assay.

Compound	IC_{50} (μM)
Gefitinib	0.031
ZR2002 [23]	0.010
JS84	0.504
JS61	1.257

The small-molecule crystal structures of **ZR2002, JS61** and **JS84** were compared with the conformations of the covalently bound EGFR inhibitors. The X-ray structures of **ZR2002** and **JS84** were overlaid on the quinazoline core of the 2J5F ligand (Fig. 11). The overlay of **ZR2002** with 2J5F (Fig. 11A, magenta structure) shows that it can adopt the critical conformation required for the reaction with Cys773; the reactive chain points towards Cys773 in a manner similar to the X-ray ligand and the C6–C7–N–C torsion angle is < ±90°. By contrast, the overlay of **JS84** with 2J5F (Fig. 11B, orange structure) shows the reactive chain pointing away from Cys773 with a C6–C7–N–C torsion angle > ±90; this is the incorrect orientation for reaction with Cys773. Thus, if we assume the X-ray conformations of **ZR2002** and **JS84** are representative of their solution phase conformational preferences, the lack of irreversible binding exhibited by **JS84** can be explained via conformational biasing in **JS84** which prevents the reactive chain from adopting a conformation conducive for reaction with Cys773. The presence of the additional methyl group in **JS84** appears to lock the reactive chain into an orientation unfavorable for reaction with Cys773. The compound **JS61** is an irreversible binder because it has two chloroalkyl groups, and at least one of these chloroalkyl groups will point towards Cys773 and react with it regardless.

3. Conclusion

The purpose of this study was primarily to determine the effect of adding a second 2-chloroethyl substituent moiety on the potency of the type II combi-molecule of the aminoquinazoline class. The study conclusively demonstrated that the formation of a mustard directly grafted onto the quinazoline moiety, while increasing DNA damaging potential, affected the EGFR targeting potency in a rather complex way. Indeed, **JS61** was shown to be more potent in the Comet assay, whereas its potency was not recapitulated regarding growth inhibition when compared with hemi-mustard combi-molecules **JS84** and **ZR2002**. This may be explained by its moderate EGFR inhibitory potency, which in contrast to its hemi-mustard counterparts, is not strong enough to synergize with its DNA damaging function. Accordingly, chlorambucil that does not possess an EGFR inhibitory moiety, is less potent than **JS61**; its mustard quinazoline counterpart. Furthermore, in contrast to **JS84**, **JS61** is capable of maintaining an irreversible mechanism of action due to the ability of at least one of the two chloroethyl moieties to adopt the reactive conformation. Finally, it is important to mention that acute toxicity studies showed that despite its strong DNA damaging potential, **JS61** (MTD: 150 mg/kg, see Supporting Information) was as well tolerated as its hemi-mustard counterparts **JS84** (MTD 150 mg/kg) and **ZR2002** (MTD 150 mg/kg) [26], which warrants further *in vivo* studies.

4. Experimental section

4.1. General procedures

All chemicals were of the best commercially available grade and

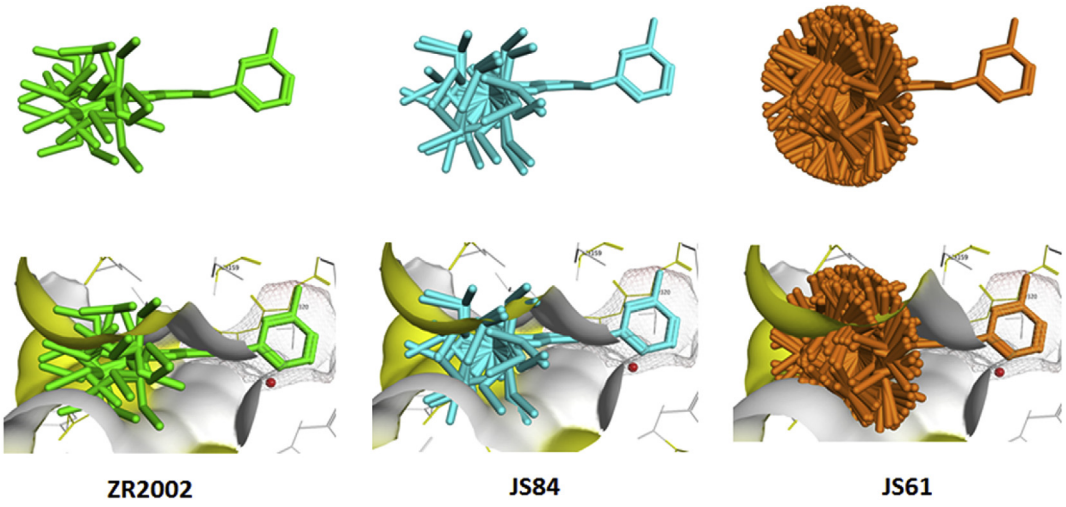

Fig. 6. Conformation ensembles of **ZR2002**, **JS84**, **JS61** in the EGFR ATP binding pocket. Conformational ensembles of **ZR2002**, **JS84** and **JS61** superimposed on their anilinoquinazoline cores are shown in free-space and overlaid in the EGFR binding pocket (PDB code 2ITY). The VDW interaction surfaces drawn around the binding pockets indicate the onset of steric clash. These VDW surfaces are colored yellow and white to indicate pocket regions formed by backbone and sidechain atoms respectively. Conformations that penetrate the interaction VDW surface would clash with the EGFR pocket. (For interpretation of the references to color in this figure legend, the reader is referred to the Web version of this article.)

used without further purification. All chemicals were purchased from Sigma Aldrich excepted for the starting material 5-fluoro-2-nitrobenzonitrile purchased from ArkPharm. Anhydrous solvents were purchased from Aldrich Chemicals. The conversion of starting materials was monitored by thin-layer chromatography (TLC) using silica gel plates (silica gel 60 F_{254} and visualization when required was achieved using UV light (254 and 365 nm). Column chromatography was performed with silica (Aldrich 60, 230–400 mesh). NMR spectra were recorded at the ambient probe temperature using Bruker 400 spectrometers. Chemical shifts are quoted as parts per million (ppm) relative to the residual peak of solvent and coupling constants (J) are quoted in Hertz (Hz). Where assignments of ^{1}H NMR spectra are given, they have been unambiguously established via COSY and HSQC experiments. In the assignments, the chemical shift (in ppm) is given first, followed, in brackets, by the multiplicity of the signal (s: singlet, d: doublet, t: triplet, m: multiplet, br s: broad signal), the value of the coupling constants in hertz if applicable, the number of protons implied, and finally the assignment. Mass spectra were obtained by using an Amazon spectrometer (ES-MS) and a Q-TOF Impact II instrument with internal calibration. RB10 has been synthesized according to a previous publication [32].

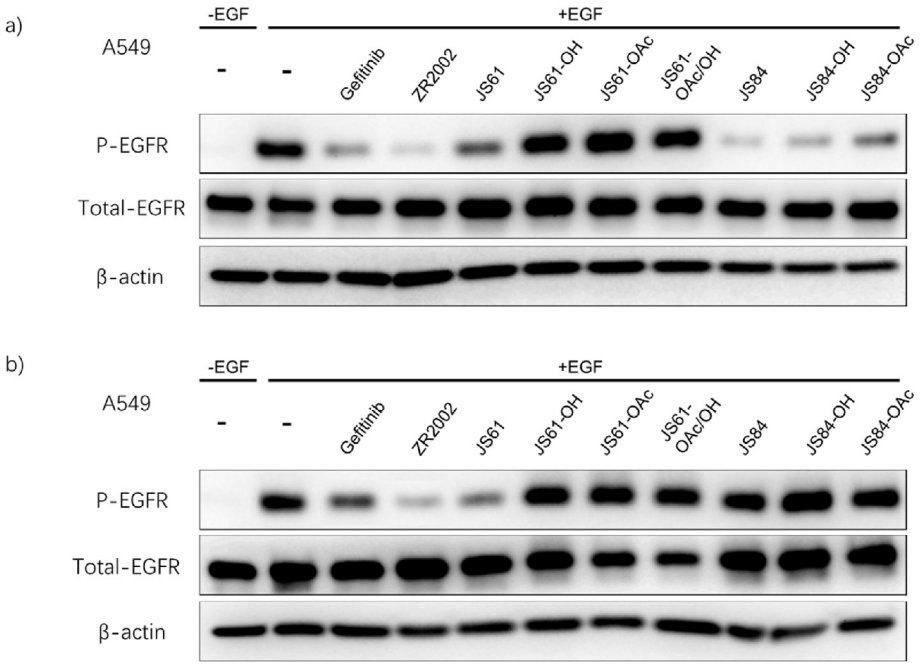

Fig. 7. Reversibility of EGFR phosphorylation of all compounds in A549 cell line by Western Blot. In (a), cells were treated with 2 μM of each compound for 2 h, EGF-stimulated and immunodetected using anti-phospho EGFR antibody. In (b), reversibility was assessed by cell treatment with drug for 2 h, removing and replacing with serum free medium every 2 h. Thereafter, this sequence was repeated three times prior to EGF stimulation.

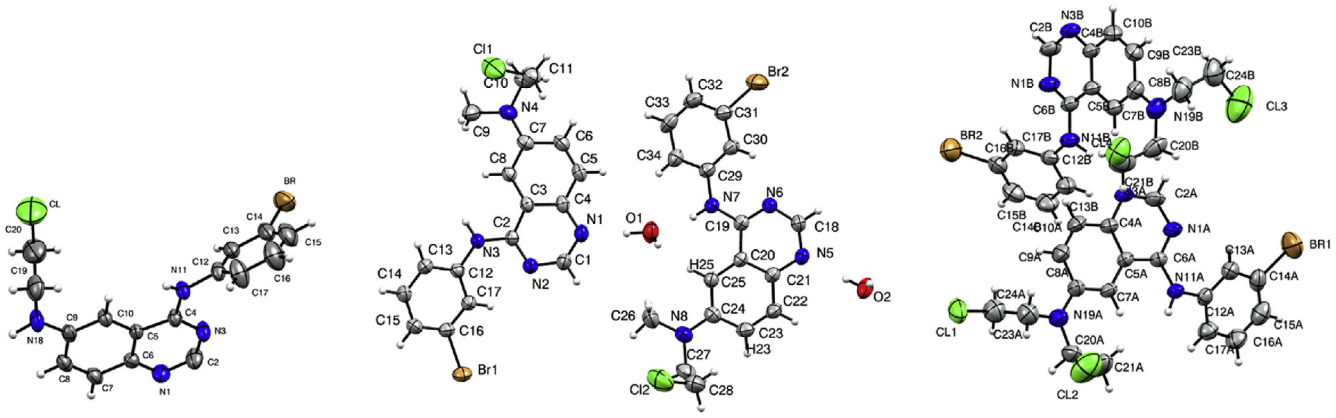

Fig. 8. X-ray structures of compound **ZR2002** *(left)*, **JS84** *(middle)* and **JS61** *(right)*, as presented in the asymmetric units.

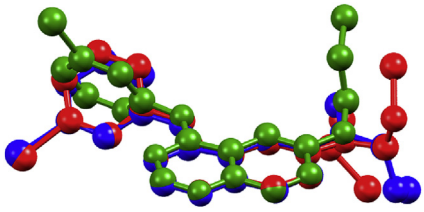

Fig. 9. Superimposition of the three crystal structures of **ZR2002** (green), **JS61** (red) and **JS84** (blue). (For interpretation of the references to color in this figure legend, the reader is referred to the Web version of this article.)

*4.1.1. 5-(bis(2-hydroxyethyl)amino)-2-nitrobenzonitrile (**1**)*

5-fluoro-2-nitrobenzonitrile (1 equiv, 500 mg, 3.01 mmol), diethanolamine (1.2 equiv, 380 mg, 3.61 mmol) and Cs_2CO_3 (1.2 equiv, 1.18 g, 3.61 mmol) were combined in DMSO (6 mL) and the reaction mixture was stirred at 100 °C overnight. The solution was cooled to room temperature, EtOAc (250 mL) was added and the solution was washed with a saturated $NaHCO_3$ solution (3 × 75 mL) and brine solution (1 × 75 mL). The organic layer was dried over Na_2SO_4, filtered and evaporated to dryness. The product was purified by silica gel column chromatography (DCM/MeOH 5%) to afford compound **1** as an orange solid in 82% yield (620 mg). ^{1}H NMR (DMSO-d_6, 400 MHz, 298K): δ = 8.13 (d, J_2 = 9.7 Hz, 1H, H_2), 7.34 (d, J_1 = 2.9 Hz, 1H, H_3), 7.08 (dd, J_1 = 2.9 Hz, J_2 = 9.7 Hz, 1H, H_1), 4.88 (s, 2H, H_6), 3.61 (s, 8H, H_4, H_5). ^{13}C NMR (DMSO-d_6, 100 MHz, 298K): δ = 152.81, 134.09, 127.78, 117.74, 114.08, 108.95, 99.49, 58.00, 53.04 ppm. ES-MS (ESI): *m/z* (%) 274.19 (100) $[M+Na]^+$

*4.1.2. 2-Amino-5-(bis(2-hydroxyethyl)amino)benzonitrile **(2)***

Compound **1** (1 equiv, 620 mg, 2.47 mmol) was suspended in aqueous EtOH (70 mL)/Water (30 mL). Iron (7 equiv, 965 mg, 17.27 mmol) and CH_3COOH (14 equiv, 1.98 mL, 34.58 mmol) were added and the reaction was stirred at 100 °C for 2 h. The solution was cooled to room temperature and EtOH was evaporated under reduced pressure. EtOAc (100 mL) and saturated $NaHCO_3$ solution (100 mL) were added. The aqueous phase was extracted with EtOAc (3 × 100 mL) and the combined organic layer was dried over Na_2SO_4, filtered and evaporated to dryness. Good product was obtained as an orange solid in 86% yield (470 mg) and was used without any further purification. ^{1}H NMR (DMSO-d_6, 400 MHz, 298K): δ = 6.89 (dd, J_1 = 2.9 Hz, J_2 = 9.0 Hz, 1H, H_1), 6.71 (d, J_2 = 9.0 Hz, 1H, H_2), 6.65 (d, J_1 = 3.1 Hz, 1H, H_4), 5.18 (br s, 2H, H_3), 4.65 (t, J = 5.5 Hz, 2H, H_7), 3.46 (q, J = 6.2 Hz, 4H, H_6), 3.27 (t, J = 6.2 Hz, 4H, H_5). ^{13}C NMR (DMSO-d_6, 100 MHz, 298K): δ = 142.69, 139.76, 120.65, 118.74, 117.11, 113.53, 94.64, 58.33, 53.67 ppm. ES-MS (ESI): *m/z* (%) 222.06 (100) $[M+H]^+$

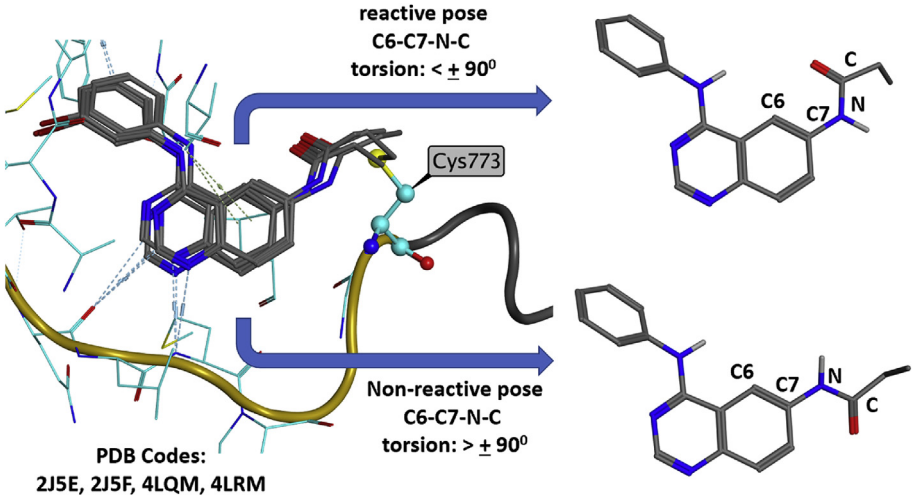

Fig. 10. Overlay of PDB complexes 2J5E, 2J5F, 4LQM and 4LRM show that the reactive sidechain adopts an orientation pointing towards the Cys773 (C6–C7–N–C torsion angle < ±90°). Reactive chain orientations pointing away from Cys773 (C6–C7–N–C torsion angle > ±90°) are far less favorable for reaction.

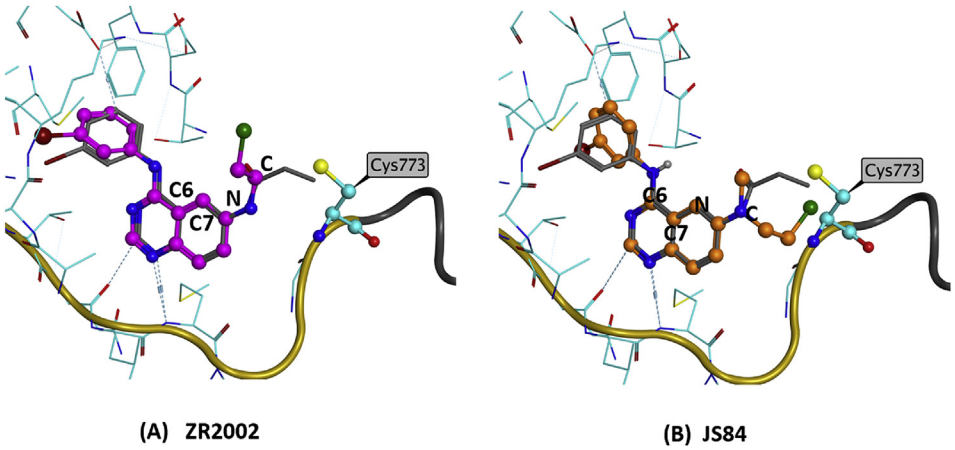

Fig. 11. Small molecule crystal structures of **ZR2002** (**A**, magenta) and **JS84** (**B**, orange) overlaid on the quinazoline core of the covalently bound ligand in PDB code 2J5F (grey) (**A**) The x-ray conformation of the **ZR2002** chloroalkyl sidechain allows for reaction with Cys773. (**B**) The x-ray conformation of the **JS84** chloroalkyl sidechain does not allow for reaction with Cys773. (For interpretation of the references to color in this figure legend, the reader is referred to the Web version of this article.)

*4.1.3. (E)-N'-(4-(bis(2-hydroxyethyl)amino)-2-cyanophenyl)-N,N-dimethylformimidamide **(3)***

Compound **2** (292 mg, 1.32 mmol) was suspended in DMF-Dimethylacetal (5 mL) and the reaction was stirred at 110 °C for 2 h. DMF-Dimethylacetal was then evaporated and the product was purified by silica gel column chromatography eluted with a gradient (DCM/MeOH 2%–8%) to afford compound **3** as a yellow solid in 75% yield (274 mg). ^{1}H NMR (DMSO-d_6, 400 MHz, 298K): δ = 7.77 (s, 1H, H_3), 6.97 (d, J_2 = 9.0 Hz, 1H, H_2), 6.90 (dd, J_1 = 3.1 Hz, J_2 = 9.0 Hz, 1H, H_1), 6.82 (d, J = 2.9 Hz, 1H, H_6), 4.72 (t, J = 5.5 Hz, 2H, H_9), 3.50 (q, J = 6.4 Hz, 4H, H_8), 3.37 (t, J = 6.1 Hz, 4H, H_7), 3.01 (s, 3H, H_4 or H_5), 2.93 (s, 3H, H_4 or H_5). ^{13}C NMR (DMSO-d_6, 100 MHz, 298K): δ = 153.42, 144.10, 143.32, 119.77, 119.26, 117.87, 113.91, 106.09, 58.14, 53.25. ppm. ES-MS (ESI): *m/z* (%) 277.15 (100) $[M+H]^+$

Synthesis of compounds **4a**, **4b** and **4c**. Compound **3** (1 equiv, 274 mg, 0.99 mmol) and 3-bromoaniline (1.1 equiv, 119 μL, 1.09 mmol) were solubilized in CH_3COOH (2 mL) and the reaction was stirred at 120 °C for 1 h. The solvent was evaporated, and the residue was purified by silica gel column chromatography eluted with a gradient (DCM/MeOH 4%–8%) to afford compounds **4a**, **4b** and **4c** as yellow solids in respectively 35% (139 mg), 16% (75 mg) and 40% (175 mg) yield.

*4.1.4. 2,2'-((4-((3-bromophenyl)amino)quinazolin-6-yl)azanediyl) bis(ethan-1-ol) **(4a)***

^{1}H NMR (DMSO-d_6, 400 MHz, 298K): δ = 9.45 (s, 1H, H_4), 8.36 (s, 1H, H_3), 8.09 (t, J = 1.8 Hz, 1H, H_5), 7.87 (d, J = 7.9 Hz, 1H, H_8), 7.62 (d, J = 9.3 Hz, 1H, H_2), 7.47 (dd, J_1 = 2.4 Hz, J_2 = 9.3 Hz, 1H, H_1), 7.36 (t, J = 7.9 Hz, 1H, H_7), 7.31 (d, J = 2.4 Hz, 1H, H_9), 7.28 (d, J = 7.9 Hz, 1H, H_6), 4.79 (br m, 2H, H_{12}), 3.63 (br s, 8H, H_{10}, H_{11}). ^{13}C NMR (DMSO-d_6, 100 MHz, 298K): δ = 52.99, 58.20, 98.86, 103.10, 121.14, 124.48, 125.67, 128.70, 130.27, 141.34, 141.91, 146.80, 149.70, 155.74 ppm. HR-MS (ESI): *m/z* calculated for $C_{18}H_{19}BrN_4O_2$ $[M+H]^+$ 403.0764. Found: $[M+H]^+$ 403.0773.

*4.1.5. ((4-((3-bromophenyl)amino)quinazolin-6-yl)azanediyl) bis(ethane-2,1-diyl) diacetate **(4b)***

^{1}H NMR (DMSO-d_6, 400 MHz, 298K): δ = 9.43 (s, 1H, H_4), 8.41 (s, 1H, H_3), 8.13 (t, J = 2.0 Hz, 1H, H_5), 7.88 (d, J = 8.1 Hz, 1H, H_8), 7.67 (d, J = 9.3 Hz, 1H, H_2) 7.55 (dd, J_1 = 2.4 Hz, J_2 = 9.3 Hz, 1H, H_1), 7.41 (d, J = 2.3 Hz, 1H, H_9),7.37 (t, J = 8.1 Hz, 1H, H_7), 7.30 (d, J = 7.5 Hz, 1H, H_6), 4.25 (t, J = 5.7 Hz, 4H, H_{11}), 3.80 (t, J = 5.7 Hz, 4H, H_{10}), 1.99 (s, 6H, H_{12}). ^{13}C NMR (DMSO-d_6, 100 MHz, 298K): δ = 170.43, 155.86, 150.30, 145.95, 142.42, 141.20, 130.34, 128.90, 125.77, 124.41, 121.02, 116.16, 99.85, 61.11, 49.02, 20.69 ppm. HR-MS (ESI): *m/z* calculated for $C_{22}H_{23}BrN_4O_2$ $[M+H]^+$ 487.0986. Found: $[M+H]^+$ 487.0975.

*4.1.6. 2-((4-((3-bromophenyl)amino)quinazolin-6-yl) (2-hydroxyethyl)amino)ethyl acetate **(4c)***

^{1}H NMR (DMSO-d_6, 400 MHz, 298K): δ = 9.43 (s, 1H, H_4), 8.39 (s, 1H, H_3), 8.12 (t, J = 2.0 Hz, 1H, H_5), 7.86–7.89 (m, 1H, H_8), 7.64 (d, J = 9.3 Hz, 1H, H_2), 7.51 (dd, J_1 = 2.7 Hz, J_2 = 9.3 Hz, 1H, H_1), 7.34–7.38 (m, 2H, H_7), 7.28–7.30 (m, 1H, H_6), 4.76 (br s, 1H, H_{12}), 4.26 (t, J = 6.0 Hz, 2H, H_{14}), 3.81 (t, J = 6.0 Hz, 2H, H_{13}), 3.62 (br s, 4H, H_{10}, H_{11}), 2.00 (s, 3H, H_{15}). ^{13}C NMR (DMSO-d_6, 100 MHz, 298K): δ = 170.45,155.77, 149.99, 146.38, 142.15, 141.26, 130.30, 128.80, 125.70, 124.41, 121.04, 116.26, 99.28, 61.07, 58.19, 52.76, 21.11, 20.73 ppm. HR-MS (ESI): *m/z* calculated for $C_{20}H_{21}BrN_4O_3$ $[M+H]^+$ 445.0870. Found: $[M+H]^+$ 445.0877.

*4.1.7. N^4-(3-bromophenyl)-N^6,N^6-bis(2-chloroethyl)quinazoline-4,6-diamine **(JS61)***

Compound **4a** (50 mg, 124 μmol) was solubilized in $POCl_3$ (0.5 mL) and the reaction mixture was heated to reflux (110 °C) for 2 h. The solvent was evaporated, and the product was purified by silica gel column chromatography eluted with a gradient (DCM/MeOH 1%–4%) to afford a yellow solid which was dissolved in EtOH. Dry K_2CO_3 was then added until the pH turned basic (colorless solution). The solution was then filtered, and the solvent evaporated to afford a yellow solid which was triturated several times with water. The solid was then dissolved in DCM and the organic solution was dried over Na_2SO_4, filtered and evaporated to afford **JS61** as a yellow solid in 75% yield (41 mg). ^{1}H NMR (DMSO-d_6, 400 MHz, 298K): δ = 9.64 (s, 1H, H_4), 8.44 (s, 1H, H_3), 8.09 (s, 1H, H_5), 7.84 (d, J = 7.6 Hz, 1H, H_8), 7.69 (d, J = 9.3 Hz, 1H, H_2), 7.54 (dd, J_1 = 2.3 Hz, J_2 = 9.3 Hz, 1H, H_1), 7.46 (d, J = 2.4 Hz, 1H, H_9), 7.38 (t, J = 7.9 Hz, 1H, H_7), 7.32 (d, J = 7.8 Hz, 1H, H_6), 3.95 (t, 4H, J = 6.4 Hz H_{10} or H_{11}), 3.84 (t, J = 6.2 Hz, 4H, H_{10} or H_{11}). ^{13}C NMR (DMSO-d_6, 100 MHz, 298K): δ = 156.01, 150.59, 145.13, 142.76, 141.14, 130.31, 129.14, 125.84, 124.56, 121.30, 121.20, 121.08, 116.20, 100.52, 51.90, 41.35 ppm. HR-MS (ESI): *m/z* calculated for $C_{18}H_{17}BrCl_2N_4$ $[M+H]^+$ 439.0086. Found: $[M+H]^+$ 439.0088.

*4.1.8. 5-((2-hydroxyethyl) (methyl)amino)-2-nitrobenzonitrile (**6**)*

5-fluoro-2-nitrobenzonitrile (1 equiv, 100 mg, 602 μmol), 2-methylamine ethanol (1.20 equiv, 55 mg, 723 μmol) and Cs_2CO_3

(1.20 equiv, 235 mg, 723 μmol) were combined in DMSO (2 mL) and the reaction mixture was stirred at 100 °C overnight. The solution was cooled to room temperature, EtOAc (50 mL) was added and the organic layer was washed with a saturated $NaHCO_3$ solution (3 × 15 mL) and brine solution (1 × 15 mL). The organic layer was dried over Na_2SO_4, filtered and evaporated to dryness. The residue was purified by silica gel column chromatography (DCM/MeOH 3%) to afford compound **6** as an orange solid in 91% yield (121 mg). ^{1}H NMR (DMSO-d_6, 400 MHz, 298K): δ = 8.16 (d, J = 9.7 Hz, 1H, H_2), 7.31 (d, J = 2.9 Hz, 1H, H_3), 7.04 (dd, J_1 = 2.9 Hz, J_2 = 9.7 Hz, 1H, H_1), 4.82–4.85 (m, 1H, H_6), 3.60–3.61 (m, 4H, H_4–H_5), 3.12 (s, 3H, H_7). ^{13}C NMR (DMSO-d_6, 100 MHz, 298K): δ = 127.79, 117.57, 113.90, 108.92, 58.18, 54.06 ppm. ES-MS (ESI): *m/z* (%) 244.01 (100) $[M+Na]^+$

4.1.9. 2-Amino-5-((2-hydroxyethyl) (methyl)amino)benzonitrile (**7**)

Compound **6** (1 equiv, 121 mg, 547 μmol) was suspended in aqueous EtOH (7 mL)/Water (3 mL). Iron (6.4 equiv, 196 mg, 3.51 mmol) and CH_3COOH (14 equiv, 438 μL, 7.66 mmol) were added and the reaction was stirred at 100 °C for 2 h. The solution was cooled to room temperature and EtOH was evaporated under reduced pressure. EtOAc (10 mL) and saturated $NaHCO_3$ solution (10 mL) were added. The aqueous phase was extracted with EtOAc (3 × 10 mL) and the combined organic layer was dried over Na_2SO_4, filtered and evaporated to dryness. Good product was obtained as an orange solid in 98% yield (103 mg) and was used without any further purification. ^{1}H NMR (DMSO-d_6, 400 MHz, 298K): δ = 6.93 (dd, J_1 = 2.9 Hz, J_2 = 9.0 Hz, 1H, H_1), 6.73 (d, J = 9.0 Hz, 1H, H_2), 6.66 (d, J = 2.7 Hz, 1H, H_4), 5.29 (br s, 2H, H_3), 4.59 (br s, 1H, H_7), 3.48 (t, J = 6.2 Hz, 2H, H_6), 3.22 (t, J = 6.2 Hz, 2H, H_5), 2.79 (s, 3H, H_8). ^{13}C NMR (DMSO-d_6, 100 MHz, 298K): δ = 143.28, 141.09, 121.36, 118.69, 117.03, 114.11, 94.41, 58.09, 55.34 ppm. ES-MS (ESI): *m/z* (%) 192.03 (100) $[M+H]^+$

4.1.10. (E)-N'-(2-cyano-4-((2-hydroxyethyl) (methyl)amino) phenyl)-N,N-dimethylformimidamide (***8***)

Compound **7** (103 mg, 539 μmol) was suspended in DMF-Dimethylacetal (2 mL) and the reaction was stirred at 110 °C for 1.5 h. DMF-Dimethylacetal was then evaporated and the product was purified by silica gel column chromatography eluted with a gradient (DCM/MeOH 1%–4%) to afford compound **8** as a yellow solid in 64% yield (85 mg). ^{1}H NMR (DMSO-d_6, 400 MHz, 298K): δ = 7.79 (s, 1H, H_3), 6.99 (d, J = 8.9 Hz, 1H, H_2), 6.92 (dd, J_1 = 3.1 Hz, J_2 = 9.2 Hz, 1H, H_1), 6.81 (d, J = 2.9 Hz, 1H, H_6), 4.64 (t, J = 5.5 Hz, 1H, H_9), 3.51 (q, J = 6.2 Hz, 2H, H_8), 3.33 (t, J = 6.0 Hz, 2H, H_7), 3.01 (s, 3H, H_4 or H_5), 2.93 (s, 3H, H_4 or H_5), 2.88 (s, 3H, H_{10}). ^{13}C NMR (DMSO-d_6, 100 MHz, 298K): δ = 153.48, 144.57, 144.46, 119.67, 119.22, 118.38, 114.38, 106.00, 58.06, 54.53 ppm. ES-MS (ESI): *m/z* (%) 247.10 (100) $[M+H]^+$

Synthesis of **9a** and **9b**. Compound **8** (1 equiv, 601 mg, 2.44 mmol) and 3-bromoaniline (1.1 equiv, 292 μL, 2.68 mmol) were solubilized in CH_3COOH (3.5 mL) and the reaction was stirred at 115 °C for 1 h. The solvent was evaporated, and the products were purified by silica gel column chromatography eluted with a gradient (DCM/MeOH 1%–4%) to afford compound **9a** and **9b** as yellow solids in respectively in 36% (326 mg) and 35% (354 mg) yield.

4.1.11. 2-((4-((3-bromophenyl)amino)quinazolin-6-yl) (methyl) amino)ethan-1-ol (***9a***)

^{1}H NMR (DMSO-d_6, 400 MHz, 298K): δ = 9.48 (s, 1H, H_4), 8.39 (s, 1H, H_3), 8.14 (t, J = 1.8 Hz, 1H, H_5), 7.90 (d, J = 8.2 Hz, 1H, H_8), 7.63 (d, J = 9.3 Hz, 1H, H_2), 7.50 (dd, J_1 = 2.4 Hz, J_2 = 9.2 Hz, 1H, H_1), 7.35 (t, J = 8.1 Hz, 1H, H_7), 7.31 (d, J = 2.4 Hz, 1H, H_9), 7.28 (d, J = 7.8 Hz, 1H, H_6), 4.72 (t, J = 4.9 Hz, 1H, H_{12}), 3.57–3.63 (m, 4H, H_{10}, H_{11}), 3.11 (s, 3H, H_{13}). ^{13}C NMR (DMSO-d_6, 150 MHz, 298K): δ = 155.74, 149.81, 147.86, 142.17, 141.37, 130.25, 128.56, 125.53, 124.17, 121.36, 121.08, 120.80, 116.27, 99.38, 58.27, 54.12. ppm. HR-MS (ESI): *m/z* calculated for $C_{17}H_{17}BrN_4O_1$ $[M+H]^+$ 373.0665. Found: $[M+H]^+$ 373.0658.

4.1.12. 2-((4-((3-bromophenyl)amino)quinazolin-6-yl) (methyl) amino)ethyl acetate (***9b***)

^{1}H NMR (DMSO-d_6, 400 MHz, 298K): δ = 9.48 (s, 1H, H_4), 8.42 (s, 1H, H_3), 8.15 (t, J = 2.0 Hz, 1H, H_5), 7.90 (d, J = 7.9 Hz, 1H, H_8), 7.66 (d, J = 9.3 Hz, 1H, H_2), 7.53 (dd, J_1 = 2.7 Hz, J_2 = 9.3 Hz, 1H, H_1), 7.34–7.38 (m, 2H, H_7, H_9), 7.28 (d, J = 8.6 Hz, 1H, H_6), 4.25 (t, J = 5.7 Hz, 2H, H_{11}), 3.79 (t, J = 5.6 Hz, 2H, H_{10}), 3.10 (s, 3H, H_{13}), 1.93 (s, 3H, H_{12}). ^{13}C NMR (DMSO-d_6, 150 MHz, 298K): δ = 155.85, 150.14, 147.42, 142.43, 141.32, 130.31, 128.67, 125.63, 124.21, 121.32, 121.12, 120.83, 116.21, 99.92, 61.17, 50.26, 20.65 ppm. HR-MS (ESI): *m/z* calculated for $C_{19}H_{19}BrN_4O_2$ $[M+H]^+$ 415.0775. Found: $[M+H]^+$ 415.0764.

4.1.13. N^4-(3-bromophenyl)-N^6-(2-chloroethyl)-N^6-methylquinazoline-4,6-diamine (***JS84***)

Compound **9a** (168 mg, 452 μmol) was dissolved in $POCl_3$ (2 mL) and the reaction mixture was heated to reflux (110 °C) for 2 h. The solvent was evaporated, and the product was purified by silica gel column chromatography eluted with a gradient (DCM/MeOH 1%–5%) to afford a yellow solid, which was dissolved in EtOH. Dry K_2CO_3 was then added until the pH turned basic (colorless solution). The solution was then filtered, and the solvent evaporated to afford a yellow solid, which was triturated several times with water. The solid was then dissolved in DCM and the organic solution was dried over Na_2SO_4, filtered and evaporated to afford **JS84** as a yellow solid in 54% yield (115 mg). ^{1}H NMR (DMSO-d_6, 400 MHz, 298K): δ = 9.52 (s, 1H, H_4), 8.42 (s, 1H, H_3), 8.14 (t, J = 1.8 Hz, 1H, H_5), 7.98 (d, J = 8.6 Hz, 1H, H_8), 7.67 (d, J = 9.2 Hz, 1H, H_2), 7.54 (dd, J_1 = 2.6 Hz, J_2 = 9.3 Hz, 1H, H_1), 7.39 (d, J = 2.6 Hz, 1H, H_9), 7.36 (t, J = 8.1 Hz, 1H, H_7), 7.29 (d, J = 8.3 Hz, 1H, H_6), 3.82–3.91 (m, 4H, H_{10}, H_{11}), 3.14 (s, 3H, H_{12}). ^{13}C NMR (DMSO-d_6, 150 MHz, 298K): δ = 155.92, 150.24, 147.11, 142.54, 141.28, 130.27, 128.77, 125.64, 124.27, 121.30, 121.09, 120.89, 116.19, 100.16, 53.14, 41.67, 38.92 ppm. HR-MS (ESI): *m/z* calculated for $C_{17}H_{16}BrClN_4$ $[M+H]^+$ 391.0320. Found: $[M+H]^+$ 391.0320.

4.1.14. N^4-(3-bromophenyl)-N^6-(2-chloroethyl)quinazoline-4,6-diamine (***ZR2002***)

RB10 (1 equiv, 500 mg, 1.59 mmol) was solubilized in MeOH (30 mL) and chloroacetaldehyde (2 equiv, 360 μL, 3.17 mmol) was added. HCl 6 M in MeOH (280 μL) was added followed by $NaBH_3CN$ (1.5 equiv, 150 mg, 2.18 mmol). The resulting mixture was stirred at r. t. overnight. The solvent was evaporated, and the product was purified by silica gel column chromatography eluted with 3% MeOH in DCM to afford **ZR2002** in 86% (518 mg). The characterizations are similar as already described in the literature.

4.1.15. Cell culture

A549, PC-9 and H1975 were purchased from ATCC. A549 was maintained in DMEM (Wisent) containing 10% FBS (Wisent), supplemented with 12.5 mL of HEPES buffer (Wisent) and 500 μL of gentamycin (Wisent), 250 μL of amphotericin B (Wisent) and 170 μL of ciprofloxacin (Fluka) as antibiotics. PC-9 and H1975 were maintained in RPMI 1640 (Wisent) containing 10% FBS (Wisent) and identical additives. All cells lines were maintained in a humidified incubator at 37 °C with 5% CO_2.

4.1.16. Sulforhodamine B (SRB) growth Inhibition assay

The assessment for growth inhibition proceeded as follows. Briefly, cells were seeded with a volume of 100 μL into 96 well

plates (Corning) at a concentration of 5000 cells/well and left to attach in a humidified incubator at 37 °C with 5% CO_2 overnight. Cells were treated with 100 μL of various drugs in media at differing dose ranges and stored in the incubator for 5 days. Cells were then fixed using 50 μL of 50% trichloroacetic acid (Alfa Aesar) for 2 h at 4 °C, subsequently rinsed with water and left to dry overnight. The cells were stained with 50 μL of 0.4% SRB solution (Alfa Aesar) for 1h at room temperature, subsequently rinsed with 1% (v/v) acetic acid (Alfa Aesar) and left to dry overnight. Dissolution of the colored complex was achieved using 200 μL of 10 mM Tris base (Fisher Scientific) and optical density was measured with a Tecan Infinite 200Pro plate reader (Serial No. 1412003451) at a wavelength of 490 nm.

4.1.17. In vitro alkylation with calf thymus DNA

Briefly, 45 mg of calf thymus DNA (Amersham Pharmacia Biotech Inc.) was vortexed and sonicated in 4.5 mL of 10 mM potassium phosphate buffer at pH 6.85 (Fisher). To each tube, 10 mM of 500 μL of corresponding treatment dissolved in DMSO (Fisher) was added. The mixture was left in a humidified incubator at 37 °C and 5% CO_2 for a period of five days. After incubation, 500 μL of 3 M sodium acetate (Fisher) and 12.5 mL of absolute ethanol (Commercial Alcohols) were added to each sample and vortexed. The mixture was centrifuged at 3900 rpm for 30 min and the supernatant discarded. The pellet was resuspended in 5 mL of 10 mM potassium phosphate buffer and 5 mL of n-butanol (Fisher). The resulting suspension was vortexed and placed in a heating block set at 100 °C for 10 min. Once the sample had reached room temperature, the n-butanol fraction was collected in a separate tube. This thermal cleavage was carried out twice more with 5 mL of fresh n-butanol each time and the fractions of n-butanol were pooled. Samples were then centrifuged once more, decanted to remove any residual water and evaporated to dryness using the heating block (S/N: 003N0332). Samples were stored at −20 °C until further analysis. For LC-MS/MS analysis, LC-MS grade solvents, acetonitrile, formic acid and water were obtained from EMD Millipore. Ammonium acetate was obtained from VWR. Analyses were performed at the Drug Discovery Platform at the Research Institute of the McGill University Health Centre on an ESI-QTOF-MS system (Impact II, Bruker, Billerica, MA) coupled with a liquid chromatography system (1290 Infinity, Agilent) and equipped with a reversed-phase InertSustain AQ-C18 column (100 × 2.1 mm, 3 μm) GL Sciences Inc. Mobile phases were 50 mM ammonium acetate in water with 0.1% formic acid (A) and acetonitrile with 0.1% formic acid (B). The following gradient elution method was used: 5% B from 0 to 1 min, 5−60% B from 1 to 12 min, a 60% B plateau for 12−16 min, 60−80% B from 16 to 20 min, an 80% B plateau for 3 min and returning to initial conditions with an equilibration for 2 min. Column temperature was set at 25 °C and the flow rate was 0.4 mL/min. The samples were kept in an autosampler at 4 °C. The ESI source was operated in positive ion mode. The operating parameters of the mass spectrometer were positive spray voltage 4000V, dry temperature 250 °C, dry gas flow 10 L/min, nebulizer 3 bar. The data were collected in an auto MS/MS mode with a mass range from 50 to 3000 *m*/*z*. The instrument was calibrated using ESI-L Low concentration tuning mix solution (Agilent).

4.1.18. Alkaline Comet Assay

The assessment for DNA damage proceeded as follows. Briefly, cells were seeded with a volume of 2 mL into 6 well plates (Corning) at a concentration of 500,000 cells/well and left to attach in a humidified incubator at 37 °C with 5% CO2 overnight. Cells were treated with 1 mL of various drugs in media at different concentrations and left to incubate in the incubator for 2 h. Treatment was then removed, the cells washed with 1 mL of PBS (Wisent) and detached using 500 μL of trypsin (Wisent). Once detached, 1 mL of media was added and the cells collected. Cells were centrifuged at 1500 rpm for 5 min, the supernatant aspirated and subsequently washed in 1 mL PBS. The cells were pelleted prior to resuspension in 1 mL PBS, mixed in a 1:10 ratio with 0.7% low melting point agarose (Fisher Scientific) solution in PBS and 200 μL of the mixture was cast over agarose support film (Lonza). Once polymerized, the film was subjected to lysis overnight in the dark at 4 °C with a solution consisting of 2.5 M sodium chloride (Fisher Scientific), 100 mM tetrasodium ethylenediaminetetraacetic acid (Sigma), 10 mM Tris base (Fisher Scientific) and 35 mM of n-Lauroylsarcosine (Sigma). The protocol hereafter was performed in the dark. The films were then washed with a solution consisting of 2.5 M sodium chloride, 100 mM tetrasodium ethylenediaminetetraacetic acid and 10 mM Tris base for 1 h in a humidified incubator at 37 °C with 5% CO2. The film was then submerged into an electrophoresis buffer consisting of 300 mM sodium hydroxide (Fisher Scientific), 10 mM ethylenediaminetetraacetic acid (Sigma), 7 mM 8-hydroxyquinoline (Fisher Scientific) and 2% dimethyl sulfoxide (Fisher Scientific) for 30 min at room temperature before electrophoresis at 20 V and 0.4 mA for 20 min using cold electrophoresis buffer. The film was submerged in a solution of 1 M ammonium acetate (Alfa Aesar) for 30 min at room temperature prior to a wash with 100% ethanol (Commercial Alcohols) for 2 h at room temperature and subsequently air dried. Staining the film was accomplished using a 1:10000 solution of CYBR gold nucleic acid stain (Molecular Probes) in water for 13 min. Comets were imaged using a Leica DFC300 FX camera (Serial No. 234762307) on a Leica DM IL fluorescence microscope (Instrument No. 521228) and scored using Comet Assay IV (Precision Instruments) software.

4.1.19. EGFR kinase binding assay

The assessment for EGFR binding affinity proceeded as follows. Briefly, 100 μL/well of a 0.25 mg/mL solution of Poly Glu:Tyr 4:1 (Sigma) was plated into 96 well plates (Nunc Maxisorp) and left to incubate in a humidified incubator at 37 °C with 5% CO_2 for 48 h. The excess Poly Glu:Tyr 4:1 was removed and the wells washed with wash buffer consisting of 200 μL of 0.1% Tween 20 (Acros) in PBS (Wisent). All solutions and drug dilutions for the kinase reaction were carried out in phosphorylation buffer consisting of 50 mM HEPES (Fisher Scientific), 125 mM sodium chloride (Fisher Scientific), 24 mM of magnesium chloride (Fisher Scientific) and 10 mM of orthovanadate (Sigma). To each well, 10 μL of drug, 7.5 μL of a 100 μg/mL EGFR (Signal Chem) solution, 2.1 μL of a 100 μg/mL EGF (Sigma) solution and 20 μL of a 50 μM ATP (Sigma) solution were added in that order to commence the kinase reaction. The plate was incubated in the dark and shaken for a duration of 8 min at room temperature. The wells were washed with 200 μL of wash buffer prior to the addition of 50 μL of a 0.2 μg/mL solution of pTyr-HRP (Santa Cruz) prepared using 3% BSA (Wisent) in wash buffer to each well and thereafter incubated in the dark for 25 min 50 μL of a 1:1 ratio of peroxidase substrate and peroxidase solution B (Perry Laboratories) was then added to each well and incubated in the dark at room temperature for 10 min to allow the colorimetric reaction to occur. The reaction was stopped using 50 μL of a 0.09 M sulfuric acid (Fisher Scientific) solution, briefly shaken and optical density measured with a Tecan Infinite 200Pro plate reader (Serial No. 1412003451) at a wavelength of 450 nm.

4.1.20. Kinase profiling

Kinase profiling of **JS61** and **ZR2002** were kindly performed by Carna Biosciences Inc. (Natick, MA, USA) according to their standardized protocol. A specified subset of 25 kinases were treated with either **JS61** or **ZR2002** at 1 μM. ATP concentration used for the

assay was set at the Km for each particular kinase.

4.1.21. Data and statistical analysis

Data analysis of all biological results was processed with GraphPad Prism version 6 (GraphPad Software Inc.). Statistical analysis was achieved using either one- or two-way ANOVA where applicable with Bonferroni correction. $P < 0.05$.

4.1.22. Western blot – Inhibition of phosphorylation

The assessment for inhibition of phosphorylation of the EGFR signaling cascade proceeded as follows. Briefly, cells were seeded in 6 well plates (Corning) at 500,000 cells/well with a volume of 2 mL and allowed to attach in a humidified incubator at 37 °C with 5% CO_2 overnight. Once confluent, cells were serum starved using 1 mL of corresponding starvation media (Wisent) for 24 h prior to the addition of 1 mL of drug diluted in serum free media for 2 h. Cells were stimulated with 50 ng/mL of EGF (Sigma) for 30 min before lysis in RIPA buffer (Cell Signaling) with 1 mM of PMSF (Bioshop Canada Inc.) over ice. Cells were scraped, harvested and lysed for 30 min over ice. Samples were centrifuged at 13,000 rpm for 20 min at 4 °C and the supernatant collected. All cell lysates had their proteins quantified using the Bradford assay and a BSA standard curve. Equal quantities of proteins prepared in Laemmli buffer (Bio-Rad) were loaded into an SDS-PAGE pre-cast gel (Bio-Rad) and run for 1 h at 100V in an electrophoresis tank (Bio-Rad). Proteins were transferred to a PVDF membrane (Bio-Rad) using a transfer apparatus (Bio-Rad) under the following conditions: 100V for 1.5 h over ice. Membranes were blocked using 5% milk in TBST 1X for 1 h prior to primary antibody incubation overnight in 5% milk according to manufacturer specifications at 4 °C. Washing 3 times with TBST 1X for 10 min preceded secondary antibody incubation according to manufacturer specifications for 1.5 h at room temperature. The membrane was again washed thrice with TBST 1X and chemiluminescent detection was accomplished using the WestPico (Thermo Fisher) reagent kit and images recording using the GE Healthcare ImageQuant LAS4000 system (Serial No. 28955810−0632092) and quantitation of protein expression by densiometry was computed using ImageJ.

4.1.23. Western blot – Irreversibility

To determine the recovery of EGFR phosphorylation by Western Blot, two groups of serum-starved cells were treated with compounds for 2 h. One group was stimulated immediately thereafter with EGF (50 ng/mL) for 30 min, whereas the other group was washed by fresh treatment and serum free media three times every 2 h prior to EGF stimulation. Both groups of cells were subsequently harvested, and the following steps were as previously described in Western Blot methodology. Immunodetection was achieved using anti-phospho EGFR antibody (Cell Signaling) and total EGFR antibody (Santa Cruz).

4.1.24. Single crystal X-ray diffraction

Single crystal X-ray diffraction data were collected on a Bruker D8 Venture diffractometer with a Photon 200 CMOS area detector and an IμS microfocus X-ray source (Madison, WI) using CuKα radiation. Single crystals were coated with paraffin oil, and data were collected at room temperature. Apex 3 software suite (Madison, WI) was used for the data collection, reduction, and unit cell assignment. Crystals were solved by an iterative dual space approach as implemented in SHELXT. Non-hydrogen atoms were located from the difference map and refined anisotropically. Hydrogen atoms bonded to nitrogen and oxygen atoms were located from the difference maps, while hydrogen atoms bonded to carbon atoms were placed in calculated positions. All hydrogen atom coordinates and thermal parameters were constrained to ride on the carrier atoms.

4.1.25. Acute toxicity

CD1 male mice were injected P.O. once daily for one week with either JS61 or JS84 at doses of 50 mg/kg, 100 mg/kg or 150 mg/kg. Mouse weights and physical symptoms were monitored throughout the course of the experiment.

Declaration of competing interest

The authors declare that they have no known competing financial interests or personal relationships that could have appeared to influence the work reported in this paper.

Acknowledgements

This study was supported by CIHR (MOP-130363). The present study was partially supported by Canada-Brazil bilateral project DFATD-CAPES-88887.137283/2017−00. We also thank DFATD-CAPES for ING and MNR fellowships. JS thanks the Research Institute of the McGill University Health Centre (RI MUHC) for financial support. The China Scholarship Council (CSC) is acknowledged for SH scholarship. We wish to thank the Center for Translational Biology (CTB) of the RI MUHC Drug Discovery Platform for NMR access and mass spectrometry data.

Appendix A. Supplementary data

Supplementary data to this article can be found online at https://doi.org/10.1016/j.ejmech.2020.112185.

Abbreviations

EGFR	epidermal growth factor receptor
DNA	Deoxyribo Nucleic Acid
NSCLC	Non-small cell lung cancer
BBB	blood brain barrier
Wt	wild-type
ATP	adenosine triphosphate
CLBC	Chlorambucil
GEF	gefitinib
HPLC	high-performance liquid chromatography
HR-MS	High resolution mass spectrometry
ES-MS	Electrospray Mass Spectrometry
DCM	dichloromethane
DMF	N,N-dimethyl- formamide
DMSO	dimethyl sulfoxide
AcOH	Acetic Acid
EtOH	Ethanol
MeOH	Methanol
EtOAc	Ethyl Acetate
rt	room temperature
h	hour(s)
min	minute
quant	quantitative
on	overnight
TLC	thin-layer chromatography
VDW	Van Der Waals

References

[1] G.V. Scagliotti, G. Selvaggi, S. Novello, F.R. Hirsch, The biology of epidermal growth factor receptor in lung cancer, Clin. Canc. Res. 10 (2004) 4227s−4232s.
[2] D. Veale, N. Kerr, G.J. Gibson, P.J. Kelly, A.L. Harris, The relationship of quantitative epidermal growth factor receptor expression in non-small cell lung cancer to long term survival, Br. J. Canc. 68 (1993) 162−165.

[3] M. Volm, W. Rittgen, P. Drings, Prognostic value of ERBB-1, VEGF, cyclin A, FOS, JUN and MYC in patients with squamous cell lung carcinomas, Br. J. Canc. 77 (1998) 663–669.
[4] G. Bethune, D. Bethune, N. Ridgway, Z. Xu, Epidermal growth factor receptor (EGFR) in lung cancer: an overview and update, J. Thorac. Dis. 2 (2010) 48–51.
[5] V.D. Cataldo, D.L. Gibbons, R. Pérez-Soler, A. Quintás-Cardama, Treatment of non–small-cell lung cancer with erlotinib or gefitinib, N. Engl. J. Med. 364 (2011) 947–955.
[6] W. Zhong, X. Yang, H. Yan, X. Zhang, J. Su, Z. Chen, R. Liao, Q. Nie, S. Dong, Q. Zhou, J. Yang, H. Tu, Y.-L. Wu, Phase II study of biomarker-guided neoadjuvant treatment strategy for IIIA-N2 non-small cell lung cancer based on epidermal growth factor receptor mutation status, J. Hematol. Oncol. 8 (2015) 54.
[7] A. Chi, S. Remick, W. Tse, EGFR inhibition in non-small cell lung cancer: current evidence and future directions, Biomarker Research 1 (2013) 2.
[8] G.M. O'Kane, T.A. Barnes, N.B. Leighl, Resistance to epidermal growth factor receptor tyrosine kinase inhibitors, T790M, and clinical trials, Curr. Oncol. 25 (2018) S28–S37.
[9] K. Politi, D. Ayeni, T. Lynch, The next wave of EGFR tyrosine kinase inhibitors enter the clinic, Canc. Cell 27 (2015) 751–753.
[10] S. Wang, S. Cang, D. Liu, Third-generation inhibitors targeting EGFR T790M mutation in advanced non-small cell lung cancer, J. Hematol. Oncol. 9 (2016) 34.
[11] B.P. Brown, Y.-K. Zhang, D. Westover, Y. Yan, H. Qiao, V. Huang, Z. Du, J.A. Smith, J.S. Ross, V.A. Miller, S.M. Ali, L. Bazhenova, A.B. Schrock, J. Meiler, C.M. Lovly, On-target resistance to the mutant-selective EGFR inhibitor osimertinib can develop in an allele specific manner dependent on the original EGFR activating mutation, Clin. Canc. Res. 25 (2019) 3341.
[12] C. Tomasello, C. Baldessari, M. Napolitano, G. Orsi, G. Grizzi, F. Bertolini, F. Barbieri, S. Cascinu, Resistance to EGFR inhibitors in non-small cell lung cancer: clinical management and future perspectives, Crit. Rev. Oncol.-Hematol. 123 (2018) 149–161.
[13] Y.-C. Zhang, Q. Zhou, Y.-L. Wu, Clinical management of third-generation EGFR inhibitor-resistant patients with advanced non-small cell lung cancer: current status and future perspectives, Canc. Lett. 459 (2019) 240–247.
[14] L.A. Knight, F. Di Nicolantonio, P. Whitehouse, S. Mercer, S. Sharma, S. Glaysher, P. Johnson, I.A. Cree, The in vitro effect of gefitinib ('Iressa') alone and in combination with cytotoxic chemotherapy on human solid tumours, BMC Canc. 4 (2004) 83.
[15] R. Banerjee, Y. Huang, Q. Qiu, J.P. McNamee, G. Belinsky, B.J. Jean-Claude, The combi-targeting concept: mechanism of action of the pleiotropic combi-molecule RB24 and discovery of a novel cell signaling-based combination principle, Cell. Signal. 23 (2011) 630–640.
[16] M.I. Todorova, A.-L. Larroque, S. Dauphin-Pierre, Y.-Q. Fang, B.J. Jean-Claude, Subcellular distribution of a fluorescence-labeled combi-molecule designed to block epidermal growth factor receptor tyrosine kinase and damage DNA with a green fluorescent species, Mol. Canc. Therapeut. 9 (2010) 869.
[17] Y. Wang, T. Ren, X. Lai, G. Sun, L. Zhao, N. Zhang, R. Zhong, Synthesis and antitumor activity evaluation of a novel combi-nitrosourea prodrug: BGCNU, ACS Med. Chem. Lett. 8 (2017) 174–178.
[18] G. Sun, T. Fan, L. Zhao, Y. Zhou, R. Zhong, The potential of combi-molecules with DNA-damaging function as anticancer agents, Future Med. Chem. 9 (2017) 403–435.
[19] R. Banerjee, Y. Huang, J.P. McNamee, M. Todorova, B.J. Jean-Claude, The combi-targeting concept: selective targeting of the epidermal growth factor receptor- and Her2-expressing cancer cells by the complex combi-molecule RB24, J. Pharmacol. Exp. Therapeut. 334 (2010) 9.
[20] M. Heravi, S. Kumala, Z. Rachid, B.J. Jean-Claude, D. Radzioch, T.M. Muanza, ZRBA1, a mixed EGFR/DNA targeting molecule, potentiates radiation response through delayed DNA damage repair process in a triple negative breast cancer model, Int. J. Radiat. Oncol. Biol. Phys. 92 (2015) 399–406.
[21] Z. Rachid, F. Brahimi, Q. Qiu, C. Williams, J.M. Hartley, J.A. Hartley, B.J. Jean-Claude, Novel nitrogen mustard-armed combi-molecules for the selective targeting of epidermal growth factor receptor overexperessing solid Tumors: discovery of an unusual Structure–Activity relationship, J. Med. Chem. 50 (2007) 2605–2608.
[22] Z. Rachid, F. Brahimi, J. Domarkas, B.J. Jean-Claude, Synthesis of half-mustard combi-molecules with fluorescence properties: correlation with EGFR status, Bioorg, Med. Chem. Lett. 15 (2005) 1135–1138.
[23] F. Brahimi, Z. Rachid, Q. Qiu, J.P. McNamee, Y.-J. Li, A.M. Tari, B.J. Jean-Claude, Multiple mechanisms of action of ZR2002 in human breast cancer cells: a novel combi-molecule designed to block signaling mediated by the ERB family of oncogenes and to damage genomic DNA, Int. J. Canc. 112 (2004) 484–491.
[24] F. Brahimi, S.L. Matheson, F. Dudouit, J.P. McNamee, A.M. Tari, B.J. Jean-Claude, Inhibition of epidermal growth factor receptor-mediated signaling by "combi-triazene" BJ2000, a new probe for combi-targeting postulates, J. Pharmacol. Exp. Therapeut. 303 (2002) 238.
[25] S. Rao, A.-L. Larroque-Lombard, L. Peyrard, C. Thauvin, Z. Rachid, C. Williams, B.J. Jean-Claude, Target modulation by a kinase inhibitor engineered to induce a tandem blockade of the epidermal growth factor receptor (EGFR) and c-Src: the concept of type III combi-targeting, PloS One 10 (2015), e0117215.
[26] Z. Sharifi, B. Abdulkarim, B. Meehan, J. Rak, P. Daniel, J. Schmitt, N. Lauzon, K. Eppert, H.M. Duncan, K. Petrecca, M.-C. Guiot, B. Jean-Claude, S. Sabri, Mechanisms and antitumor activity of a binary EGFR/DNA–Targeting strategy overcomes resistance of glioblastoma stem cells to temozolomide, Clin. Canc. Res. 25 (2019) 7594–7608.
[27] B. Marvania, P.-C. Lee, R. Chaniyara, H. Dong, S. Suman, R. Kakadiya, T.-C. Chou, T.-C. Lee, A. Shah, T.-L. Su, Design, synthesis and antitumor evaluation of phenyl N-mustard-quinazoline conjugates, Biorg. Med. Chem. 19 (2011) 1987–1998.
[28] S. Li, X. Wang, Y. He, M. Zhao, Y. Chen, J. Xu, M. Feng, J. Chang, H. Ning, C. Qi, Design and synthesis of novel quinazoline nitrogen mustard derivatives as potential therapeutic agents for cancer, Eur. J. Med. Chem. 67 (2013) 293–301.
[29] S. Lin, Y. Li, Y. Zheng, L. Luo, Q. Sun, Z. Ge, T. Cheng, R. Li, Design, synthesis and biological evaluation of quinazoline–phosphoramidate mustard conjugates as anticancer drugs, Eur. J. Med. Chem. 127 (2017) 442–458.
[30] B.J. Jean-Claude, Z. Rachid, F. Brahimi, Novel Combi-Molecules Having EGFR and DNA Targeting Properties, in, canada, 2004.
[31] A.-L. Larroque, B. Peori, C. Williams, Y.Q. Fang, Q. Qiu, Z. Rachid, B.J. Jean-Claude, Synthesis of water soluble bis-triazenoquinazolines: an unusual predicted mode of binding to the epidermal growth factor receptor tyrosine kinase, Chem. Biol. Drug Des. 71 (2008) 374–379.
[32] Z. Rachid, F. Brahimi, A. Katsoulas, N. Teoh, B.J. Jean-Claude, The combi-targeting Concept: chemical dissection of the dual targeting properties of a series of "combi-triazenes", J. Med. Chem. 46 (2003) 4313–4321.
[33] D. Yan, Y. Ge, H. Deng, W. Chen, G. An, Gefitinib upregulates death receptor 5 expression to mediate rmhTRAIL-induced apoptosis in Gefitinib-sensitive NSCLC cell line, OncoTargets Ther. 8 (2015) 1603–1610.
[34] I. Kenessey, K. Kói, O. Horváth, M. Cserepes, D. Molnár, V. Izsák, J. Dobos, B. Hegedűs, J. Tóvári, J. Tímár, KRAS-mutation status dependent effect of zoledronic acid in human non-small cell cancer preclinical models, Oncotarget 7 (2016) 79503–79514.
[35] Y. Zhang, Z. Chen, Y. Lou, Y. Yu, 2,3-Disubstituted 8-arylamino-3H-imidazo [4,5-g]quinazolines: a novel class of antitumor agents, Eur. J. Med. Chem. 44 (2009) 448–452.
[36] C. Han, Z. Huang, C. Zheng, L. Wan, L. Zhang, S. Peng, K. Ding, H. Ji, J. Tian, Y. Zhang, Novel hybrids of (Phenylsulfonyl)furoxan and anilinopyrimidine as potent and selective epidermal growth factor receptor inhibitors for intervention of non-small-cell lung cancer, J. Med. Chem. 56 (2013) 4738–4748.
[37] C. Avendaño, J.C. Menéndez, Chapter 5 - DNA alkylating agents, in: C. Avendaño, J.C. Menéndez (Eds.), Medicinal Chemistry of Anticancer Drugs, Elsevier, Amsterdam, 2008, pp. 139–176.
[38] J.-Y. Fan, S.J. Ohms, M. Boyd, W.A. Denny, DNA adducts of 9-anilinoacridine Mustards: characterization by NMR, Chem. Res. Toxicol. 12 (1999) 1166–1172.
[39] N. Müller, G. Eisenbrand, The influence of N7 substituents on the stability of N7-alkylated guanosines, Chem. Biol. Interact. 53 (1985) 173–181.
[40] T. Tanaka, A. Munshi, C. Brooks, J. Liu, M.L. Hobbs, R.E. Meyn, Gefitinib radiosensitizes non-small cell lung cancer cells by suppressing cellular DNA repair capacity, Clin. Canc. Res. 14 (2008) 1266–1273.
[41] D.W. Fry, A.J. Bridges, W.A. Denny, A. Doherty, K.D. Greis, J.L. Hicks, K.E. Hook, P.R. Keller, W.R. Leopold, J.A. Loo, D.J. McNamara, J.M. Nelson, V. Sherwood, J.B. Smaill, S. Trumpp-Kallmeyer, E.M. Dobrusin, Specific, irreversible inactivation of the epidermal growth factor receptor and erbB2, by a new class of tyrosine kinase inhibitor, Proc. Natl. Acad. Sci. U.S.A. 95 (1998) 12022.